HEAVY ATOM INDUCED PHOSPHORESCENCE OF ORGANIC MATERIALS USING MONO- AND TRIFUNCTIONAL ORGANOMERCURY DERIVATIVES

A Dissertation

by

CHARLOTTE NICOLE BURRESS

Submitted to the Office of Graduate Studies of
Texas A&M University
in partial fulfillment of the requirements for the degree of

DOCTOR OF PHILOSOPHY

December 2006

Major Subject: Chemistry

HEAVY ATOM INDUCED PHOSPHORESCENCE OF ORGANIC MATERIALS USING MONO- AND TRIFUNCTIONAL ORGANOMERCURY DERIVATIVES

A Dissertation

by

CHARLOTTE NICOLE BURRESS

Submitted to the Office of Graduate Studies of
Texas A&M University
in partial fulfillment of the requirements for the degree of

DOCTOR OF PHILOSOPHY

Approved by:

Chair of Committee,	François P. Gabbaï
Committee Members	Eric Simanek
	Raymond Schaak
	Michael Bevan
Head of Department	David Russell

December 2006

Major Subject: Chemistry

ABSTRACT

Heavy Atom Induced Phosphorescence of Organic Materials using Mono- and Trifunctional Organomercury Derivatives. (December 2006)
Charlotte Nicole Burress, B.S., Tulane University
Chair of Advisory Committee: Dr. François P. Gabbaï

This dissertation focuses on the phosphorescence of organic chromophores using perfluoro-*ortho*-phenylene mercury (**1**) and bis(pentafluorophenyl)mercury (**2**) as external heavy atom effect inducers. To ascertain the suitability of these luminescent adducts for OLED applications, several research objectives have been investigated.

To further shorten the triplet lifetimes of adducts involving **1**, a strategy was developed which combines both internal and external heavy atom effects. Specifically, complexes involving **1** and *N*-methylcarbazole, *N*-methylindole and the 1-halonaphthalenes were investigated. The existence and stability of the complexes could be confirmed in solution by fluorescence spectroscopy. In the solid state, these adducts form supramolecular binary stacks where the molecules of **1** alternate with the aromatic substrate. As a result of the mercury external heavy atom effect, all of these adducts display intense room temperature phosphorescence of the free arene. With the *N*-heterocycles, the triplet lifetimes were drastically reduced to below 100 μs.

To appreciate the origin of the unusual heavy atom effects observed in arene adducts with **1**, **2** was studied as a monofunctional analog to **1**. By utilizing fluorescence spectroscopy, naphthalene, biphenyl, and fluorene complexes of **1** and **2** have been detected in solution. The solid state structure of the adducts with **2** reveal supramolecular binary stacks. Comparison of the photophysical results supports the occurrence of cooperative effects between the Lewis acidic mercury centers of **1**, which make it a more efficient external heavy-atom effect inducer.

Polymeric materials which are amenable to deposition in thin layers were investigated as substrates for **1** and **2**. Both poly(vinyl-2-naphthalene) and poly(vinylcarbazole) interact with **1** and **2** in solution as evidenced by fluorescence spectroscopy. With the solid blend **1**•PVK, a small doping percentage of **1** results in white emission, while larger percentages of **1** yield bright orange emission.

This dissertation presents the first structurally characterized ternary complex with **1**, carbazole, and coordinating solvents THF and triethylamine. IR spectroscopy and short N···O and N···N distances in the solid state indicates that the acidic N-H moiety of carbazole interacts with the solvent by hydrogen bonding. In the extended structure, molecules of **1** and the hydrogen bonded complex alternate to form supramolecules.

DEDICATION

For my Grandad

ACKNOWLEDGMENTS

I would like to thank my research advisor, Prof. François P. Gabbaï, for his dedication and support during the last four years. He was especially helpful in my efforts to learn more photophysics and avoid synthesis as long as possible. I would also like to thank my committee members, Dr. Raymond Schaak, Dr. Eric Simanek, and Dr. Michael Bevan for their support outside of formal committee duties. I was able to form a relationship with each of them, and I feel honored to have them serve as my advising committee.

I would also like to show appreciation for the members of the Gabbai group during my tenure here. Thomas J. Taylor and I both joined the group in 2002, and we have worked well together despite our drastic differences in thinking. I would also like to thank Dr. Mason R. Haneline, who started this project and has continued to be a dear friend, Ching-Wen Chiu, Christopher Dorsey, Todd Hudnall, Dr. Mieock Kim, Dr. Julie King, Dr. Mohand A. Melaimi, Dr. Alexandre Picot, Dr. Stephane Solé, Dr. Mitsukimi Tsunoda, and Dr. Huadong Wang. Martha I. Bodine was an NSF-REU undergraduate student who worked with me on some of the monofunctional organomercurial complexes. She was an excellent coworker, and I know she will do well in the future.

Our collaborators at the University of North Texas, Dr. Oussama El-bjeirami and Prof. Mohammad Omary, deserve a big thank you for their hard work and dedication to the completion of this project.

I would also like to thank my undergraduate professors at Tulane University, specifically Dr. S. Thayumanavan, now of the University of Mass. Amherst, for preparing me for graduate school and beyond.

Additionally, I would like to acknowledge the Texas Advanced Technology Program, the Welch Foundation, and NSF for research funding, and the Department of Chemistry for a travel grant through the Arthur Martell award program.

Last but by no means least, I want to express my deepest gratitude to my family for their love and patience throughout the years, especially Richard, my other half, Pixie, my baby girl, Jacqueline, Sally, and Carl.

TABLE OF CONTENTS

LIST OF FIGURES

FIGURE Page

FIGURE Page

FIGURE Page

FIGURE Page

LIST OF TABLES

CHAPTER I

INTRODUCTION AND RESEARCH OBJECTIVES

I.1. Background

Organic light emitting devices (OLEDs) have great potential for use in flat panel displays because of their advantageous properties such as robustness, low operating voltages, light weight, and wide viewing angles and ease of processing.[1] Generally, devices consist of thin layers of materials which fulfill a specific purpose such as charge injection, charge transport, or emission.[2] When voltage is applied in a typical device, holes are injected into the hole transport layer (HTL), while electrons are injected into the electron transport layer (ETL). These electrons and holes then recombine in the emitting layer, forming an excited state or exciton. Relaxation of the excited state or exciton is radiative and gives rise to light emission. In order to improve device efficiency, multilayer devices are commonly utilized to prevent recombination occurring in any layer other than the emitting layer (Figure I.1).[2]

This dissertation follows the style and format of the *Journal of the American Chemical Society.*

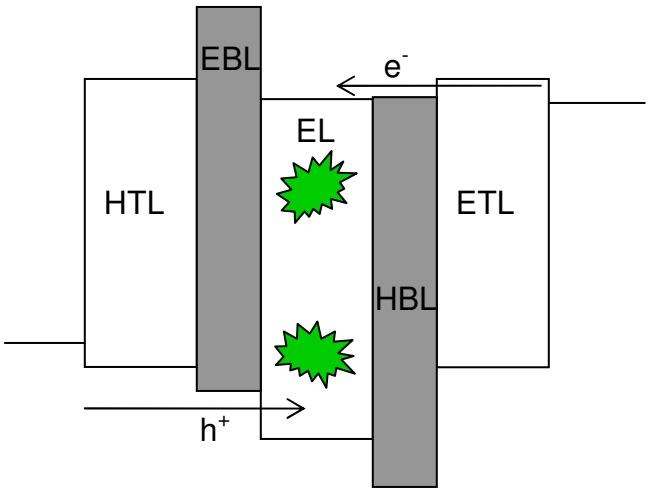

Figure I.1. Schematic energy-level diagram of a high-efficiency electrophosphorescent OLED adopted from ref 2. Holes (h^+) transport along the HOMO energy levels, and the electrons (e^-) along the LUMO levels. Excitons are shown as starbursts. Abbreviations: HTL, hole transport level; EBL, electron blocking layer; EL, emitting layer; HBL, hole blocking layer; ETL, electron transport level. The EBL or HBL prevent holes, electrons, or excitons from traveling through the EL to the HTL or ETL respectively.

Despite the promising progress in the field of OLEDs, there are still obstacles in bringing the devices to market, including rapid aging and deterioration of the device.[3] The most problematic barrier to mass producing devices is the low electroluminescent device efficiency. Luminescent compounds generally found in OLEDs emit fluorescence from the singlet state, thereby restricting the device efficiency to 25% due to spin statistics.[4] Other complications arise from the fact that intermolecular interactions in the solid state of the chromophores greatly reduce the device efficiency due to self-quenching and excimer formation.[1,3]

In order to increase the device efficiency, the electroluminescent emitting layer has been doped with phosphorescent dyes. Due to the radiative relaxation pathway of the triplet exciton in these dyes, the theoretical device efficiency is increased to 100% as derived from spin statistics. Heavy metal complexes, predominantly those containing Pt(II) and Ir(III), have been extensively studied as phosphorescent dyes in OLEDs.[2] The emission of the triplet excitons results from the spin orbit coupling provided by the

heavy atom. Devices involving Ir(III) complexes with cyclometalating ligands have the highest device efficiencies to date due to the harvesting of both the singlet and triplet excitons.[5] In these devices, an organic host material is doped with a small percentage of the Ir(III) complex, which acts as the emitter.

In contrast to these phosphorescent dye devices, this dissertation describes a strategy which uses the external heavy atom effect to induce the phosphorescence of the organic host material. In particular, the Lewis acid perfluoro-*ortho*-phenylene mercury (**1**) has been investigated as a heavy atom effect inducer. This compound forms 1:1 adducts with arenes such as triphenylene, pyrene, naphthalene, and biphenyl (Scheme I.1).[6,7] In the solid state, these adducts consist of extended binary stacks where eclipsed molecules of **1** alternate with the arene substrate. The sandwich structure of these adducts precludes arene-arene intermolecular interactions in the solid state, which will help increase device efficiency. All of these adducts display intense room temperature phosphorescence of the arene resulting from the mercury heavy atom effect.[4] The heavy atom effect also leads to significantly shorter triplet lifetimes than those seen by pure arenes, where phosphorescence is spin-forbidden.[8] For example, the naphthalene adduct has a lifetime of 0.985 ms at 77 K, while naphthalene in an EPA matrix has a lifetime of 2.3 s at 77 K.[4,5] These shorter lifetimes are crucial for OLED applications due to the rapid on/off switching required for flat panel displays.[2]

Scheme I.1. Reaction of **1** with naphthalene

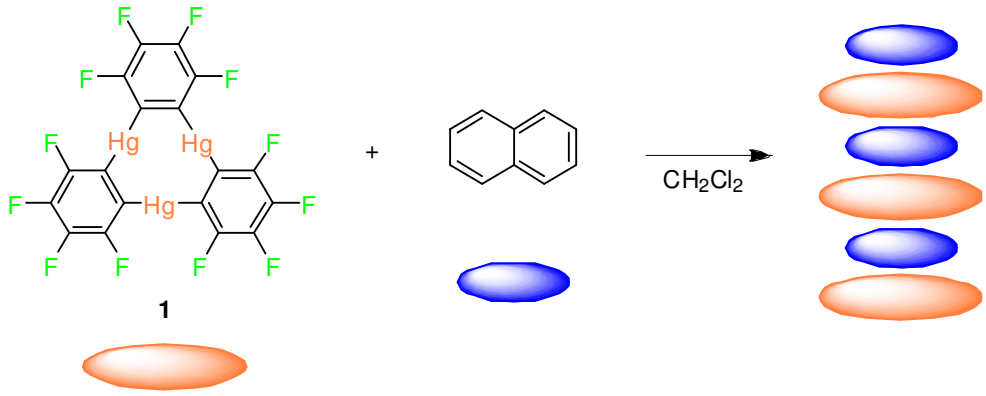

I.2. Research objectives

Altogether, adducts involving **1** and unsaturated chromophores show great promise as light emitting materials. It is the purpose of this dissertation to ascertain the suitability of these materials for the design of OLEDs. To fulfill this overarching goal, a number of specific objectives must first be examined. First, although the triplet lifetimes of the arene complexes with **1** are drastically shortened due to the heavy atom effect, they remain too long for the rapid on/off switching of the emission required in displays. For this reason, it became the objective of this dissertation to explore strategies allowing for a greater shortening of the triplet lifetimes.

In order to better appreciate the origin of the unusual heavy-atom effects observed in arene complexes with **1,** a second objective of this dissertation is to compare the properties of trinuclear **1** to those of its monofunctional analog bis(pentafluorophenyl) mercury (**2).** This dissertation presents a set of structural and solution studies which suggest that cooperative effects are involved in the spin-orbit perturbation that **1** provides to aromatic substrates.

With applications in OLEDs as an ultimate goal, a third research objective is to investigate the use of **1** and **2** as heavy atom effect inducers in polymeric materials which are amenable to deposition in thin layers by spin-coating techniques. Due to the affinity of the organomercurials **1** and **2** to aromatic substrates, polymeric organic materials with pendant aromatic groups as complexation sites. This dissertation reports a set of solution and solid state photophysical studies concerning the interaction of **1** and **2** with PVK and PV2N.

CHAPTER II

BACKGROUND*

In this chapter, recent literature concerning organomercury derivatives as well as heavy atom effects is presented. Organomercurials continue to be widely used in organic and organometallic synthesis. In addition to their synthetic utility, organomercury derivatives have been investigated as complexing agents for aromatic substrates, polyfunctional Lewis acids, anionic receptors as well as building blocks for supramolecular assemblies.

II.1. Complexation of aromatic substrates by organomercurials

Structural examples of mercury–arene π complexes with a variety of coordination modes, including η^2, η^3, and η^6, have been reported. In a continuation of earlier studies dealing with $[Hg_2(1,3,5\text{-}Me_3C_6H_3)_2]\bullet(AlCl_4)_2$,[9] Kloo and coworkers studied the $Hg_2Cl_2/GaCl_3$/benzene system using Raman spectroscopy and liquid X-ray scattering. Their data, complemented by DFT calculations, are in agreement with the existence of an $Hg_2(C_6H_6)_2^{2+}$ complex with the benzene ligand coordinated in an η^1 / *quasi* – η^3 – fashion along the Hg-Hg bond (Figure II.1).[10]

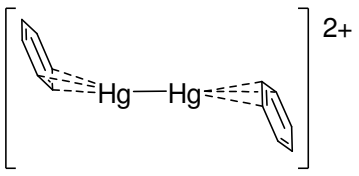

Figure II.1. Calculated structure of $Hg_2(C_6H_6)_2^{2+}$

* Reprinted in part with permission from *Comprehensive Organometallic Chemistry – 3rd Edition*, "Mercury and Cadmium," by Burress, C. N.; Melaimi, M.; Taylor, T. J.; Gabbaï, F. P., *in press*, Elsevier, New York, NY, Copyright 2006 by Elsevier.

In addition to [Hg(η^2-toluene)$_2$•(GaCl$_4$)$_2$][11], other mercury-arene complexes of general formula [Hg(η^2-arene)$_2$•(AlCl$_4$)$_2$] have been prepared.[12,13] These include the bis(toluene) **3**, the bis(*o*-xylene) **4** as well as the bis(1,2,3-trimethylbenzene) complexes **5** whose structures have all been determined experimentally (Figure II.2). While the arene in **3** and **4** is coordinated in an asymmetrical η^2-fashion, the η^2-1,2,3-trimethylbenzene ligands of **5** form two nearly equal Hg-C bonds of 2.45 and 2.46 Å. DFT calculations also show that the Hg···arene interactions are mostly ionic.[12]

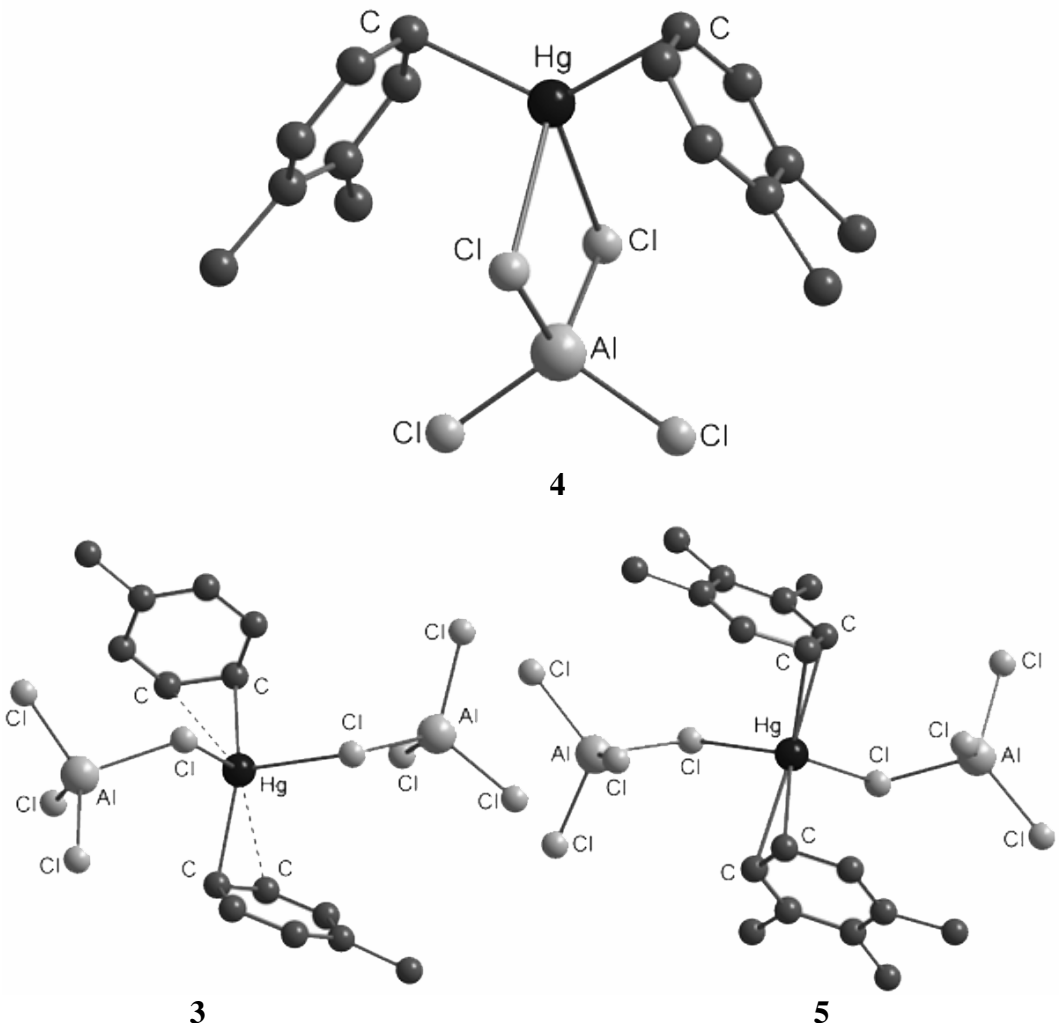

Figure II.2. Molecular structure of Hg(C$_6$H$_5$Me)$_2$•(AlCl$_4$)$_2$ **3**; [Hg(C$_6$H$_4$Me$_2$)$_2$(AlCl$_4$)][AlCl$_4$] **4** and Hg(C$_6$H$_3$-1,2,3-Me$_2$)$_2$•(AlCl$_4$)$_2$ **5**. Hydrogen atoms omitted for clarity

Longer Hg-π interactions are observed in the p-*tert*-butylcalix[4]arene mercury complex **6** (Figure II.3). The mercury atom forms primary bonds with the two sulfur atoms and engages in weaker secondary interactions with two arene rings of the calixarene. Each of these rings is coordinated to the mercury center in a polyhapto-fashion with the centroid of each ring sitting at 3.07 to 3.11 Å from the mercury center.[14]

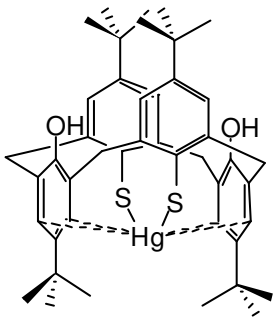

Figure II.3. Complex **6**

In an effort to characterize the species formed in vapors containing mercury and arenes upon irradiation with UV-light, the formation of exciplexes between excited mercury atoms and arenes has been investigated theoretically. For benzene, these investigations suggest the formation of an exciplex involving the Hg atom in the $^3P_1$ state and an η^2-bound molecule of benzene. This loose complex (^{3}[Hg(η^2-arene)]) with estimated Hg-C bonds of 2.36 Å, allows for transfer of the triplet excited state to the arene. In the case of alkyl-substituted benzenes, population of the triplet states triggers a number of subsequent reactions including C-C bond scissions.[15,16]

To prepare compounds which contain Hg–π interactions along with other types of associative interactions such as Hg–X (X = halides), large aromatic ligands such as anthracene have been employed. The compound 9-chloromercurioanthracene (**7**) has

been isolated and characterized by NMR and X-ray crystallography. In the solid state structure, the mercury center of **7** exhibits a trihapto-π-interaction of a neighboring anthracenyl ligand resulting in a polymeric extended structure (Figured II.4).[17] The anthracenyl ligands are slipped with respect to each other, yielding a staircase structure held together by Hg–Cl, π–π, and Hg–π interactions.

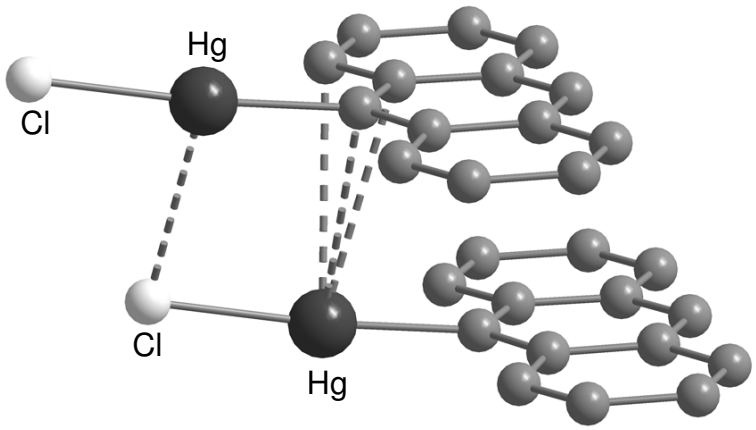

Figure II.4. Molecular structure of **7**. Hydrogen atoms omitted for clarity

II.2. Organomercurials as polydentate Lewis acids

II.2.1. Anion complexation

In the presence of electron-withdrawing substituents, organomercurials, which do not typically exhibit any significant Lewis acidity, form adducts with a number of neutral and anionic Lewis basic substrates. Bis(trifluoromethyl)mercury (**8**), for example, complexes fluoride, bromide, iodide, and thiocyanate to afford anionic complexes which all have been structurally characterized. The fluoride complex ([**8**•μ_2•F]$^{2-}$) (Figure II.5), formed by reaction with TASF, adopts a dimeric structure with the fluoride bridging the mercury atoms.[18] Dinuclear anionic complexes ([**8**•μ_2•X]$^{2-}$, X

= Br, I, SCN) are also formed when **8** is allowed to react with $[MePPh_3]^+Br^-$, $[MePPh_3]^+I$, and $[(18\text{-c-}6)\bullet K]^+[SCN]^-$.[19] In all cases, the bonds formed between the anions and the mercury centers are longer than typical covalent interactions but remain well within the sum of the van der Waals radii (Table II.1). Anion binding to the mercury center also leads to a detectable deviation of the C-Hg-C angle from linearity (Table II.1).

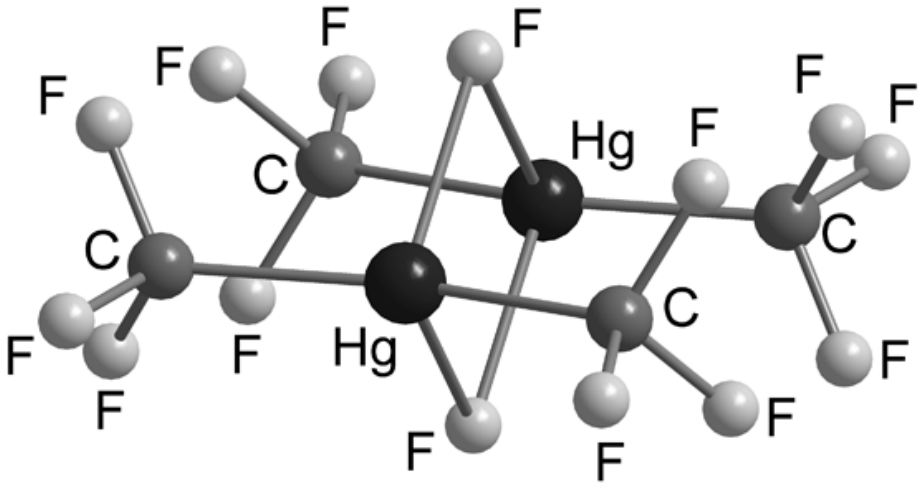

Figure II.5. Structure of ($[\mathbf{8}\bullet\mu_2\bullet F]^{2-}$)

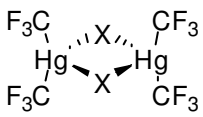

$[\mathbf{8}\cdot\mu_2\cdot X]^{2-}$

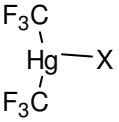

$[\mathbf{8}\cdot X]^-$

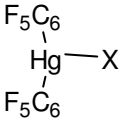

$[\mathbf{2}\cdot X]^-$

Table II.1. Comparison of geometrical parameters of organomercury-anion complexes

	X	F	Br	I	SCN
$[\mathbf{8}\bullet\mu_2\bullet X]^{2-}$	Hg-X [Å]	2.39; 2.41	2.97; 3.00	3.17; 3.19	2.99; 3.01
	C-Hg-C [°]	162.1	164.6	162.8	166.1
$[\mathbf{8}\bullet X]^-$	Hg-X [Å]	-	2.85	3.01	-
	C-Hg-C [°]	-	165.0	161.4	-

For bromide and iodide, the nature of the counter-cation influences the structure of the anionic complex. In fact, when the $[(18\text{-c-}6)\bullet K]^+Br^-$ and $[(18\text{-c-}6)\bullet K]^+I^-$ salts are used, the anionic complexes ($[\mathbf{8}\bullet X]^-$, X = Br, I) remain mononuclear and adopt a T-shaped structure. In both cases, the Hg-X bonds are shorter than those observed in the corresponding dinuclear complexes in agreement with the terminal location of the anion. The reaction of bis(pentafluoro)phenylmercury (**2**) with $[(18\text{-c-}6)\bullet K]^+Br^-$ and $[(18\text{-c-}6)\text{-}K]^+I^-$ also afford T-shaped complexes $[\mathbf{2}\bullet Br]^-$ and $[\mathbf{2}\bullet I]^-$ (Figure II.6). The Hg-Br (2.93 Å) and Hg-I (3.12 Å) bonds found in these complexes are longer than those observed in $[\mathbf{8}\bullet Br]^-$ and $([\mathbf{8}\bullet I]^-$ indicating that **2** is a weaker Lewis acid than **8.**[20]

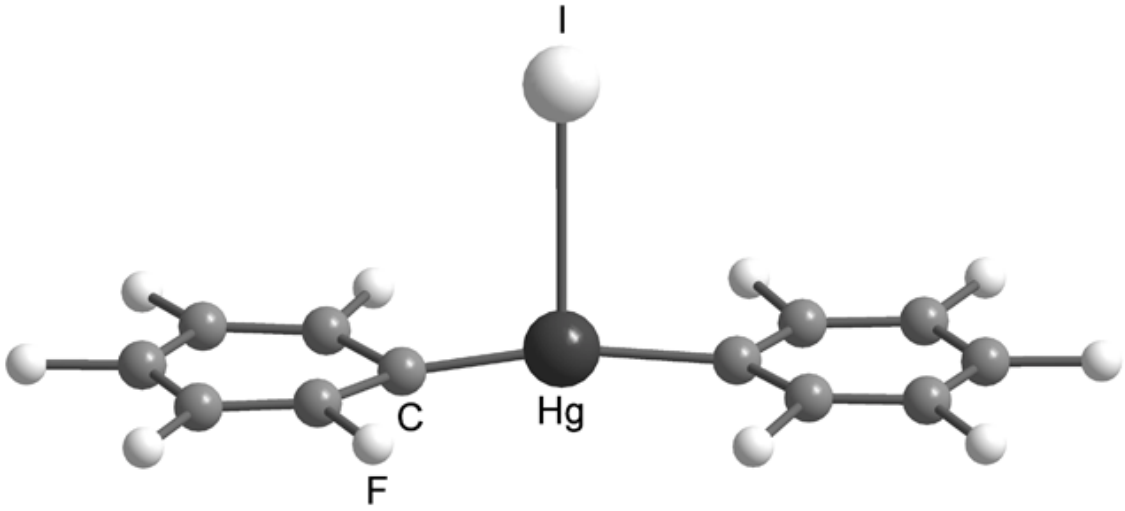

Figure II.6. Structure of [**2**•I]$^-$

Electron-withdrawing substituents have also been used to enhance the Lewis acidity of polyfunctional organomercurials. Trimeric perfluoro-*ortho*-phenylene mercury (**1**) has been extensively studied as an anion acceptor. While [**1**•Cl]$^-$, [**1**•Br]$^-$ and [**1**•I]$^-$ have been previously isolated,[21] recent ESI mass spectrometric studies suggest the gas phase formation of stable 2:1 complexes ([(**1**)$_2$•X]$^-$, X = F, Cl, Br, I) in which the halide is sandwiched by two molecules of **1** (Figure II.7).[22] Related anionic sandwich complexes have been obtained by reaction of $[B_{10}H_{10}]^{2-}$ or $[B_{12}H_{12}]^{2-}$ with **1**.[23,24] Structural characterization of $([(\mathbf{1})_2\bullet[B_{10}H_{10}]]^{2-}$ and $([(\mathbf{1})_2\bullet[B_{12}H_{12}]]^{2-}$ indicates the presence of multiple H-Hg bridges ranging from 2.5 to 2.8 Å. A sandwich complex ($[(\mathbf{1})_2\bullet[Fe(CN)_6]]^{3-}$) has also been isolated with the hexacyanoferrate anion (Figure II.8).[25] The cohesion of this sandwich results from multiple Hg-N interactions whose length (2.72 to 2.91 Å) is well within the sum of the van der Waals radii of mercury and nitrogen.

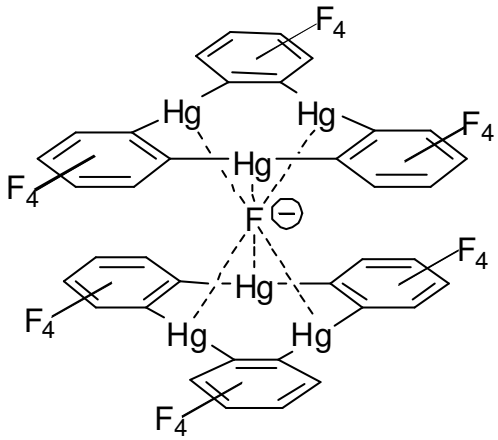

Figure II.7. Compound $[(\mathbf{1})_2 \bullet F]^-$

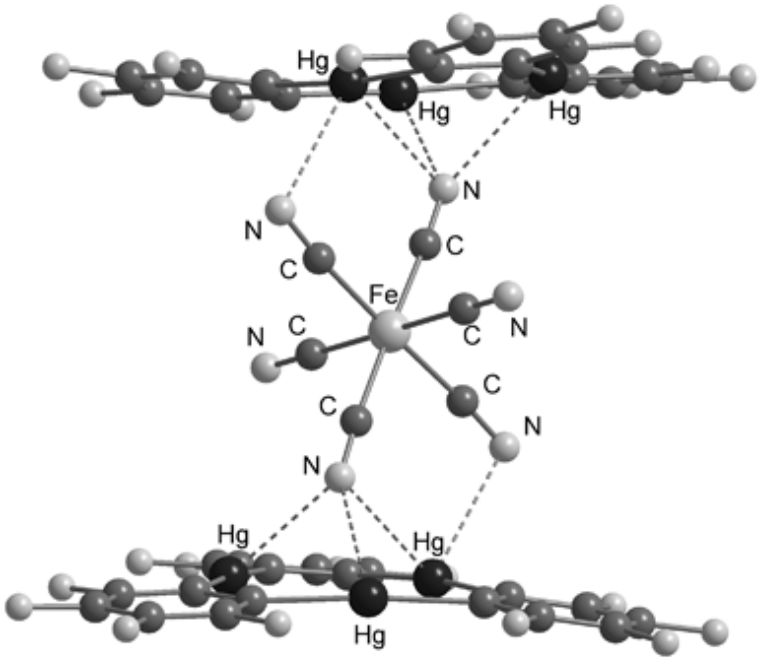

Figure II.8. Structure of $([(\mathbf{1})_2 \bullet [Fe(CN)_6]]]^{3-}$

Reaction of **1** with NBu_4SCN leads to formation of the anionic complex ([**1**•SCN]$^-$ which adopts a multidecker structure with the anion sandwiched between successive molecules of **1** (Figure II.9). The sulfur atoms of the SCN^- ion in [**1**•SCN]$^-$ interact unsymmetrically with the mercury atoms of the neighboring molecules of **1** forming four short Hg···S bonds that range from 3.06(1) to 3.36(1) Å and two long bonds of 3.74(1) and 3.87(1) Å. While the longer Hg-S bonds approach the limit for the involvement of dative interactions, the shorter ones are comparable to those observed in [**8**•SCN]$^-$.

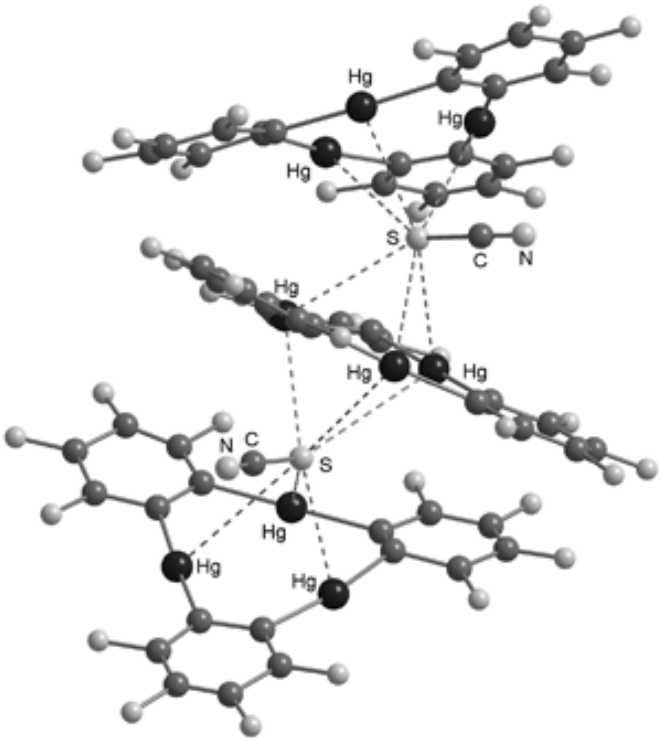

Figure II.9. Stack of repeating units of ([**1**•SCN]$^-$)

II.2.2. Supramolecular self-assembly

Polyfunctional organomercurials have emerged as useful building blocks for the constructions of supramolecular species. For instance, 1,2-bis(chloromercurio)tetrafluorobenzene (**9**) has been shown to form a supramolecular sandwich η^1 – μ complex with benzene [**9**•C_6H_6] (Figure II.10).[26] Secondary Hg–π interactions are observed between one carbon of the benzene and the mercury center as evidenced by the short Hg–C distances of 3.16 and 3.24 Å.

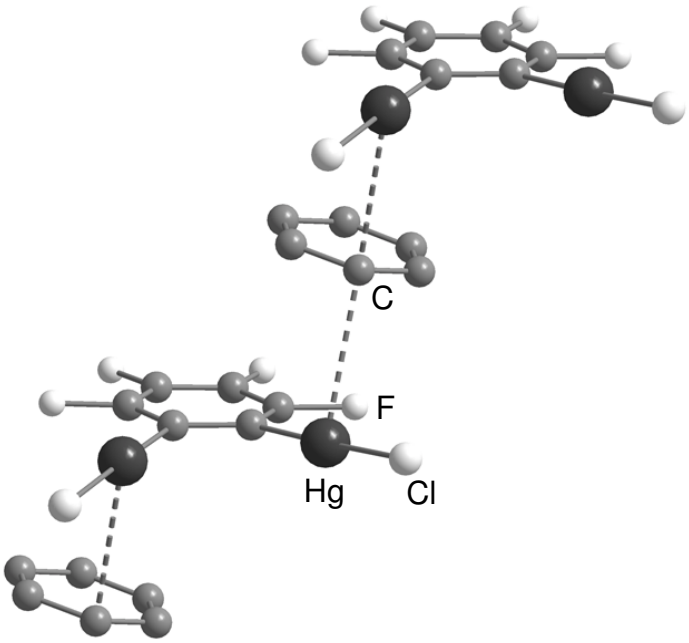

Figure II.10. Molecular structure of [**9**•C_6H_6]. Hydrogens are omitted for clarity.

Compound **1** was also shown to complex benzene, yielding extended binary stacks where the two components alternate (Figure II.11).[27] These stacks are rather compact (centroid distance of 3.24 Å) so that secondary π-interactions occur between the benzene molecule and the mercury centers. Each of the six C-C bonds of the benzene molecule interacts with one of the six mercury centers of the two juxtaposed molecules

of **1**. The short Hg···C contacts must be relatively weak as no change could be detected in the C-C bond lengths of the aromatic substrate. As indicated by wideline deuterium NMR, the sandwiched benzene molecules undergo an in-plane 60° reorientation with an activation energy of 52 ± 4 kJ/mol.[28] The magnitude of this activation energy suggests the presence of directional interactions between the mercury atoms of **1** and the benzene molecules.

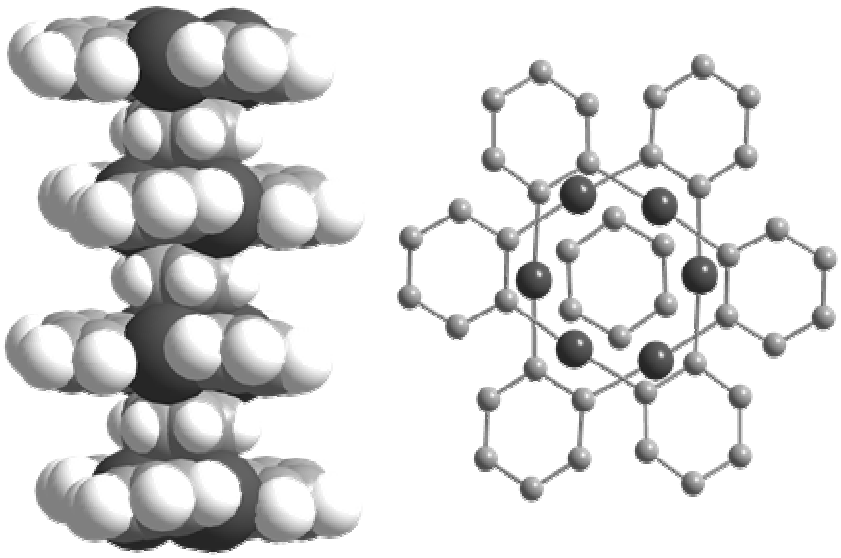

Figure II.11. Side and top views of a stack formed between [**1**•C_6H_6]

In order to assess how the bulk of the arene influences the structure of such stacked assemblies, the adducts of **1** with toluene, *o*-, *m*-, and *p*-xylenes, and mesitylene have been synthesized and structurally characterized.[29] In all cases, these adducts form extended binary stacks similar to those found in [**1**•C_6H_6]. The substituted benzene molecules adopt an apparently random orientation with respect to the trinuclear core of **1** thus suggesting that the binding might be largely dispersive and/or electrostatic. The interaction of **1** with larger aromatic substrates such as biphenyl, naphthalene, pyrene

and triphenylene has also been investigated.[6,7] The structure of the resulting adducts consists of extended stacks where eclipsed molecules of **1** alternate with the aromatic substrate (Figure II.12). These complexes all have short Hg···C contacts in the 3.2–3.4 Å range, reflecting the presence of secondary polyhapto–π interactions occurring between the electron rich aromatic molecules and the acidic mercury centers. Recent investigations indicate that **1** also complexes to the π-face of heteroatom containing substrates such as tetrathiafulvalene (TTF).[30]

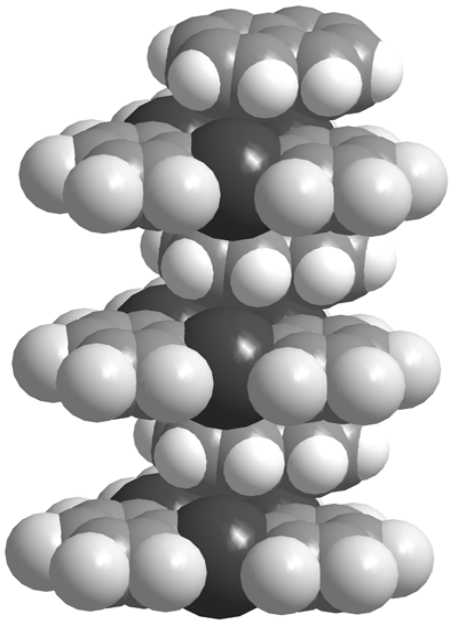

Figure II.12. Space filling view of [**1**•$C_{10}H_8$]

Simple mixing of **1** with ferrocene or nickelocene results in the formation of supramolecular electrophilic double-sandwiches in which each cyclopentadienide ring of the metallocene is capped by a molecule of **1** (Figure II.13). The shortest Hg···C distances range from 3.20–3.24 Å and indicate that the carbon atoms of the Cp rings are in close contact with the mercury centers. [31]

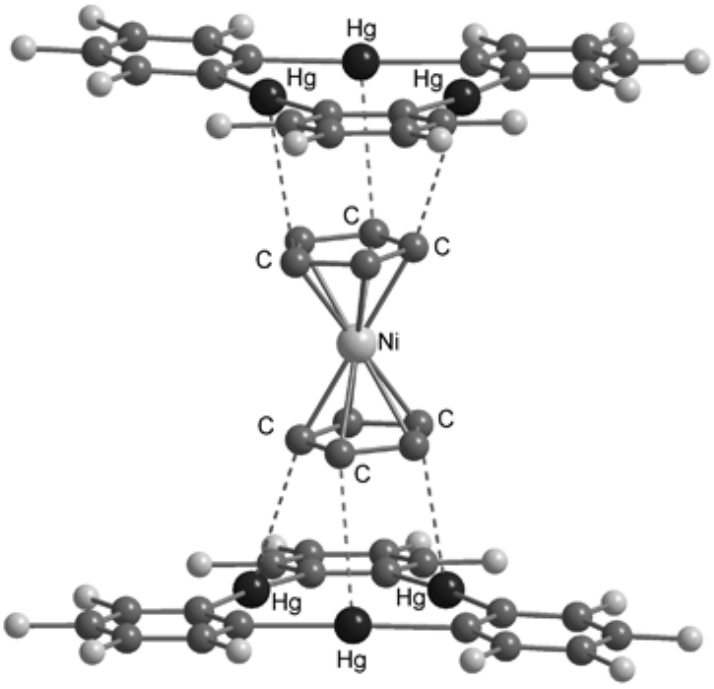

Figure II.13. Molecular structure of [**1**•$NiCp_2$]

II.3. External heavy atom effects

In atoms which have near-filled or filled valence shells and large atomic numbers *Z*, significant spin orbit coupling can be expected.[8] Spin orbit coupling occurs when there is interaction between the spin and orbital angular momenta of an electron and, thus, formerly forbidden transitions ($\Delta S \neq 0$) may take place. For example, rare gases and halogens are typical "heavy atoms" which gives rise to considerable spin orbit coupling. As a result, forbidden transitions, such as phosphorescence ($T_1 \rightarrow S_0$) in organic chromophores, can be observed in the presence of an internal or external heavy atom. Direct substitution of a heavy atom on the chromophore results in an internal heavy atom effect, while external heavy atom effects are observed when a heavy atom containing molecule interacts with the chromophore via non-covalent interactions

(Figure II.14).[8] The spin orbit perturbation provided by the heavy atom to the organic chromophore also leads to a shortening of the triplet lifetime (τ^P).

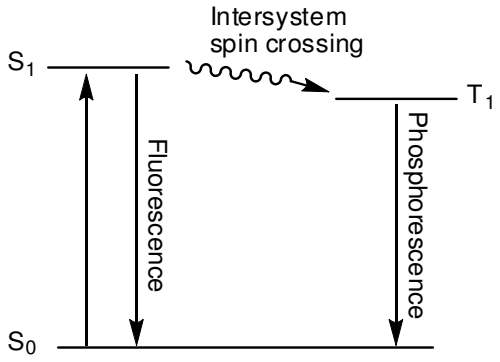

Figure II.14. Simplified Jablonski diagram for organic chromophores.

The external heavy atom effect provided by halogenated solvents to solute organic chromophores has been extensively studied in the literature. In his classic experiment, Kasha reported that upon mixing ethyliodide with 1-chloronaphthalene, an increase in phosphorescence of naphthalene was observed.[32] To grasp the mechanism of the external heavy atom effect, many studies have been pursued, and regrettably there does not seem to be a consensus on the mechanism. It has been suggested that the interaction is due to charge transfer, where the electron acceptor is the heavy atom containing molecule and the electron donor is the organic chromophore.[8,33,34] Unfortunately, in external heavy atom systems, the distinctive charge-transfer complex absorption peaks have not been observed. In addition to halogenated solvents, traditional external heavy atom effect inducers include halogen salts and rare gas matrices, and due to the extensive literature using these types of heavy atom containing systems, they will not be detailed here.

Mixed crystal systems have been employed to determine the effect of external heavy atoms on triplet lifetimes. For instance, the triplet emission and lifetime of

naphthalene has been measured in 1,4-dichloromobenzene, 1,4-dibromobenzene, and 1,4 diiodobenzene crystalline matrices (Figure II.15).[35-42] As expected, the triplet lifetime decreases as the atomic number *Z* of the halogen increases (Figure II.15).[35] It was determined from a series of lifetime experiments using these mixed crystal systems that the heavy atom effect generally perturbs the T_1–S_0 radiative rate rather than nonradiative transitions.

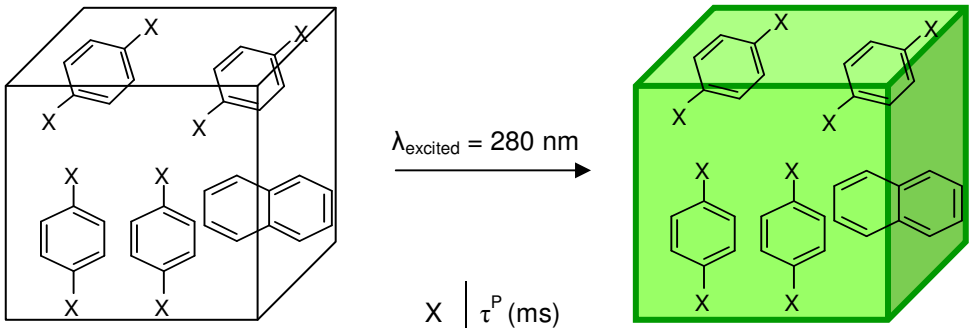

X	τ^P (ms)
Cl	776
Br	33
I	14

Figure II.15. Phosphorescent crystal of 1,4-dihalobenzene doped with naphthalene.

Recently, it has been demonstrated that the external heavy atom effect can propagate through the walls of a hemicarcerand. The triplet lifetime of biacetyl trapped in a hemicarcerand was measured in different halogenated solvents such as $CHBr_3$ and CH_2I_2, and a significant decrease in lifetimes was observed as the size of the halogen increased (Figure II.16).[43] This shortening is a result of the stronger spin orbit perturbation provided by the larger halogen to the biacetyl.

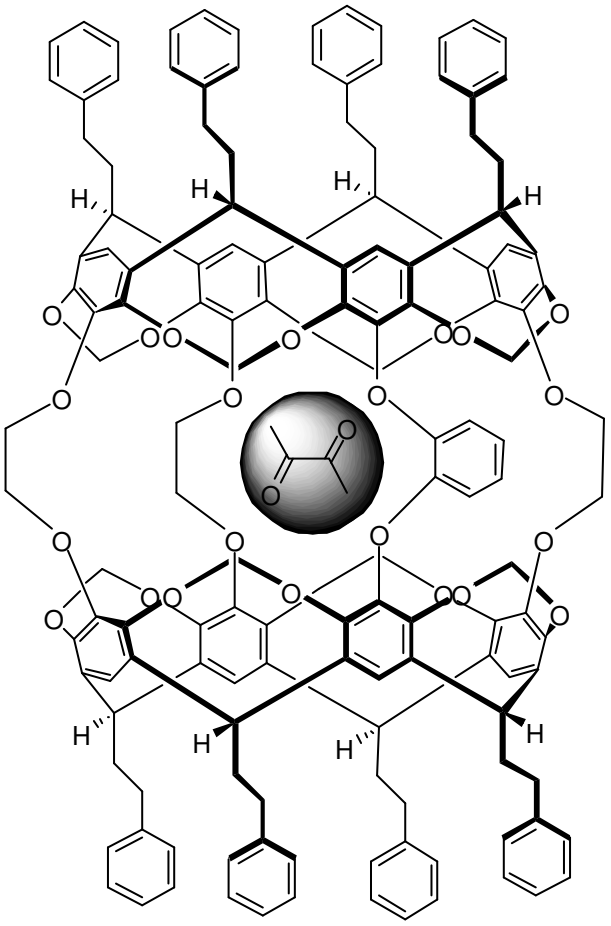

Figure II.16. Biacetyl encapsulated in a hemicarcerand.

While salts of Hg^{2+}, Ag^{+}, Pb^{2+}, and Tl^{+} have been commonly used as heavy atom effect inducers,[44] simple organometallic compounds have also been studied. For instance, dimethylmercury, tetraethyllead, and tetramethyltin have been used as heavy atom solvents for the observation of phosphorescence of aromatics.[45,46]

In order to observe room-temperature phosphorescence in aqueous solutions, cyclodextrins have been utilized as a means to force contact between the chromophore and heavy atom effect inducer. In most cases, the organic chromophore enters the interior of the cyclodextrin to afford an inclusion complex, whose formation is facilitated

by the hydrophobic nature of the organic.[47] Addition of an external heavy atom effect inducer such as KI or 1, 2-dibromoethane results in the observation of the chromophore phosphorescence.[48,49] Specifically, *N*-heterocycles, dibenzofuran, dibenzothiophene, biphenyl, fluorene, and other aromatics have been encapsulated in β-cyclodextrin along with 1,2-dibromoethane which provides spin orbit coupling to the aromatic chromophore (Scheme II.1).[50] Cyclodextrins have also been functionalized with halogens (Br and I) so that an additional heavy atom perturber is not required.[48,51] A recent review of the literature gives a detailed summary of the advances in room temperature phosphorescence of aqueous solutions using cyclodextrins.[47]

Scheme II.1. Heavy atom induced phosphorescence of biphenyl in aqueous media using cyclodextrins.

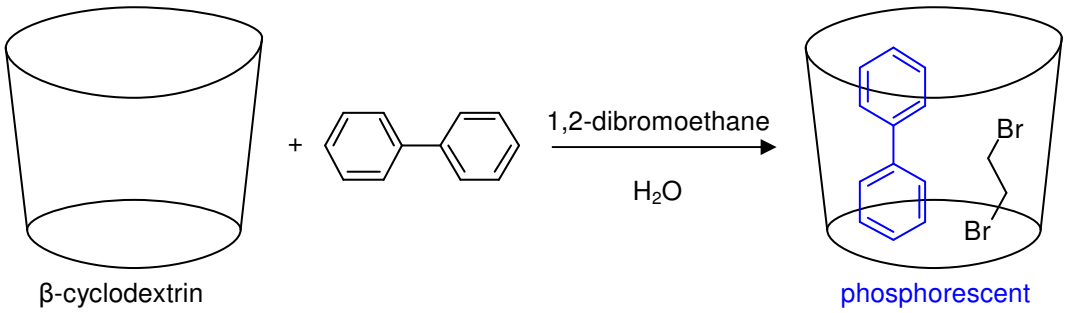

For detection of phosphorescence in solids, the heavy atom effect of zeolites has been explored with various arenes, diphenylpolyenes, and olefins. By using several types of zeolites with heavy countercations such as Rb^+, Cs^+, and Tl^+, phosphorescence of these chromophores has been observed.[52,53] The heavy cation effect in zeolites is reported as a general phenomenon, and room temperature phosphorescence can be observed with organic chromophores that are small enough to fit into the pore or window of the zeolite cage environment.[53]

Although external heavy atom effects are expected to yield weaker spin orbit coupling than internal heavy atom effects, Fackler and coworkers have shown that using gold as an external heavy atom effect inducer yields similar results as using an internal heavy atom. Electron rich $Au_3(p\text{-tolN=COEt})_3$ (**10**) was shown to form a 1:1 adduct with octafluoronaphthalene [**10**•$C_{10}F_8$], and the extended structure of [**10**•$C_{10}F_8$] shows supramolecular columnar stacks where π-base **10** alternates with the octafluoronaphthalene π-acid (Figure II.17).[54] In [**10**•$C_{10}F_8$], the phosphorescence of the octafluoronaphthalene is observed, and the triplet lifetime is shortened from 0.25 *seconds* to 3.25 *ms*. This shortening is more drastic than commonly expected with external heavy atom effects and, in fact, is comparable to lifetime reductions due to internal heavy atom effects. It is likely that this strong spin orbit coupling perturbation is a result of the extended structure of these stacks where the octafluoronaphthalene is surrounded by six metal atoms.[54]

Similar to the gold adduct [**10**•$C_{10}F_8$], adducts of **1** have been shown to display luminescent properties resulting from the mercury heavy atom effect. The adducts of **1** with naphthalene, biphenyl, pyrene, and triphenylene mentioned above display intense room temperature phosphorescence of the arene due to the external heavy atom effect.[30,31] Because of the extended structure of these adducts, the aromatic substrate is surrounded by six mercury atoms, which provides significant spin orbit coupling to the arene. The triplet lifetimes of these adducts range from 0.3–1 ms and are much shorter than those of the free arenes (~ seconds). This lifetime reduction is even more drastic than that observed by Fackler and coworkers. Unlike pure nickelocene which is air sensitive and displays a green color, the double sandwich nickelocene adduct [$\mathbf{1}_2$•$NiCp_2$] is a dark red solid and air stable. The unusual color of this complex results from an increase in the intensity of the formally spin forbidden $^3A_{2g} \rightarrow {}^1E_{1g}$ transition indicating the occurrence of a mercury heavy atom effect.[31]

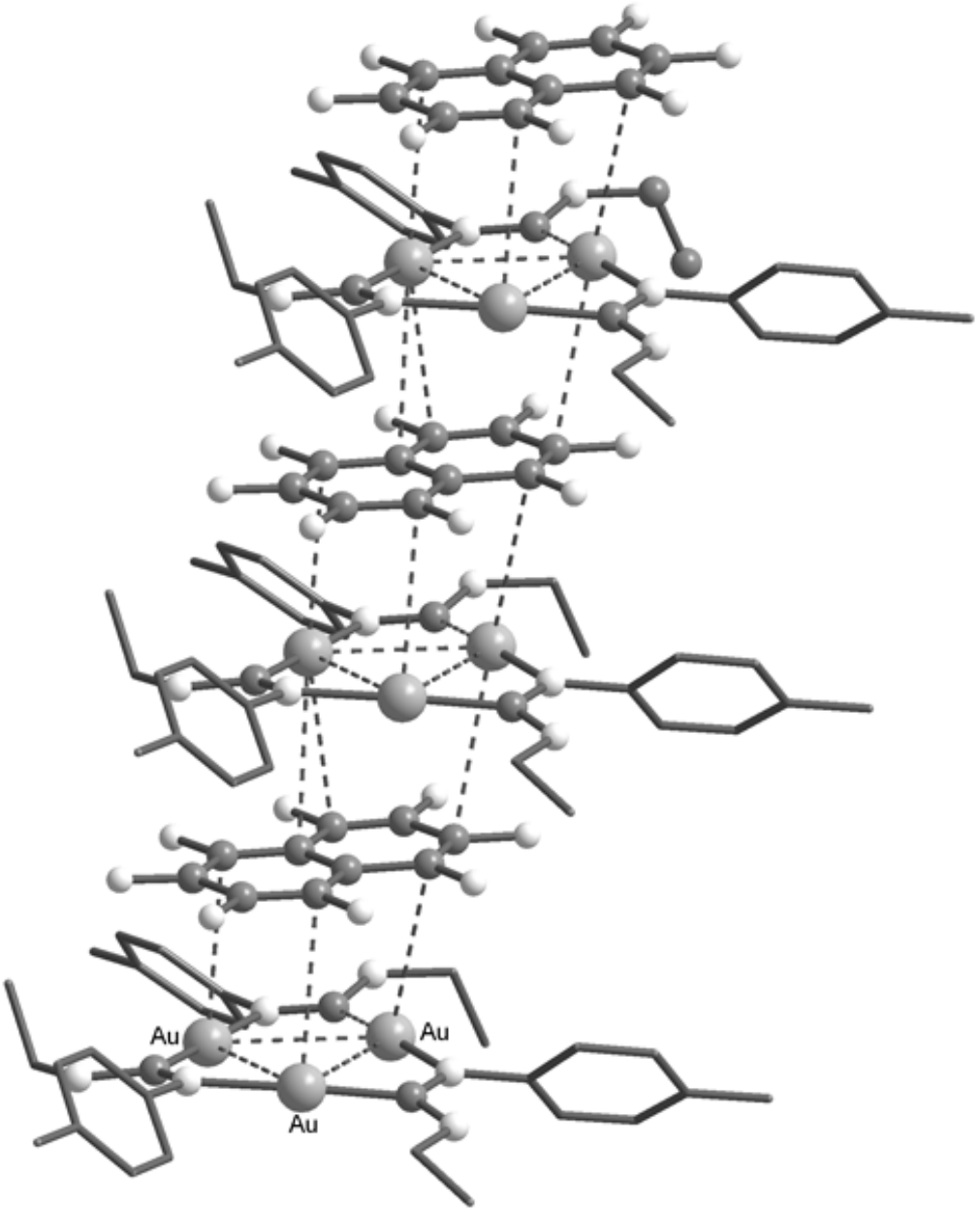

Figure II.17. Supramolecular stack of [**10**•$C_{10}F_8$] with short Au-C interactions.

CHAPTER III

REDUCTION OF TRIPLET LIFETIMES OF ORGANIC CHROMOPHORES BY COMPLEXATION TO $[(o\text{-}C_6F_4)Hg]_3$*

III.1. Introduction

The heavy-atom induced phosphorescence of organic chromophores originates from spin-orbit coupling and is always accompanied by a reduction of the triplet excited state lifetime. This phenomenon, which has been observed for a plethora of aromatic chromophores, can be triggered by both internal and external heavy atom effects.[8,32,55] In the latter case, a reduction of the triplet excited state lifetime by one to three orders of magnitude has been observed.[55,56]

As shown by some of our recent work, trimeric perfluoro-*ortho*-phenylene mercury (**1,** Chart III.1) "sticks" to the π-face of aromatic substrates.[28,31,57] In the case of pyrene, naphthalene, and biphenyl, this interaction leads to the formation of extended binary supramolecules in which **1** and the arene alternate.[6,7] In these supramolecules, each arene is surrounded by six mercury atoms that are positioned 3.3-3.6 Å from the arene molecular plane. As a result, the arene experiences a heavy atom effect that is manifested by an intense $T_1 \rightarrow S_0$ monomer phosphorescence. This supramolecular approach allows for a systematic synthesis of bright phosphors whose emission colors can be coarse- and fine-tuned simply by varying the identity of the arene substrate.[6,7]

---

* Reprinted in part with permission from *J. Am. Chem. Soc. 127* Burress, C.; Elbjeirami, O.; Omary, M. A.; Gabbaï, F. P. "Five-Order-of-Magnitude Reduction of Triplet Lifetimes of *N*-heterocycles by Complexation to a Trinuclear Mercury Complex," 12166, Copyright 2005 by the American Chemical Society, *J. Phys. Chem. A* submitted for publication, Elbjeirami, O; Burress, C. N.; Gabbaï, F. P.; Omary, M. A. "Simultaneous External and Internal Heavy Atom Effects in Binary Adducts of 1-Halonaphthalenes with Trinuclear Perfluoro-*ortho*-phenylene Mercury(II): A Structural and Photophysical Study," Unpublished work copyright 2006 American Chemical Society.

Moreover, the triplet excited state lifetimes fall in the *ms* range, which represents shortening by three to four orders of magnitude in comparison to those of the free arene. With the incorporation of such materials in OLEDs as an ultimate application,[58] we are currently exploring strategies that would afford lifetimes in the *μs* range.[59] Since chromophores with internal spin-orbit perturbation are typically more sensitive to external heavy-atom effects,[60] we have become interested in the photophysical properties of complexes involving **1** and *N*-heterocycles as well as 1-halonaphthalenes, (Chart III.1) wherein the nitrogen atom present in the *N*-heterocycles and the halogen atom (Cl, Br, and I) in the 1-halonaphthalenes act as internal spin-orbit coupling perturbers.[55b,61]

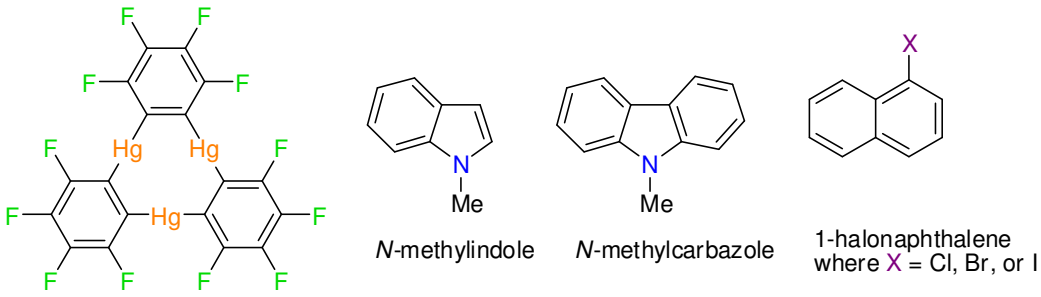

Chart III.1.

III.2. Solution studies

Incremental addition of **1** to a CH_2Cl_2 solution of the *N*-methylcarbazole results in a progressive quenching of the fluorescence of the heterocycle (Figure III.1). The observed quenching most likely results from a mercury heavy-atom effect,[6,7] which depopulates the S_1 state of the heterocycle. Analysis of the fluorescence quenching data herein provides the first evidence for the complexation of aromatic substrates by **1** in solution. Thus, a Stern-Volmer analysis[62] yields a K_{SV} value of 383 ± 24 M^{-1} for *N*-methylcarbazole (Figure III.2). The magnitude of this constant suggests that the quenching observed is static rather than dynamic. This conclusion is reinforced by measurements of the fluorescence lifetimes, which remain constant during the titration

experiment (Figure III.2). The photoluminescence spectra of frozen CH_2Cl_2 solutions containing equimolar amounts of **1** and *N*-methylcarbazole; *N*-methylindole; and 1-chloronaphthalene exhibit only the phosphorescence of the chromophore with emission energies that correspond to those reported for the respective T_1 states.[63,64] The observed phosphorescence results from substantial spin-orbit coupling provided by the mercury centers of **1** to the chromophore, consistent with the existence of complexes [**1**•*N*-methylindole] (**11**), [**1**•*N*-methylcarbazole] (**12**), and [**1**•1-chloronaphthalene] (**13**) in solution. Measurements performed by Dr. Oussama Elbjeirami in frozen CH_2Cl_2 solutions indicate drastic lifetime shortening upon complexation (τ^P = 66 ± 3 μs for **11** 176 ± 6 μs for **12;** 248 ± 6 μs for **13** vs 2.1 s for *N*-methylindole; 5.1 s for *N*-methylcarbazole; and 20.5 ms for 1-chloronaphthalene), certainly corroborating the above conclusion.

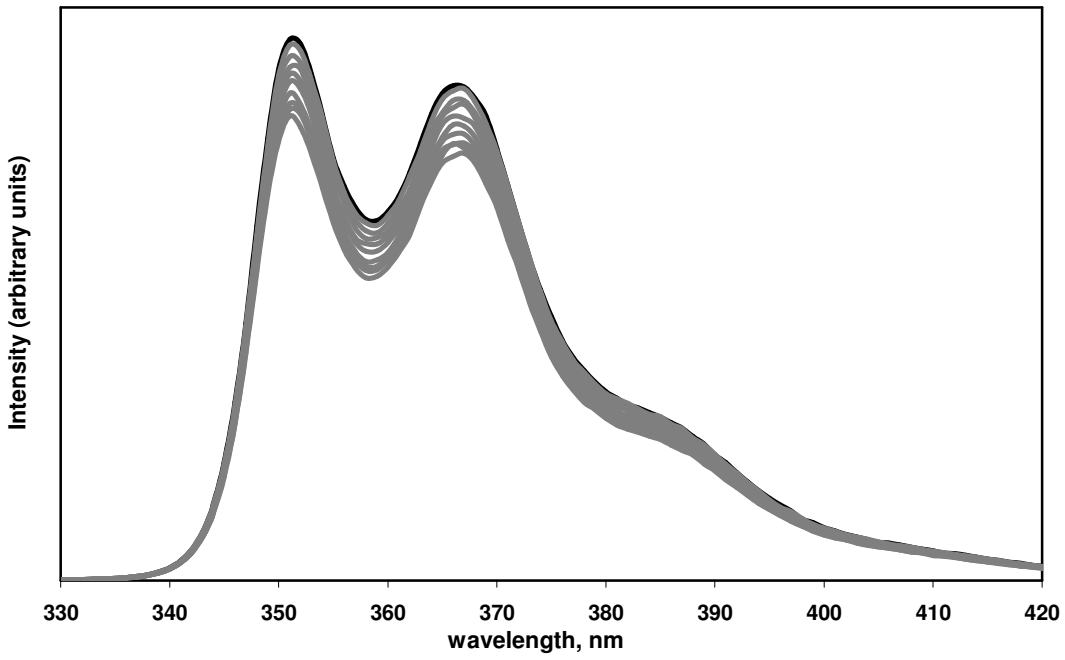

Figure III.1. Fluorescence quenching of *N*-methylcarbazole with **1**.

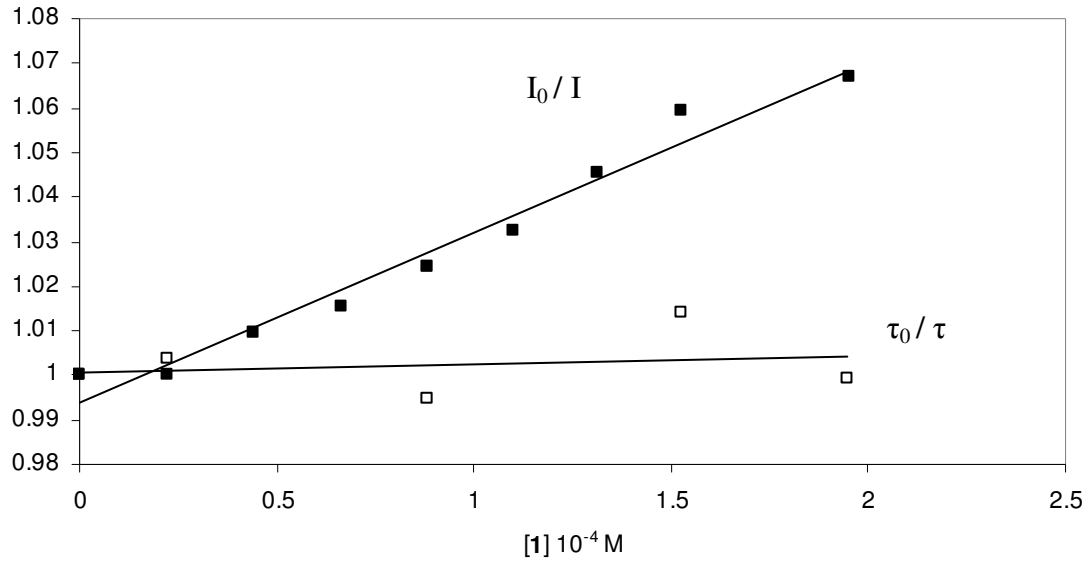

Figure III.2. Stern-Volmer plots for the fluorescence quenching of *N*-methylcarbazole (2.18 x 10^{-5} M) with **1** (6.6 x 10^{-3} M). The sample was excited at $\lambda_{excited}$ = 320 nm, and the emission intensities at 356 nm were monitored during the titration Measurement of lifetimes performed by Dr. Oussama Elbjeirami of UNT.

III.3. Solid state structures of the adducts

While it is difficult to ascertain their structure in solution, the binary complexes **11** and **12** precipitate from concentrated CH_2Cl_2 solutions containing equimolar amounts of **1** and *N*-methylcarbazole or *N*-methylindole. As indicated by elemental analysis, the solid adducts have a 1:1 stoichiometry. While we have not been able to elucidate the solid state structure of **11**, single crystals of **12** can be readily obtained (Figure III.3). The crystal structure of this adduct reveals the formation of extended binary stacks with alternating molecules of **1** and *N*-methylcarbazole (Figure III.3). As a result, the π-faces of the heterocycle are directly exposed to the trinuclear mercury core of adjacent molecules of **1**. Because of the presence of two independent molecules of [**1**•*N*-methylcarbazole] in the asymmetric unit, there are two crystallographically independent types of stacks which differ by the orientation of the *N*-methylcarbazole unit with respect

to the trinuclear mercury core of **1**. In one of the two orientations, there is a short Hg-N distance of 3.39 Å, which is within the van der Waals radii of mercury (r_{vdw} = 1.7 Å)[65] and nitrogen (r_{vdw} = 1.5 Å).[66] In both stacks, there are short Hg-$C_{aromatic}$ contacts ranging from 3.26 to 3.44 Å, suggesting the presence of secondary Hg-π interactions.[6,7] The coexistence of two distinct orientations of the *N*-methylcarbazole unit suggests that these interactions are not directional but perhaps largely dispersive and/or electrostatic.

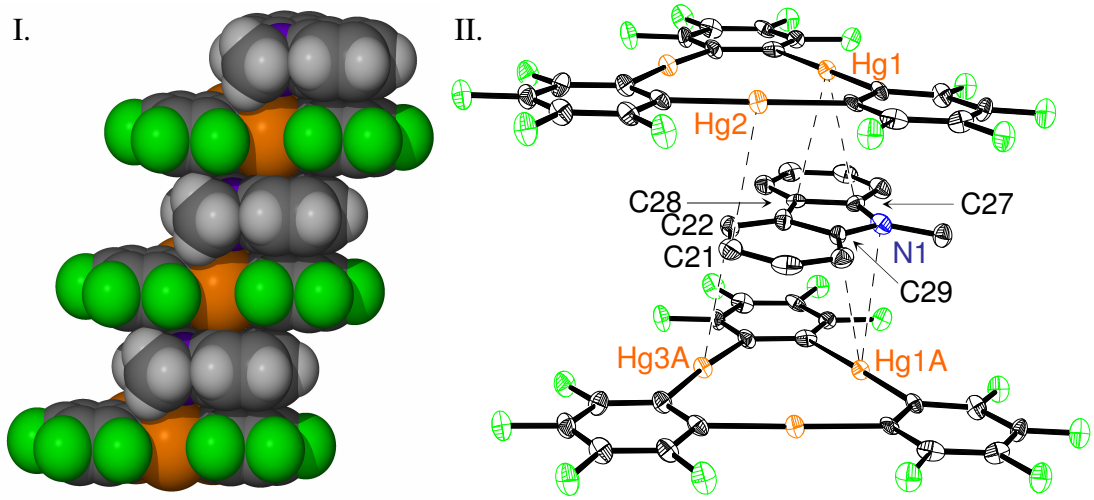

Figure III.3. Space filling (I) and ORTEP view (50% ellipsoid, II) of a portion of a stack in the structure of **12**. Only one of the two crystallographically independent stacks is shown. Representative intermolecular distances (Å): Hg(1)-C(27) 3.37, Hg(1)-C(28) 3.27, Hg(1A)-C(29) 3.33, Hg(1A)-N(1) 3.39, Hg(2)-C(21) 3.29, Hg(3A)-C(22A) 3.38.

In a similar fashion, when concentrated CH_2Cl_2 solutions containing equimolar amounts of **1** and 1-chloro-, 1-bromo, or 1-iodo-naphthalene slowly evaporate, the binary complexes **13**, [**1**•1-bromonaphthalene] (**14**), and [**1**•1-iodonaphthalene] (**15**) readily precipitate. The solid adducts are colorless, air stable, and have been analyzed by elemental analysis and their structures have been determined (Figures III.4–6). All three adducts display extended binary stacks where molecules of **1** alternate with the halogenated naphthalene.

Compounds **13, 14,** and **15** crystallize in the space groups $P2_1/n$, P-1, and $P2_1/c$, respectively (Table III.1). Examination of the cell packing diagram for all three adducts confirms the formation of extended stacks as observed in [**1**•naphthalene].[6] All three adducts display short Hg···$C_{aromatic}$ distances ranging from 3.28–3.43 Å, indicating secondary Hg–π interactions. These distances are all within the van der Waals radii for Hg (r_{vdw} = 1.73-2.00 Å)[65] and $C_{aromatic}$ (r_{vdw} = 1.7 Å)[66]. In **13**, the molecule of 1-chloronaphthalene of the asymmetric unit is disordered over two equally occupied positions, with the 8-position of the naphthalene ring acting as the pivot point between the two molecules. In the first orientation, the chlorine atom Cl(1) points outward from the stack and does not form any short contacts with the mercury centers (Figure III.4). In the second orientation, the chlorine atom Cl(2) interacts simultaneously with two mercury centers (Hg(1A)···Cl(2) 3.419 Å and Hg(3)···Cl(2) 3.501 Å), and these distances are within the sum of the van der Waals radii for Hg and Cl (r_{vdw} = 1.58–1.78 Å). [67] It is also important to note that these distances fall in the range typically observed for secondary Hg···Cl interactions.[17,26] While the crystal structure of **13** is affected by positional disorder, compound **14** has two distinguishable units of 1-bromonaphthalene located between the molecules of **1** similar to that observed in adduct **12** (Figure III.5). Each molecule of **1** exhibits a different type of interaction, with one molecule displaying mostly Hg···C_{arene} interactions and the other displaying Hg···Br interactions. In the unit where the two components interact only via Hg···C_{arene} interactions, the bromine atom Br(2) is positioned near the periphery of the stacks and does not interact with any of the mercury centers (Figure III.5). In the other unit, however, the bromine is coordinated to all three Hg atoms with distances from 3.57–3.84 Å, which are within the van der Waals radii of mercury and bromine (r_{vdw} = 1.54–1.84 Å).[67] Finally, compound **15** has only one molecule of 1-iodonaphthalene in the asymmetric unit. The sandwiched 1-iodonaphathalene interacts with the two neighboring molecules of **1** by secondary Hg···C_{arene} and Hg···I interactions (Figure III.6). The three distances between the three mecury centers Hg(1), Hg(2), and Hg(3) and the iodine atom I(1) are 3.814, 3.836, and 3.626 Å, respectively, which fall within the range of the van der Waals radii of the two

elements (r_{vdw} (I) = 1.98–2.13 Å).[67] These distances are close to those found in complexes involving tetranuclear mercuracarborand hosts and iodocarborane guests (3.6 Å).[68]

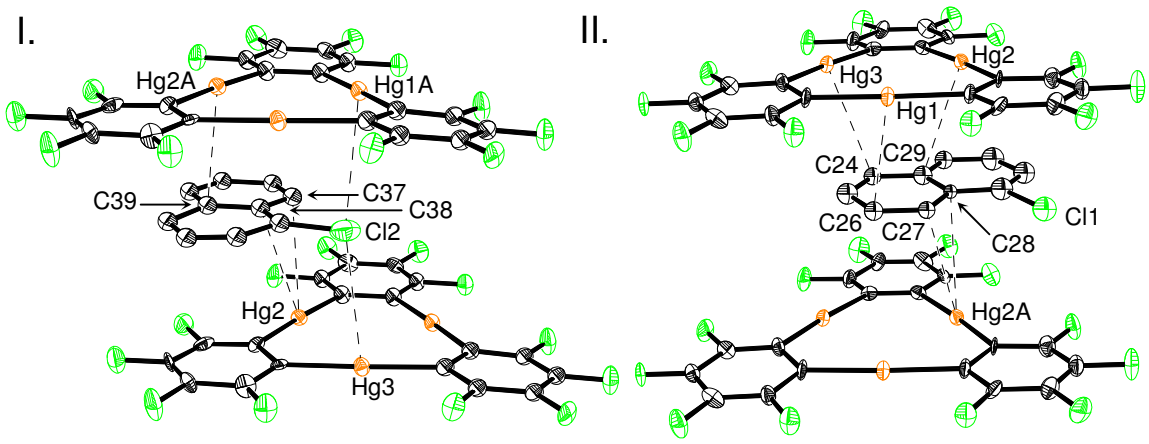

Figure III.4. Molecular structure of **13.** Thermal ellipsoids are at 50%. Hydrogen atoms are omitted for clarity. I. Significant contacts (Å): Cl(2)-Hg(1A) 3.500(12), Cl(2)-Hg(3) 3.419(14), C(37)-Hg(2A) 3.250(20), C(38)-Hg(2) 3.400(20), C(39)-Hg(2A) 3.359(19). II. Significant contacts (Å): C(24)-Hg(3) 3.374(12), C(26)-Hg(1) 3.358(14), C(27)-Hg(2A) 3.277(14), C(28)-Hg(2A) 3.402(14), C(29)-Hg(2) 3.406(19).

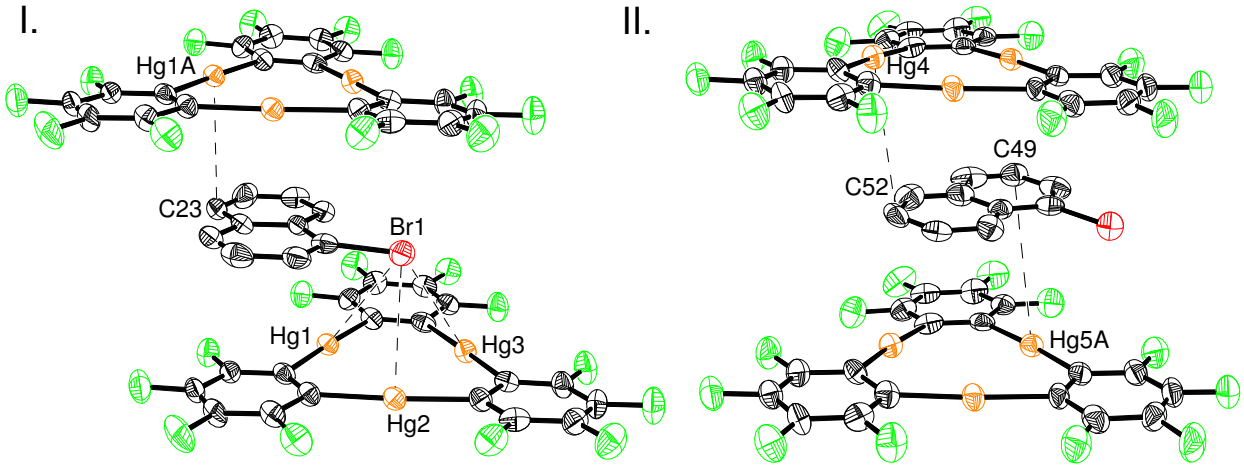

Figure III.5. Molecular structure of **14.** Thermal ellipsoids are at 30%. Hydrogen atoms are omitted for clarity. I. Significant contacts (Å): Br(1)-Hg(1) 3.843(2), Br(1)-Hg(2) 3.565(2), Br(1)-Hg(3) 3.809(2), C(23)-Hg(1A) 3.439(17), C(28)-Hg(1) 3.421(13). II. Significant contacts (Å): C(52)-Hg(4) 3.388(11), C(49)-Hg(5A) 3.426(20).

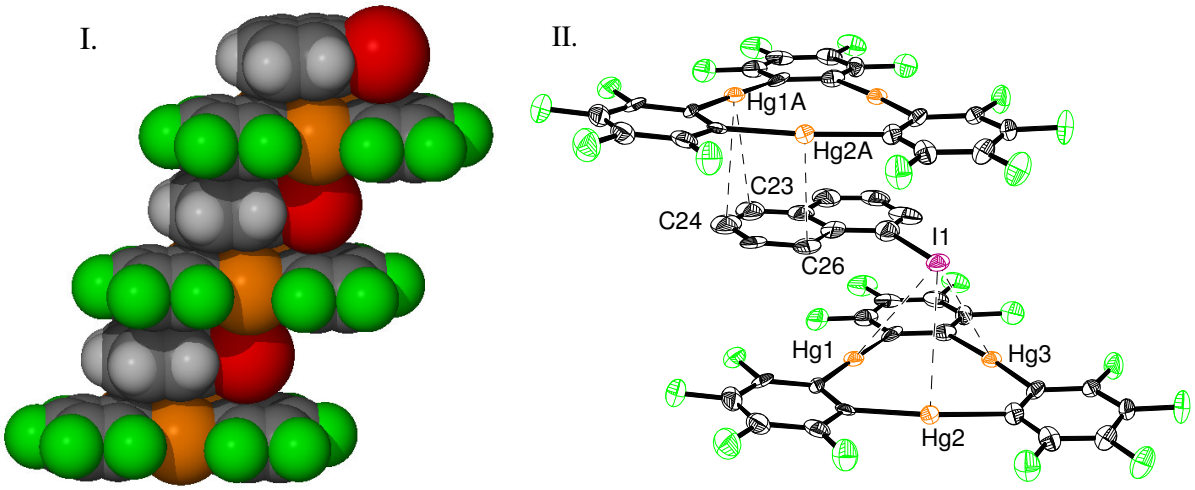

Figure III.6. I. Space-filling model of the binary stacks observed in the extended structure of **15.** II. Molecular structure of **15.** Thermal ellipsoids are at 50%. Hydrogen atoms are omitted for clarity. Significant contacts (Å): I(1)-Hg(1) 3.814(16), I(1)-Hg(2) 3.836(14), I(1)-Hg(3) 3.626(13), C(23)-Hg(1A) 3.325(17), C(24)-Hg(1A) 3.324(17), C(26)-Hg(2A) 3.421 (13).

Table III.1.Crystal data, data collection, and structure refinement for **12**, **13**, **14**, and **15**.

Crystal data	**12**	**13**	**14**	**15**
Formula	$C_{31}H_{11}F_{12}Hg_3N$	$C_{28}H_7ClF_{12}Hg_3$	$C_{28}H_7BrF_{12}Hg_3$	$C_{28}H_7IF_{12}Hg_3$
M_r	1227.18	1208.56	1253.02	1300.01
Crystal size (mm^3)	0.25 x 0.06 x 0.13	0.26 x 0.11 x 0.08	0.27 x 0.10 x 0.07	0.38 x 0.19 x 0.08
Crystal system	Triclinic	Monoclinic	Triclinic	Monoclinic
Space group	P-1	P2(1)/n	P-1	P2(1)/c
A (Å)	6.9082(14)	20.069(4)	7.5525(15)	15.993(3)
B (Å)	21.246(4)	6.8937(14)	15.968(3)	7.5544(15)
C (Å)	21.650(4)	20.918(4)	22.542(5)	22.787(5)
α(°)	64.24(3)		88.35(3)	
β(°)	81.37(3)	115.00(3)	85.00(3)	98.43(3)
γ(°)	82.51(3)		86.94(3)	
V ($Å^3$)	2822.0(10)	2622.9(9)	2703.5(9)	2723.3(9)
Z	4	4	4	4
ρ_{calc} (gcm^{-3})	2.888	3.060	3.079	3.171
μ(Mo K_α)(mm^{-1})	16.386	17.724	18.575	18.107
F(000) (e)	2208	2160	2232	2304
Data Collection				
T/K	110(2)	110(2)	273(2)	110(2)
Scan mode	ω	ω	ω	ω
hkl range	-7→7, -24→24, -24→24	-25→20, -2→9, -25→23	-8→8, -18→18, -25→24	-21→21, -10→9, -30→30
Measured refl.	18526	14488	17952	22349
Unique refl., [R_{int}]	8767 [0.0287]	5366 [0.0325]	8462 [0.0340]	6517 [0.0643]
Refl. used for refinement	8767	5366	8462	6517
Absorption correction	SADABS	SADABS	SADABS	SADABS
T_{min}/T_{max}	0.208681	0.358426	0.295691	0.323027
Refinement				
Refined parameters	847	357	781	397
R1, wR2 [I>2σ(I)]	0.0369, 0.0922	0.0434, 0.1013	0.0433, 0.0993	0.0577, 0.1080
ρ_{fin} (max/min) ($eÅ^{-3}$)	2.952, -2.893	4.119, -2.697	2.264, -1.310	3.821, -2.308

[a] R1 = $(F_o - F_c)/ F_o$.[b] wR2 = $\{[w(F_o^2 - F_c^2)^2]/ [w(F_o^2)^2]\}^{1/2}$; $w = 1/[\sigma^2(F_o^2) + (ap)^2 + bp]$; $p = (F_o^2 + 2F_c^2)/3$; a = 0.0500 (**12**), 0.050 (**13**), 0.012 (**14**), 0.010 (**15**); b = 40.0000 (**12**), 66.0 (**13**), 41.0 (**14**), 141.0 (**15**).

The coexistence of two distinct orientations of **14** and **15** suggests that the interactions responsible for the formation of the adducts are not directional and most certainly dispersive. It also indicates that the Hg···Cl and Hg···Br interactions are not

sufficiently strong to dictate the supramolecular structures of these adducts. This conclusion cannot be extended to the case of **15** in which the Hg···I interaction largely dominates the stacking motif. These structural differences highlight the preference that the soft mercury Lewis acidic sites display for the softer halogen.[69]

III.4. Solid state luminescence and phosphorescence lifetimes

Crystals of **13, 14,** and **15** display green luminescence, the intensity of which is enhanced by lowering the temperature. The emission can be attributed to the phosphorescence of the naphthalene chromophore (Figure III.7). In order to further assess the extent of the heavy atom effects induced by **1** in the solid state, we analyzed the kinetics of the radiative decay. The resulting phosphorescence lifetimes (τ^P) of adducts **13, 14,** and **15** were determined to be 1.557 ms, 1.018 ms, and 0.991 ms at 77 K as measured by Dr. Oussama Elbjeirami of UNT. In comparison, the τ^P of [**1**•naphthalene] had been previously measured at 0.723 ms at 77 K.[7] Although adducts **13, 14,** and **15** show a significant decrease in the radiative decay of the triplet state of free naphthalene (2.3 *seconds* in EPA at 77 K)[85], the triplet lifetimes of the adducts remain in the same order of magnitude as [**1**•naphthalene]. This could be explained by the presence of Hg···halogen interactions which prevent the arene chromophore from interacting with the strong spin orbit coupling provided by **1**.

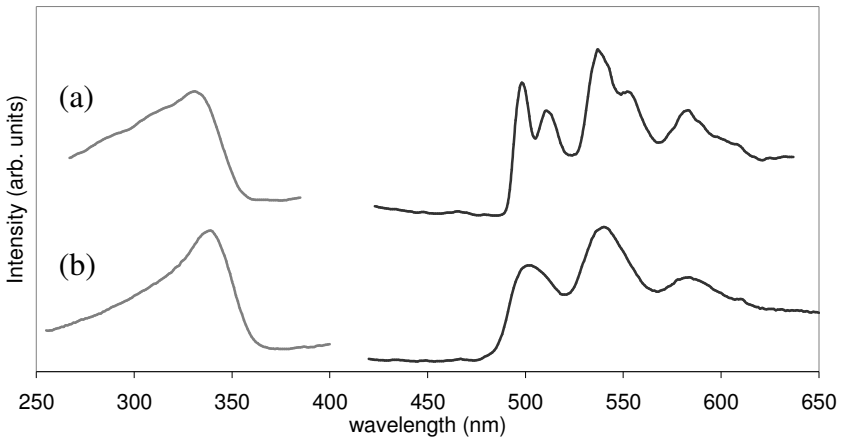

Figure III.7. Photoluminescence excitation and emission spectra of crystals of **13** at 77 K (a) and RT (b). Measurements performed by Dr. Oussama Elbjeirami of UNT.

The solid state photoluminescence spectra of crystalline **11** and **12** are almost identical to those observed for the corresponding frozen CH_2Cl_2 solutions (Figure III.8). The intense emissions of the binary solids are attributed to monomer phosphorescence of *N*-methylindole and *N*-methylcarbazole, respectively.[63,64] In addition, the excitation spectrum of compound **11** features a series of bands that are distinctly red-shifted from the singlet absorption of the unperturbed heterocycle. These bands (Figure III.8, I) most likely correspond to direct $S_0 \rightarrow T_1$ excitation. Nevertheless, the low intensity of these bands suggests that they play little role in the excitation route.

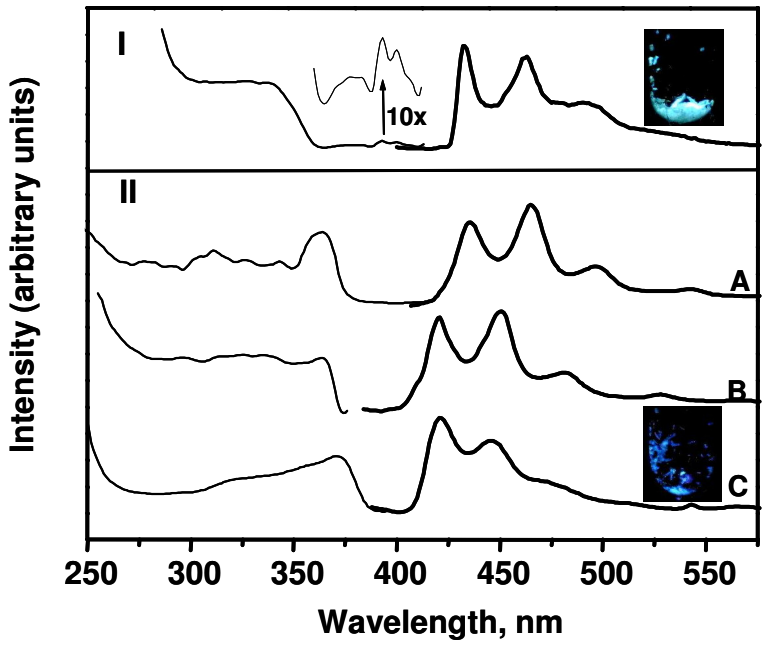

Figure III.8. Photoluminescence excitation and emission spectra of crystals of **11** at 77 K (I) and of **12** (II) in CH_2Cl_2 frozen solution (A), crystals at 77 K (B) and crystals at room temperature (C). Measurements performed by Dr. Oussama Elbjeirami of UNT.

The phosphorescence lifetimes for solid **11** and **12** are below 100 μs at room temperature (RT) and 77 K (Table III.2). The lifetimes at 77 K are shortened by five orders of magnitude, when compared to those of the free *N*-heterocycles in EPA glass[63, 64] (Table III.2). Such a startling reduction highlights the difference that exists in the spin-orbit perturbation provided by an innocent matrix such as EPA and the heavy-atom environment provided by the mercury atoms of **1** in the adducts. We also note that these lifetime reductions are more drastic than those obtained when comparing the triplet emissions of [**1**•biphenyl] or [**1**•naphthalene] to those of the respective free arenes.[6,7] Hence, the dramatic lifetime reduction observed for **11** and **12** most likely results from the synergy of the external mercury and internal nitrogen heavy atom effects. The combination of these effects is also manifested by the appearance of $S_0 \rightarrow T_1$ bands in the excitation spectrum of **11**.

Table III.2. Triplet lifetimes for *N*-heterocycles and their adducts with **1.** Measurements performed by Dr. Oussama Elbjeirami of UNT.

	EPA	Frozen CH_2Cl_2		Frozen CH_2Cl_2	Solid 77 K	Solid RT
N-methylindole	6.7 s	2.1s	**11**	66 μs	57 μs	29 μs
N-methylcarbazole	7.5 s	5.1s	**12**	176 μs	99 μs	49 μs

III.5. Conclusions

The results presented in this chapter indicate that complexes involving **1** and aromatic substrates exist in solution. Their presence is reflected by the intense phosphorescence observed in frozen solutions, and their formation can be readily quantified by fluorescence spectroscopy. The observed fluorescence quenching can be rationalized on the basis of the mercury heavy atom effect, which effectively depopulates the S_1 state. Additionally, these studies clearly demonstrate that **1** forms supramolecular stacks with *N*-heterocycles and 1-halonaphthalenes. These adducts display short Hg···C and Hg···X (where X = N, Cl, Br, or I) interactions which are probably dispersive and/or electrostatic in nature. As a direct result of the mercury external heavy atom effect which provides intense spin orbit coupling to the aromatic substrate, all of these adducts exhibit room temperature phosphorescence of the free arene. In the case of the 1-halonaphthalene adducts, the triplet lifetimes are significantly decreased as compared to the triplet lifetime of free naphthalene; however, the lifetimes of the adducts are similar to [**1**•naphthalene]. Dramatic triplet lifetime reductions have been observed in the case of **11** and **12**, whose lifetimes are below 100 μs. This five order of magnitude reduction of triplet lifetimes likely results from the simultaneous internal nitrogen and external mercury heavy atom effects present in the adducts.

III.6. Experimental details

General. Due to the toxicity of the mercury compounds discussed, extra care was taken at all times to avoid contact with solid, solution, and air-borne particulate mercury compounds. The studies herein were carried out in a well aerated fume hood. Atlantic Microlab, Inc., Norcross, GA, performed the elemental analyses. All commercially available starting materials and solvents were purchased from Aldrich Chemical and VWR, Inc. and used as provided. Compound **1** was prepared according to the published procedure.[70]

Synthesis of [1•*N*-methylindole] (11). Compound **1** (0.020 g, 0.0191 mmol) was dissolved in CH_2Cl_2 (8 mL). In a separate vial, a CH_2Cl_2 (2 mL) solution of *N*-methylindole (0.0025 g, 0.0191 mmol) was prepared. The two solutions were mixed. Upon concentration by slow evaporation of the solvent, crystals of **11** formed in a 93% yield (0.021 g, 0.0191 mmol). mp 285 - 288 ° C (decomp). Anal. Calcd for $C_{27}H_9NF_{12}Hg_3$: C, 27.55; H, 0.77. Found: C, 27.79; H, 0.61.

Synthesis of [1•*N*-methylcarbazole] (12). Compound **1** (0.020 g, 0.0191 mmol) was dissolved in CH_2Cl_2 (8 mL). In a separate vial, *N*-methylcarbazole (0.0035 g, 0.0191 mmol) was dissolved in CH_2Cl_2 (2 mL). The two solutions were mixed. Upon concentration by slow evaporation of the solvent, crystals of **12** formed in a 95% yield (0.0223 g, 0.0191 mmol). mp 314 - 316 °C (decomp.). Anal. Calcd for $C_{31}H_{11}NF_{12}Hg_3$: C, 30.34; H, 0.90. Found: C, 30.45; H, 0.68.

Synthesis of [1•1-chloronaphthalene] (13). Compound **1** (0.020 g, 0.0200 mmol) was dissolved in CH_2Cl_2 (5 mL). In a separate vial, 1-chloronaphthalene (0.0031 g, 0.0200 mmol) was dissolved in CH_2Cl_2 (2 mL). The two solutions were mixed. Upon concentration by slow evaporation of the solvent, crystals of **13** formed in a 99% yield (0.024 g, 0.0200 mmol). mp 292 - 294 ° C (decomp). Anal. Calcd for $C_{28}H_7ClF_{12}Hg_3$: C, 27.72; H, 0.58. Found: C, 27.72; H, 0.58.

Synthesis of [1•1-bromonaphthalene] (14). Compound **1** (0.020 g, 0.0198 mmol) was dissolved in CH_2Cl_2 (5 mL). In a separate vial, 1-bromonaphthalene (0.004 g, 0.0198 mmol) was dissolved in CH_2Cl_2 (2 mL). The two solutions were mixed. Upon

concentration by slow evaporation of the solvent, crystals of **14** formed in a 96% yield (0.0238 g, 0.0198 mmol). mp 302–304 °C (decomp.). Anal. Calcd for $C_{28}H_7BrF_{12}Hg_3$: C, 26.75; H, 0.56. Found: C, 26.94; H, 0.42.

Synthesis of [1•1-iodonaphthalene] (15). Compound **1** (0.020 g, 0.0191 mmol) was dissolved in CH_2Cl_2 (5 mL). In a separate vial, 1-iodonaphthalene (0.004 g, 0.0191 mmol) was dissolved in CH_2Cl_2 (2 mL). The two solutions were mixed. Upon concentration by slow evaporation of the solvent, crystals of **15** formed in a 95% yield (0.019 g, 0.0191 mmol). mp 290 °C (decomp.). Anal. Calcd for $C_{28}H_7IF_{12}Hg_3$: C, 25.77; H, 0.54. Found: C, 26.59; H, 0.67.

Crystal Structure Determinations. X-ray data for **12**, **13**, **14**, and **15** were collected on a Bruker SMART-CCD diffractometer using graphite-monochromated Mo Kα radiation (λ = 0.71073 Å). Specimens of suitable size and quality were selected and glued onto a glass fiber with freshly prepared epoxy resin. The structure was solved by direct methods, which successfully located most of the non-hydrogen atoms. Subsequent refinement on F^2 using the SHELXTL/PC package (version 5.1) allowed location of the remaining non-hydrogen atoms.

Luminescence Titrations. The luminescence spectra were recorded with a SLM/AMINCO, Model 8100 spectrofluorometer equipped with a xenon lamp. Titration experiments were performed by adding aliquots of a CH_2Cl_2 solution of **1** (10 μL of 6.6 x 10^{-3} M) to a quartz cuvette containing 3.00 mL of a 2.18 x 10^{-5} M (*N*-methylcarbazole) CH_2Cl_2 solution of the arene. The sample was excited at $\lambda_{excited}$ = 320 nm, and the emission intensities at λ_{max} = 356 nm were monitored during the titration. The intensities were corrected for dilution and absorption using the following formula: . $I_{corrected} = I_{observed}\left(\frac{V}{V_{initial}}\right)10^{0.5A}$, where V = volume of the sample, V_{intial} = volume of the sample prior to additions, and A = absorbance of the sample at 320 nm.

CHAPTER IV

ENHANCEMENT OF EXTERNAL SPIN-ORBIT COUPLING EFFECTS CAUSED BY METAL-METAL COOPERATIVITY*

IV.1. Introduction

With electron-withdrawing substituents, organomercurials, which do not typically exhibit any significant Lewis acidity, form adducts with a number of neutral and anionic Lewis basic substrates. For instance, bis(pentafluorophenyl)mercury (**2**) complexes bromide and iodide to afford T-shaped anionic complexes in which the anion is terminally ligated to the mercury center.[20] In an analogous fashion, trimeric perfluoro-*ortho*-phenylene mercury (**1**, $[o\text{-}C_6F_4Hg]_3$) complexes halides including bromide and iodide.[21] In both cases, structural studies indicate the occurrence of cooperative effects between the mercury atoms of **1** which simultaneously participate in the binding of the anion. Similar cooperative effects have been observed in adducts involving **1** and a number of neutral or anionic electron rich substrates.[57] As part of our contribution to this general area, we found that **1** interacts with aromatic substrates to form extended binary supramolecules in which **1** and the arene alternate.[28-31,71,72] This approach has now been extended to a number of aromatic substrates[73] including pyrene, naphthalene, and biphenyl.[6,7] The mercury centers of the trinuclear complex approach the π-face of the aromatic substrate and engage in polyhapto secondary Hg–C interactions in the 3.3–3.6 Å range. Because of the extended structures of these solids, each arene is surrounded by six mercury atoms. As a result, the arene experiences an intense spin-orbit perturbation manifested by the $T_1 \rightarrow S_0$ monomer phosphorescence of the arene.

---

* Reproduced in part with permission from *Inorg. Chem.* submitted for publication Burress, C. N.; Elbjeirami, O.; Omary, M. A.; Gabbaï, F. P. "Enhancement of External Heavy Atom Effects Caused by Metal-Metal Cooperativity," Unpublished work copyright 2006 by the American Chemical Society.

Moreover, the triplet excited state lifetimes fall in the ms range, which represents a shortening by 3-4 orders of magnitude in comparison to the lifetimes of the free arene. [7] More drastic lifetime shortenings are observed in the case of aromatic *N*-heterocycles such as *N*-methylcarabazole whose triplet lifetime is reduced by five orders of magnitude when complexed to **1**![71] The intensity of the external heavy-atom effects induced by **1** is unusually high and exceeds that sometimes observed in the presence of internal heavy-atoms. For example, the triplet lifetime of naphthalene in [**1**•naphthalene] (τ^P = 0.987 ms) [7] is distinctly shorter than that of the internal heavy-atom containing 1-iodonaphthalene (τ^P = 2.50 ms).[74] In order to better appreciate the origin of these unusual heavy-atom effects, we have decided to compare the properties of trinuclear **1** to those of its monofunctional analog, **2**. In this chapter, we present a set of structural and solution studies which suggest that cooperative effects are involved in the spin-orbit perturbation that **1** provides to aromatic substrates. We also demonstrate that the mononuclear derivative **2** is a useful supramolecular synthon which readily assembles with various arenes to form room-temperature-phosphorescent supramolecules. These studies are part of our ongoing effort to discover novel materials for organic light emitting diodes.

IV.2. Results and discussion

IV.2.1. Experimental determination of K_{SV}

In order to probe for possible cooperative effects in the binding of naphthalene by the trifunctional Lewis acid **1**, we first studied mixtures of **1** and naphthalene using fluorescence spectroscopy. Incremental addition of the organomercurial **1** to a CH_2Cl_2 solution of naphthalene results in quenching of the fluorescence (Figure IV.1). The observed quenching results from the spin-orbit perturbation provided by the organomercurial to the arene (Scheme IV.1). This perturbation facilitates intersystem crossing leading to the depopulation of the S_1 state of the arene. When the same experiment was repeated with **2**, no fluorescence quenching could be observed. For biphenyl and fluorene, fluorescence quenching experiments could not be carried out

because of a large overlap between the absorption spectrum of the quencher **2** and the excitation spectrum of the arene. The Stern-Volmer constant (K_{SV}), which can be obtained from these experiments, is presented in Scheme IV.1.[62]

Scheme IV.1.

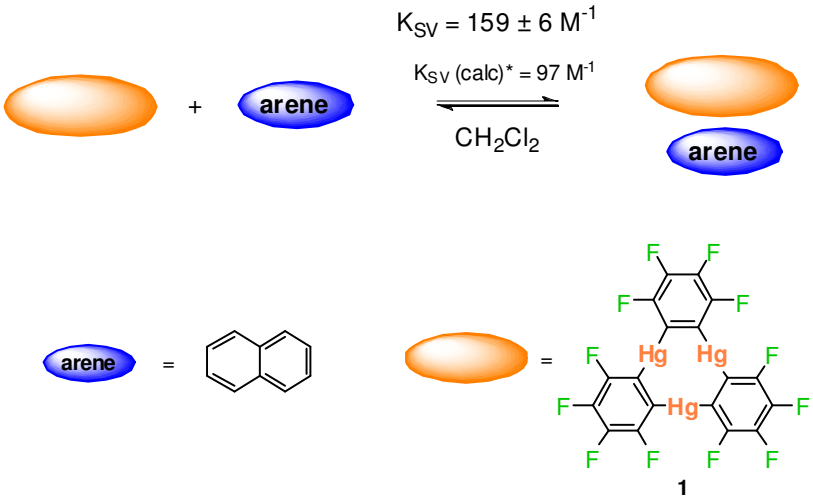

*The collisional quenching K_{sv} value has been calculated using the Smoluchowski equation.

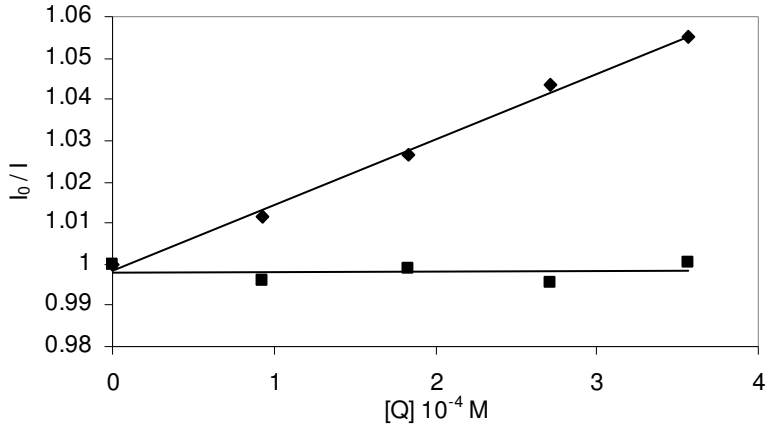

Figure IV.1. Stern-Volmer plots of the fluorescence quenching of naphthalene (7 x 10^{-3} M) in CH_2Cl_2 at ambient temperatures with **1** (♦; 5.7 x 10^{-3} M) and **2** (■; 6 x 10^{-3} M). The samples were excited at 327 nm, and the emission intensities were monitored at 337 nm during the titration.

IV.2.2. Calculation of the diffusion-controlled K_{SV}

The diffusion-controlled bimolecular rate constant, k_0, can be calculated using Smoluchowski's equation:

$$k_0 = \frac{4\pi N}{1000}(R_f + R_q)(D_f + D_q)$$

where R_f and R_q are the molecular radii of the fluorophore and quencher, respectively, D_f and D_q are the diffusion coefficients of the fluorophore and quencher respectively, and N is Avogadro's number.[62] The diffusion coefficients are obtained from the Stokes-Einstein equation:

$$D = \frac{kT}{6\pi\eta R}$$

k = 1.38 x 10^{-16} g cm^2 / s^2

η (CH_2Cl_2) = 4.13 x 10^{-3} g / cm s

where k is the Boltzmann constant ,η is the solvent viscosity, and R is the molecular radius. The resulting k_0 can be used to calculate the expected K_{SV} if the mechanism of quenching results from dynamic or collisional quenching.[62]

$$K_{SV} = k_q \tau_0$$

To determine the bimolecular rate constant for **1** and naphthalene, the molecular radii of **1** and naphthalene were calculated as 4.20 x 10^{-8} cm^{-1} and 3.47 x 10^{-8} cm^{-1}, respectively, as derived from the crystallographic volumes of each component.[75,76] Assuming the collision radius to be the sum of the two components molecular radii, the resulting k_0 was determined to be 1.61 x $10^{10} M^{-1}s^{-1}$. In order to calculate the theoretical K_{SV}, the fluorescence lifetime of naphthalene was measured in CH_2Cl_2 prior to addition of the quencher. By multiplying the measured fluorescence lifetime of 6.0 ns by the calculated k_0, the theoretical K_{SV} value of 97 M^{-1} was found.

IV.2.3. Discussion of experimental and calculated K_{SV}

The experimental K_{SV} constant of naphthalene quenched by **1** (159 ± 6 M^{-1}) is higher than the value of 97 M^{-1} which can be theoretically predicted from the singlet lifetime of the chromophore and the collisional frequency. In turn, this Stern-Volmer constant suggests that the observed quenching is static rather than dynamic (Scheme IV.1). The occurrence of static quenching is corroborated by the values of the fluorescence lifetimes, measured by Dr. Oussama Elbjeirami of UNT, which remain constant throughout the naphthalene titration with **1** as a quencher (Figure IV.1).

The high quenching efficiency of **1** may result from two factors. As a first factor, it can be proposed that **1** possess an increased affinity for naphthalene possibly originating from the planarity of the molecule, which facilitates the approach and complexation of the aromatic substrate. Although **2** is able to access a planar conformation (*vide infra*), available crystal structures indicate that the two pentafluorophenyl rings prefer to be twisted,[77] which would hinder the approach and complexation of flat aromatic substrates. As a second factor, we can also invoke the

occurrence of more acute external heavy atom effects in the case of **1** which contains three rather than one mercury atom. In order to further assess the spin orbit coupling perturbation provided by **1** and **2**, we turned our attention to the study of solid adducts.

IV.2.4. Synthesis and structure of the adducts

The coordination chemistry of **2** is much less developed than that of **1**. In fact, only a handful of adducts involving **2** have been thus far reported. These adducts involve Lewis basic substrates containing nitrogen,[78] phosphorus, and arsenic[79] as donor atoms. To our knowledge, however, adducts involving unsubstituted arenes have remained unknown. Encouraged by the foregoing fluorescence quenching experiments which indicate the formation of ground state complexes involving **2** and naphthalene, biphenyl, or fluorene, we decided to attempt the solid state isolation of the complexes. Combination of **2** with naphthalene, biphenyl or fluorene in CH_2Cl_2 followed by slow evaporation of the solvent leads to the crystallization of [**2**•naphthalene], [**2**•biphenyl], and [**2**•fluorene] whose composition has been confirmed by elemental analysis. These adducts, which are air stable and melt at 184 ºC, 169 ºC, and 204 ºC for [**2**•naphthalene], [**2**•biphenyl], and [**2**•fluorene], respectively, have been studied by single crystal X-ray analysis (Table IV.1). In the solid state, these adducts form extended binary stacks where molecules of **2** alternate with the arene (Figure IV.2). In all three adducts, there are no unusual intramolecular bond distances and angles in the structure of the individual components. The closest known analog of such binary compounds is an adduct involving **2** and 2,2'-dipyridyl diselenide.[80] This adduct forms extended stacks that are supported by Hg–Se interactions, rather than Hg–C interactions.

Table IV.1. Crystal data, data collection, and structure refinement for [**2**•naphthalene], [**2**•biphenyl], [**2**•fluorene], and [**1**•fluorene]

Crystal data	[**2**•naphthalene]	[**2**•biphenyl]	[**2**•fluorene]	[**1**•fluorene]
Formula	$C_{22}H_8F_{10}Hg$	$C_{24}H_{10}F_{10}Hg$	$C_{25}H_{10}F_{10}Hg$	$C_{31}H_{10}F_{12}Hg_3$
M_r	662.87	688.91	700.92	2424.32
Crystal size (mm^3)	0.23 x 0.07 x 0.05	0.23 x 0.18 x 0.04	0.45 x 0.11 x 0.03	0.35 x 0.20 x 0.05
Crystal system	Monoclinic	Triclinic	Triclinic	Monoclinic
Space group	P2(1)/c	P-1	P-1	P2(1)/c
a (Å)	9.948(2)	6.3754(13)	7.0988(14)	7.0469(14)
b (Å)	6.8142(14)	8.0460(16)	8.1504(16)	44.805(9)
c (Å)	14.627(3)	10.918(2)	10.740(2)	17.337(4)
α(°)		90.13(3)	91.37(3)	
β(°)	105.33(3)°	102.04(3)	107.29(3)	91.36(3)
γ(°)		102.75(3)	108.90(3)	
V ($Å^3$)	956.3(3)	533.54(19)	556.34(19)	5472.3(19)
Z	2	1	1	4
ρ_{calc} (gcm^{-3})	2.302	2.144	2.092	2.943
μ(Mo $K\alpha$)(mm^{-1})	8.151	7.309	7.012	16.897
F(000) (e)	620	324	330	4352
Data Collection				
T/K	110(2)	273(2)	273(2)	110(2)
Scan mode	ω	ω	ω	ω
hkl range	-12→12, -8→8, -18→18	-8→8, -10→10, -14→14	-8→8, -9→9, -12→14	-7→7, -49→49, -18→19
Measured refl.	7171	4739	5052	34002
Unique refl., [R_{int}]	1873 [0.0272]	2498 [0.0297]	2634 [0.0571]	7851 [0.0305]
Refl. used for refinement	1873	2498	2634	7851
Absorption correction	SADABS	SADABS	SADABS	SADABS
T_{min}/T_{max}	0.720398	0.660439	0.2275	0.286218
Refinement				
Refined parameters	154	165	119	829
R1, wR2 [I>2σ(I)]	0.0280, 0.0754	0.0323, 0.0610	0.0457, 0.0991	0.0442, 0.1004
ρ_{fin} (max/min) ($eÅ^{-3}$)	1.913, -0.780	0.541, -0.497	0.615, -0.630	3.546, -1.222

[a] $R1 = (F_o - F_c)/ F_o$. [b] $wR2 = \{[w(F_o^2 - F_c^2)^2]/ [w(F_o^2)^2]\}^{1/2}$; $w = 1/[\sigma^2(F_o^2) + (ap)^2 + bp]$; $p = (F_o^2 + 2F_c^2)/3$; *a* = 0.0500 (**12**), 0.050 (**13**), 0.012 (**14**), 0.010 (**15**); *b* = 40.0000 (**12**), 66.0 (**13**), 41.0 (**14**), 141.0 (**15**).

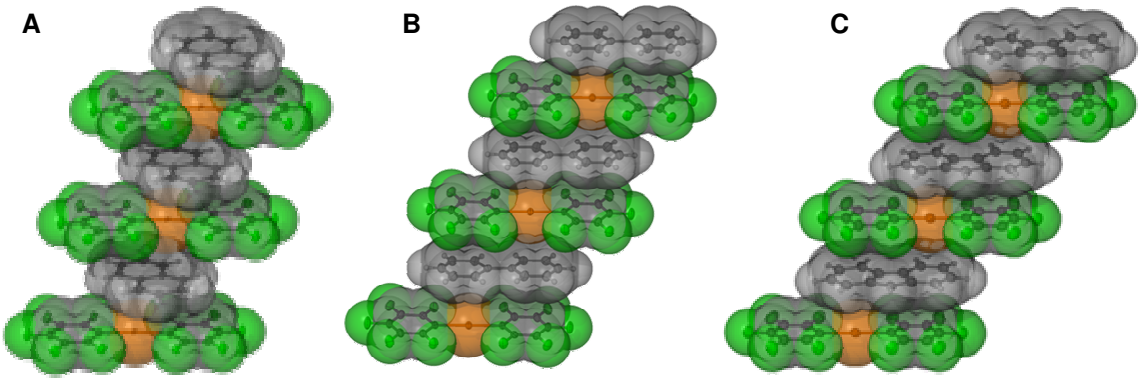

Figure IV.2. ORTEP view with transparent van der Waals spheres of a stack in each of the structures of [**2**•naphthalene] (A), [**2**•biphenyl] (B), and [**2**•fluorene] (C).

Adduct [**2**•naphthalene] crystallizes in the monoclinic space group $P(2)_1/c$ with half a molecule of **2** and half a molecule of naphthalene in the asymmetric unit (Figure IV.2A, Figure IV.3). The naphthalene molecule is weakly π–coordinated to the mercury centers of two neighboring molecules of **2** (Figure IV.2A). The two mercury centers Hg(1) and Hg(1A) effectively sandwich the naphthalene molecule via η^3-interactions involving the carbon atoms C(7), C(10), and C(11) and their symmetry related equivalents C(7A), C(10A), and C(11A) (Figure IV.3). These Hg–C interactions fall in the range 3.21–3.49 Å, which are some of the shortest distances observed in arene adducts of organomercurials[26] and are within the van der Waals radii for Hg (r_{vdw} = 1.73–2.00 Å)[65] and $C_{aromatic}$ (r_{vdw} = 1.7 Å)[66] (Figure IV.3). As a result of these interactions, the naphthalene molecule is slightly tilted with respect to the plane containing **2** with which it forms an angle of 4.6°. We also note that the naphthalene does not engage in arene–perfluoroarene interactions with the pentafluorophenyl groups

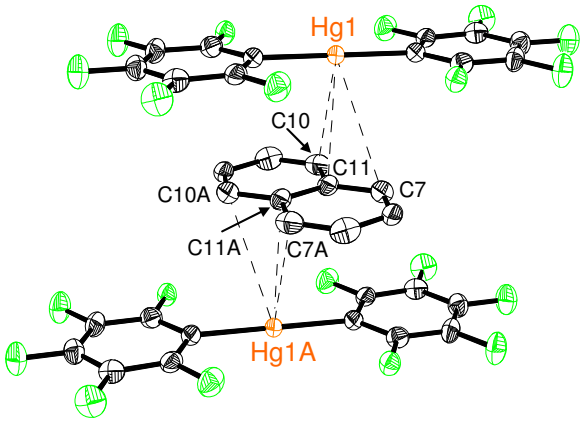

Figure IV.3. ORTEP view (50% ellipsoid) of a portion of a stack in the structure of [**2**•naphthalene]. Representative intermolecular distances (Å): Hg(1)-C(7) 3.49, Hg(1)-C(10) 3.27, Hg(1)-C(11) 3.21.

of **2**. Adduct [**2**•biphenyl] crystallizes in the triclinic space group *P*-1 with half a molecule of **2** and half a molecule of biphenyl in the asymmetric unit (Figure IV.4). Unlike in [**2**•naphthalene], one of the pentafluorophenyl groups of the organomercurial form an arene-perfluoroarene interaction with the biphenyl molecules (Figure IV.2B). The presence of this interaction is supported by the short distance of 3.65 Å separating the centroids of the phenyl ring containing C(8) and pentafluorophenyl ring containing C(1B) (Figure IV.4). Cohesion of the components is further assisted by a secondary mercury–π interaction of 3.51 Å involving Hg(1) and C(8) and their symmetry equivalent atoms Hg(1A) and C(8A). As in [**2**•naphthalene], the biphenyl molecule is slightly tilted with respect to the plane containing **2** with which it forms an angle of 4.4°. Both components are planar; the biphenyl occupies a crystallographic inversion center resulting in a Ph–Ph dihedral angle of 0°. This situation differs from that observed in the gas phase where the Ph–Ph dihedral angle is close to 44.4°.[81] According to computations, this twisted conformation corresponds to an energy minimum while the flat conformation corresponds to a maximum which is about 2–3 kcal higher in energy.[82]

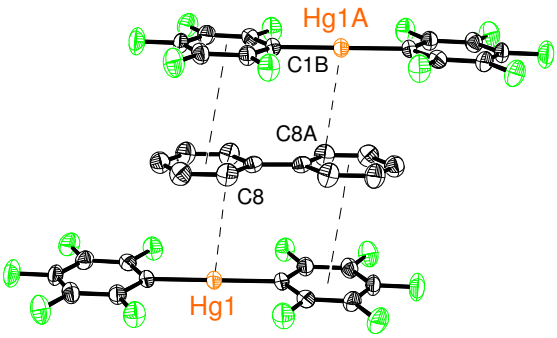

Figure IV.4. ORTEP view (30% ellipsoid) of a portion of a stack in the structure of [**2**•biphenyl]. The representative intermolecular distance Hg(1)-C(8) is 3.51 Å.

It can be argued that supramolecular Hg–C and arene–perfluoroarene interactions are sufficient to overcome the repulsions present in the flat conformation of biphenyl. The observation of planar biphenyl molecules is a rare phenomenon which has only been reported to occur in a few other supramolecular systems.[83] Adduct [**2**•fluorene] crystallizes in the triclinic space group *P*-1 with half a molecule of **2** and half a molecule of fluorene in the asymmetric unit (Figure IV.2C). The fluorene molecule, which is affected by positional disorder, was refined as a rigid unit over two positions of equal occupancy. Although the quality of the refinement is satisfactory, a detailed discussion of the intramolecular interaction is somewhat superfluous. It remains that the distance separating the plane of the fluorene molecule to that of **2** is around 3.5 Å, a distance that is commensurate with the existence of both Hg–C and arene–fluoroarene interactions (Figure IV.2C).

The structure of **2** was computationally optimized using DFT methods (B3LYP, 6-31G for C and F atoms, Stuttgart RSC 1997 ECP for the Hg atom). The mercury adopts a linear geometry, and the two pentafluorophenyl rings are twisted by 90.0°, which can be compared to the value of 59.4° determined crystallographically.[77] Since in adducts [**2**•naphthalene], [**2**•biphenyl], and [**2**•fluorene] the molecule of **2** is essentially planar, we repeated the optimization of **2** with its structure constrained to the D_{2h} point group. The resulting calculated geometry corresponds closely to that observed in

adducts [**2**•naphthalene], [**2**•biphenyl], and [**2**•fluorene]. These DFT calculations were also used to map the electrostatic potential on the electron density surface of **2** (Figure IV.5). Examination of the electrostatic potential map shows that the mercury atom and, to some extent, the core of the pentafluorophenyl ring develop a positive character while the fluorine atoms bear most of the negative charges. The electrostatic potential surface of **2** shows an opposite polarization when compared to those of biphenyl, naphthalene and fluorene which display a negative potential at their centers and a positive potential at the periphery (Figure IV.5). The respective positioning of **2** and the arene in the crystal agrees well with the complementarity of the electrostatic potential surfaces of the two components. In turn, the observed structures suggest that electrostatic interactions are partly responsible for the formation of these adducts. Keeping in mind that mercury is soft and polarizable, the involvement of dispersion forces should not be ruled out and may also contribute to the stability of the adducts.

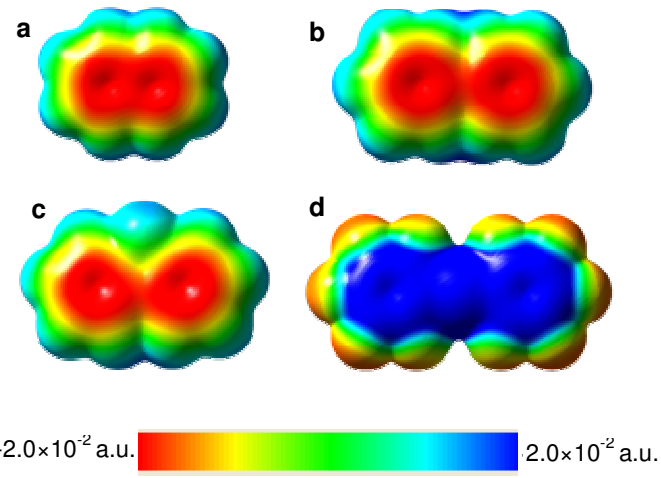

Figure IV.5. Electrostatic potential surfaces of (a) naphthalene, (b) biphenyl, (c) fluorene, and (d) **2**.

We have previously isolated and characterized complexes [**1**•naphthalene] and [**1**•biphenyl], which can be regarded as the trifunctional analogs of [**2**•naphthalene] and [**2**•biphenyl].[6] To prepare the corresponding trifunctional analog of [**2**•fluorene], we have synthesized [**1**•fluorene]. Colorless crystals of [**1**•fluorene] can be easily obtained by slow evaporation of a CH_2Cl_2 solution of **1** and fluorene. Elemental analysis confirmed the 1:1 stoichiometry of the adduct. This adduct crystallizes in the monoclinic space group $P2_1/c$ with two independent molecules of [**1**•fluorene] in the asymmetric unit (Table IV.1). Consequently, there are two crystallographically independent types of stacks which differ by the orientation of the fluorene unit with respect to the trinuclear mercury core of **2** (Figure IV.6). In both stacks, secondary Hg–π interactions contacts are observed between the aromatic rings of the fluorene molecule and the mercury centers of the trinuclear mercury complex. The resulting Hg–C contacts fall in the range 3.27–3.39 Å and are thus within the sum of the van der Waals radii of mercury and carbon. The existence of two orientations in the asymmetric unit indicates that these interactions are not directional but perhaps largely dispersive and/or electrostatic.

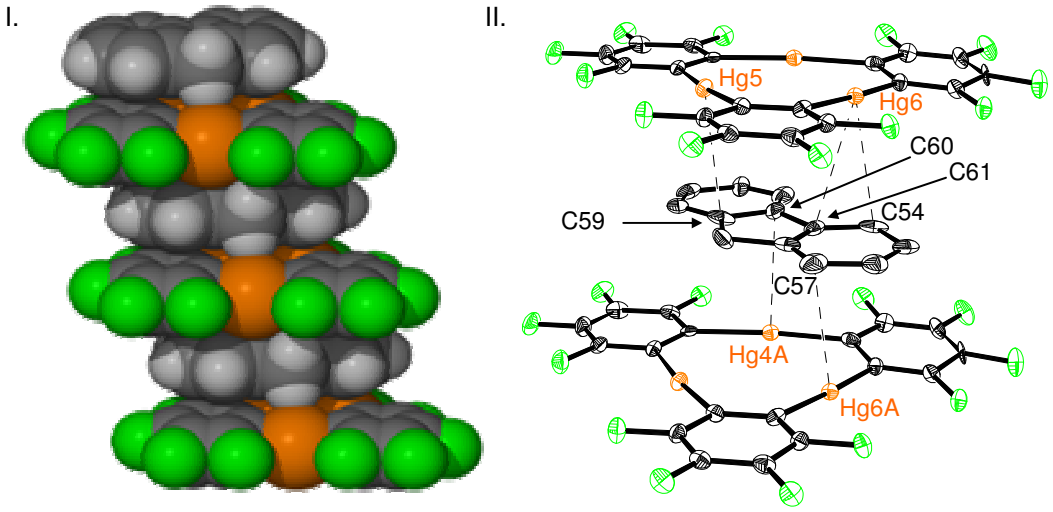

Figure IV.6. Space filling (left) and ORTEP view (50% ellipsoids, right) of a portion of a stack in the structure of [**1**•fluorene]. Only one of the two crystallographically independent stacks is shown. Representative intermolecular distances (Å): Hg(4A)-C(60) 3.29, Hg(5)-C(59) 3.29, Hg(6)-C(54) 3.27, Hg(6)-C(61) 3.39, Hg(6A)-C(57) 3.36.

IV.2.5. Solid state luminescence and triplet lifetimes

All adducts give rise to a very intense photoluminescence in the visible region. The adducts [**2**•biphenyl] and [**2**•fluorene] emit blue light while [**2**•naphthalene] and [**1**•fluorene] give rise to green emission (Figure IV.7). The energy and vibronic progression observed for the emission of [**2**•naphthalene] and [**2**•biphenyl] correspond almost exactly to that observed for the phosphorescence of free naphthalene or biphenyl in an EPA matrix at 77 K.[84,85] Similar observations have been made for arene adducts of the trinuclear complex **1**, which also display intense phosphorescence of the arene.[6,7] As previously proposed for [**1**•naphthalene] and [**1**•biphenyl],[6,7] the observed phosphorescence of [**2**•naphthalene] and [**2**•biphenyl] results from an external mercury heavy-atom effect which affects the photophysical properties of the arene. Taking into account the fact that the mercury atom of **2** is coordinated to the π-faces of the arene,

such an external heavy-atom effect seems to constitute a valid explanation for the observed phosphorescence.

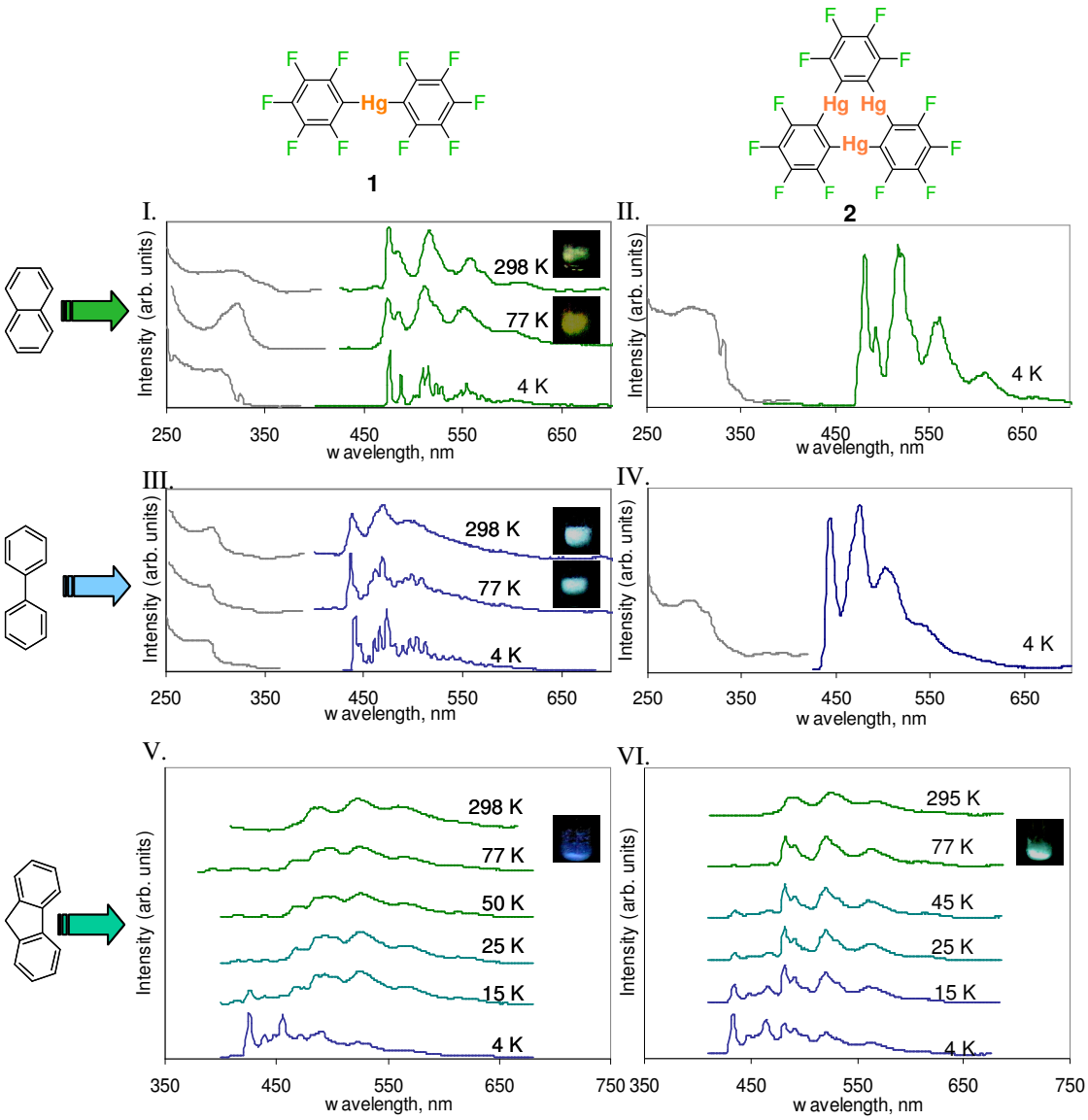

Figure IV.7. Excitation and emission of the solid adduct of [**1**•naphthalene] (I); [**2**•naphthalene] (II) ; [**1**•biphenyl] (III); [**2**•biphenyl] (IV); [**1**•fluorene] (V); and [**2**•fluorene] (VI) at the temperatures noted. Measurements performed by Dr. Oussama Elbjierami of UNT.

In the case of the fluorene adducts, the emission spectrum shows a remarkable temperature dependence. At 4 K, the emission spectra of [**1**•fluorene] and [**2**•fluorene], measured by Dr. Oussama Elbjierami of UNT, show similar energies and vibronic features to those reported for pure fluorene.[86] Upon warming, the intensity of the high energy vibronic peaks, especially the 0,0 transition, decreases and ultimately disappears above 15 K for [**2**•fluorene] and 45 K for [**1**•fluorene]. Changes in the vibronic peak distribution are not unusual for molecular systems; factors such as temperature, excitation wavelength, and sample phase or morphology can affect the relative intensities of vibronic transitions. To better compare the extent of the heavy-atom effects induced by **1** and **2** in the solid state, we have measured the kinetics of the radiative decay for each adduct. The triplet state lifetimes for [**2**•naphthalene], [**2**•biphenyl], [**2**•fluorene], and [**1**•fluorene] as well as those previously reported[7] are shown for comparison in Table IV.2. In all cases, the lifetimes are shorter than those of the free arenes (2.3, 4.4, and 6.3 *seconds* for naphthalene in EPA glass, biphenyl in EPA glass, and fluorene in ethanol glass, respectively),[84,86] which is indicative of the heavy-atom effect caused by the presence of mercury. However, the arene adducts of the trinuclear organomercurial **1** have triplet state lifetimes that are significantly shorter than those of [**2**•naphthalene], [**2**•biphenyl], and [**2**•fluorene]; see Table IV.2. The $(\tau^P)^{-1}$ values measured at 77 K or RT represent the sum of the radiative (k_r) and non-radiative (k_{nr}) decay rate constants, which cannot be readily separated. Hence, we have carried out low–temperature lifetime measurements down to 4 K (Table IV.2). Extrapolation of the low temperature data down to 0 K provides estimation for the k_r values, which are presented in Table IV.2. In all cases, arene adducts of **1** have a higher k_r than the corresponding arene adducts of **2**. The ratios k_r([**1**•arene])/k_r([**2**•arene]) are almost equal (4.8 for naphthalene; 5.5 for biphenyl, and 5.2 for fluorene). The drastic shortening in the lifetimes and increase in k_r values for arene adducts of **1** vs. **2** demonstrate cooperative effects between the three mercury centers in **1** that lead to more efficient phosphorescence via external heavy-atom effects. These cooperative effects are even more drastic than those known for organic systems with internal heavy-atom effects. For

example, the τ^P value changes from 17.6 ms to 4.96 ms on going from 2-bromonaphthalene to 1,2,4-tribromonaphthalene in EPA glass.[87]

Table IV.2. Radiative rate constants and triplet lifetimes for naphthalene, biphenyl, and fluorene adducts of **1** and **2.** Measurements performed by Dr. Oussama Elbjierami of UNT.

	k_r/s^{-1}	τ_{4K}/ms	τ_{77K} /ms	τ_{RT} /ms
[**2**•naphthalene]	139	7.71	5.15	3.11
[**2**•biphenyl]	209	4.77	2.96	2.60
[**2**•fluorene]	264	3.32	1.56	0.976
[**1**•naphthalene]	669	1.42	0.985 *	0.712 *
[**1**•biphenyl]	1091	0.891	0.337 *	0.454 *
[**1**•fluorene]	1469	0.657	0.436	0.265

* Values taken from ref 7

In order to provide a tentative explanation for these observations, we propose the following analysis. It has been previously explained that external heavy-atom effects result from the formation of a transient charge transfer complex between a chromophore and a heavy-atom containing compound.[8,88] An extrapolation of this idea to the supramolecular adducts discussed in this study lead us to invoke transient transfer of charge from the arene to the organomercurial as a mechanism for the mediation of spin–orbit coupling. Elaborating on the charge transfer nature of external heavy-atom effects, we propose that the accepting orbital is the LUMO of the organomercurial. Unlike in **2** where the LUMO bears the contribution of a single mercury 6p orbital, the LUMO of **1** results from the mixing of three mercury 6p orbitals and is therefore expected to have a lower energy.[89] In turn, the LUMO of **1** may in fact be energetically more accessible, which favors the transient transfer of charge from the arene to the organomercurial. In other words, the proximity of the three mercury centers serves to enhance the Lewis acidity of **1** which becomes a better acceptor and a more effective heavy-atom effect inducer.

IV.3. Concluding remarks

The results reported in these studies indicate that simple mononuclear organomercurials such as **2** readily assemble with arenes to form room temperature phosphorescent supramolecules with short triplet lifetimes. Keeping in mind that **2** can be prepared in one step from simple starting materials, these results are important and may provide new routes to luminescent materials, a venue that we are currently investigating. The second important aspect of this work concerns the fluorescence quenching studies, which allow us to witness the complexation of the arene by the electron deficient organomercurial in solution. These studies clearly demonstrate that the trinuclear derivative **1** forms more stable complexes with arenes. As previously proposed, the planarity of the molecule as well as its electron deficiency and polarizability are most likely responsible for this unusual chemical trait.[28] Last but not least, the photophysical results reported herein support the occurrence of cooperative effects between the Lewis acidic mercury centers. These cooperative effects lead to an increase in the acceptor properties of the trinuclear derivative **1** and make it a more efficient external heavy-atom effect inducer.

IV.4. Experimental details

General. *Warning! Due to the toxicity of the mercury compounds discussed, extra care was taken at all times to avoid contact with solid, solution, and air-borne particulate mercury compounds.* The studies herein were carried out in a well aerated fume hood. Atlantic Microlab, Inc., Norcross, GA, performed the elemental analyses. All commercially available starting materials and solvents were purchased from Aldrich Chemical and VWR, Inc. and used as provided. Compounds **1** and **2** were prepared according to published procedures.[70,90]

Synthesis of Adducts. All compounds were prepared by mixing compound **1** or **2** with the corresponding arene in CH_2Cl_2 (5–10 mL). Crystals formed upon slow evaporation of the solvent. Reagent quantities, yields, elemental analysis results, and melting points are provided for each adduct hereafter.

[**2**•naphthalene]: **2** (0.020 g, 0.0374 mmol), naphthalene (0.0048 g, 0.0374 mmol). Yield: 0.0184 g, 92%. Anal. Calcd for $C_{22}H_8F_{10}Hg$: C, 39.86; H, 1.22. Found: C, 39.89; H, 1.05. mp 184 °C.

[**2**•biphenyl]: **2** (0.020 g, 0.0374 mmol), biphenyl (0.0058 g, 0. 0374 mmol). Yield: 0.0252 g, 98%. Anal. Calcd for $C_{24}H_{10}F_{10}Hg$: C, 41.84; H, 1.46. Found: C, 41.63; H, 1.29. mp 169 °C.

[**2**•fluorene]: **2** (0.020 g, 0.0374 mmol), fluorene (0.0062 g, 0.0374 mmol). Yield: 0.0249 g, 95%. Anal. Calcd for $C_{25}H_{10}F_{10}Hg$: C, 42.84; H, 1.44. Found: C, 42.76; H, 1.24. mp 204 °C.

[**1**•fluorene]: **1** (0.020 g, 0.0191 mmol), fluorene (0.0030 g, 0.0191 mmol). Yield: 0.022 g, 96%. Anal. Calcd for $C_{31}H_{10}F_{12}Hg_3$: C, 30.71; H, 0.83. Found: C, 30.97; H, 0.76. mp 312 °C(decomp).

Crystal Structure Determinations. X-ray data for [**2**•naphthalene], [**2**•biphenyl], [**2**•fluorene], and [**1**•fluorene] were collected on a Bruker SMART-CCD diffractometer using graphite-monochromated Mo Kα radiation (λ = 0.71073 Å). Specimens of suitable size and quality were selected and glued onto a glass fiber with freshly prepared epoxy resin. The structure was solved by direct methods, which successfully located most of the non-hydrogen atoms. Subsequent refinement on F^2 using the SHELXTL/PC package (version 6.1) allowed location of the remaining non-hydrogen atoms.

Theoretical Calculations. The theoretical calculations have been carried out with the Gaussian 98[91] implementations of B3LYP [Becke three-parameter exchange functional (B3)[92] and the Lee-Yang-Parr correlation functional (LYP)[93]] density functional theory (DFT).[94] The DFT calculations used the default SCF convergence for geometry optimizations (10^{-8}). The 6-31G basis sets of Pople and co-workers[95] were used for all the carbon, hydrogen, and fluorine atoms, and the Stuttgart RSC 1997 ECP[96] basis sets were used for the mercury atom. The structure was constrained to D_{2h} symmetry and then fully optimized, and analytical frequency calculations were

performed to ensure either a minimum or a first-order saddle point was achieved. The electrostatic potential surface calculations were carried out on the optimized structure.

Luminescence Titrations. The solution luminescence spectra were recorded with a SLM/AMINCO, Model 8100 spectrofluorometer equipped with a xenon lamp. Titration experiments were performed by adding aliquots of a CH_2Cl_2 solution of **1** (50 μL of 5.7 x 10^{-3} M) or **2** (50 μL of 6 x 10^{-3} M) to a quartz cuvette containing 3.00 mL of a 7 x 10^{-3} M CH_2Cl_2 solution of naphthalene. The samples were excited at 327 nm and the emission intensities at λ_{max} = 337 nm were monitored during the titration. The intensities were corrected for dilution and absorption using the following formula: $I_{corrected} = I_{observed}\left(\frac{V}{V_{initial}}\right)10^{0.5A}$ where V = volume of the sample, V_{intial} = volume of the sample prior to additions, and A = absorbance of the sample at 337 nm.

Photophysical Measurements. Completed by Dr. El-bjeriami from the Omary group at the University of North Texas. Steady-state luminescence spectra were acquired with a PTI QuantaMaster Model QM-4 scanning spectrofluorometer. The excitation and emission spectra were corrected for the wavelength-dependent lamp intensity and detector response, respectively. Lifetime data were acquired using fluorescence and phosphorescence subsystem add-ons to the PTI instrument. The pulsed excitation source was generated using the 337.1 nm line of the N_2 laser pumping a freshly prepared 1 × 10^{-2} M solution of the continuum laser dye, Coumarin-540A, in ethanol, the output of which was appropriately tuned and frequency doubled to attain the excitation wavelengths needed based on the luminescence excitation spectra for each compound. Cooling in temperature-dependent measurements for the crystals was achieved using an Oxford optical cryostat, model Optistat CF ST, interfaced with a liquid nitrogen tank.

CHAPTER V

USING MONO- AND TRIFUNCTIONAL ORGANOMERCURIALS AS HEAVY ATOM EFFECT INDUCERS IN LUMINESCENT POLYMERIC MATERIALS

V.1. Introduction

As shown by some of our recent work, trimeric perfluoro-*ortho*-phenylene mercury (**1,** Chart 1) "sticks" to the π-face of aromatic substrates.[6,7,27,28,30,31] In the case of pyrene, naphthalene, and biphenyl, this interaction leads to the formation of extended binary supramolecules in which **1** and the arene alternate.[6,7] In these supramolecules, each arene is surrounded by six mercury atoms that are positioned 3.3-3.6 Å from the arene molecular plane. As a result, the arene experiences a heavy atom effect that is manifested by an intense $T_1 \rightarrow S_0$ monomer phosphorescence.[6,7] Moreover, the triplet excited state lifetimes fall in the *ms* range, which represents shortening by three to four orders of magnitude in comparison to those of the free arene.[7] More drastic shortenings are observed in the case of aromatic *N*-heterocycles such as *N*-methylcarbazole whose triplet lifetimes are reduced by five orders of magnitude when complexed to **1**.[71] Likewise, chapter IV shows the ability of **2** to complex arenes such as naphthalene, biphenyl, and fluorene. With applications in OLEDs as an ultimate goal, we decided to investigate the use of **1** and **2** as heavy atom effect inducers in polymeric materials which are amenable to deposition in thin layers by spin-coating techniques. Due to the affinity of the organomercurials **1** and **2** to aromatic substrates, we studied polymeric organic materials with pendant aromatic groups as complexation sites for **1** and **2**. Specifically, we studied poly(vinyl-2-naphthalene) (PV2N) and poly(vinylcarbazole) (PVK). PVK has been actively employed as a hole transport layer in multilayer OLEDs due to its ease of processing by spin coating and its adequate hole transporting properties.[97] In this chapter, we report a set of solution and solid state photophysical studies concerning the interaction of **1** and **2** with PVK and PV2N.

V.2. Solution studies

The luminescence properties of both PV2N[98] and PVK[99] have been extensively studied, and both polymers exhibit excimer fluorescence emission in solution at room temperature. In addition to excimer fluorescence, PV2N also displays bands at higher energies attributed to monomer fluorescence. Upon addition of **1** to a CH_2Cl_2 solution of PV2N, progressive quenching of both monomer and excimer fluorescence occurs. When the same experiment was repeated with **2**, no fluorescence quenching could be observed. An example of the fluorescence spectra is presented in Figure V.1. Likewise, addition of **1** or **2** to PVK yields progressive quenching of the excimer fluorescence. This quenching is likely the result of the mercury heavy atom effect which effectively depopulates the singlet excimer as well as the S_1 state of the monomer in the case of PV2N. The Stern-Volmer[62] analysis of the fluorescence quenching of the excimer band of PV2N by **1** yields a K_{SV} of 198 ± 30 respectively, indicating interaction of the organomercurial with the polymer in solution (Figure V.2). Monitoring the monomer emission wavelengths resulted in similar Stern-Volmer values. The Stern-Volmer constants for the fluorescence quenching of PVK by **1** or **2** are 2567 ± 91 and 151 ± 15 M^{-1}. In the case of **1**, this is the highest observed K_{SV} we have observed (Figure V.3). The magnitude of these constants along with the constant fluorescence lifetimes during the titrations suggests that the quenching is static in nature. As previously observed for simple arenes, compound **1** displays a greater affinity for the polymer arene chromophores when compared to **2**. Although structural data cannot be inferred from the measured K_{SV} values, the observation of an interaction between the organomercurial and the polymer chain suggests that solution processable techniques can be utilized to generate blends involving the polymer and the organomercurial.

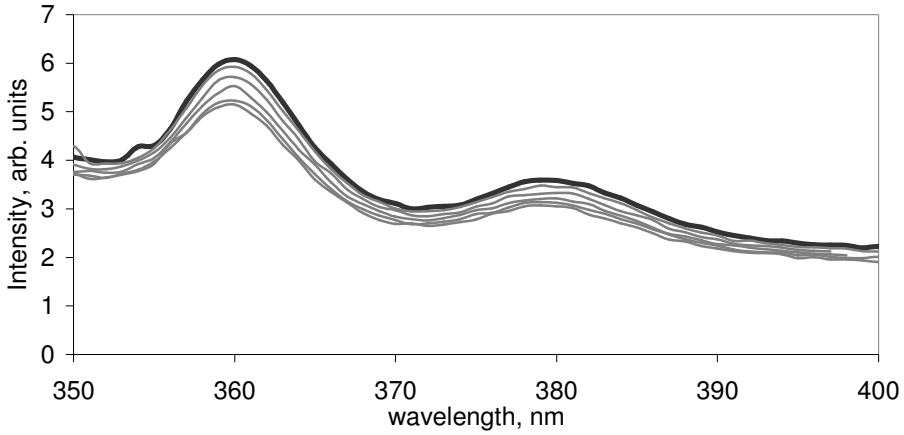

Figure V.1. Fluorescence quenching of PV2N by **1**.

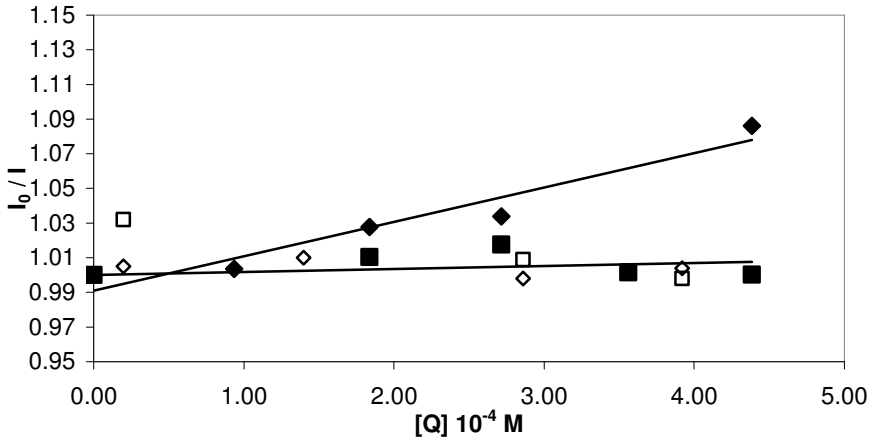

Figure V.2. Stern-Volmer plots of the fluorescence quenching of PV2N (6 x 10^{-4} M) in CH_2Cl_2 at ambient temperatures with **1** (♦(I_0 /I), ◊ (τ_0 / τ); 5.7 x 10^{-3} M) and **2** (■ (I_0 /I), □ (τ_0 / τ); 6 x 10^{-3} M). The samples were excited at 337 nm, and the emission intensities were monitored at 379 nm during the titration. The R^2 values for the decay fit of the lifetime measurements were in the range of 0.98 to 0.99.

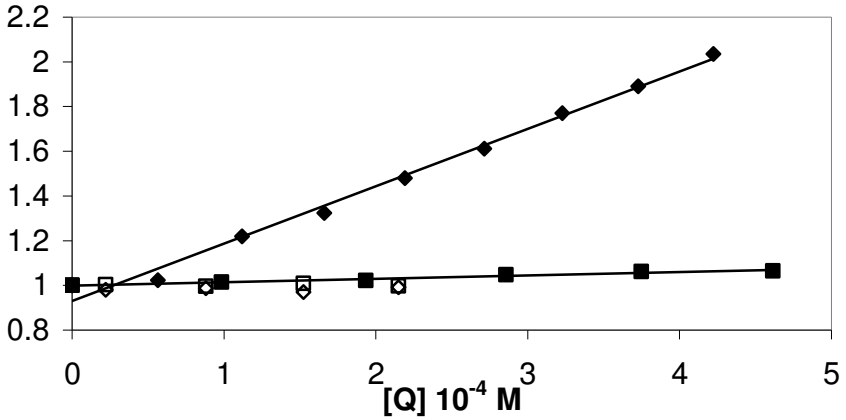

Figure V.3. Stern-Volmer plots of the fluorescence quenching of PVK (2 x 10^{-5} M) in CH_2Cl_2 at ambient temperatures with **1** (♦(I_0 /I), ◊ (τ_0 / τ); 5.7 x 10^{-3} M) and **2** (■ (I_0 /I), □ (τ_0 / τ); 6 x 10^{-3} M). The samples were excited at 334 nm, and the emission intensities were monitored at 383 nm during the titration. The R^2 values for the decay fit of the lifetime measurements were in the range of 0.98 to 0.99.

V.3. *N*-methylcarbazole adduct with **2**

In order to model the interactions between PVK and the organomercurials **1** and **2**, the representative compound *N*-methylcarbazole was utilized. The 1:1 adduct of *N*-methylcarbazole and **1** has been previously reported, and due to the combined internal and heavy atom effects, the triplet lifetime of *N*-methylcarbazole was reduced by five orders of magnitude upon complexation with **1**.[71] In a similar fashion, slow evaporation of a CH_2Cl_2 solution containing *N*-methylcarbazole and **2** yields the crystalline 1:1 adduct **16** as confirmed by elemental analysis. The extended structure shows binary stacks with alternating molecules of *N*-methylcarbazole and **2** (Figure V.4 and Table V.1).

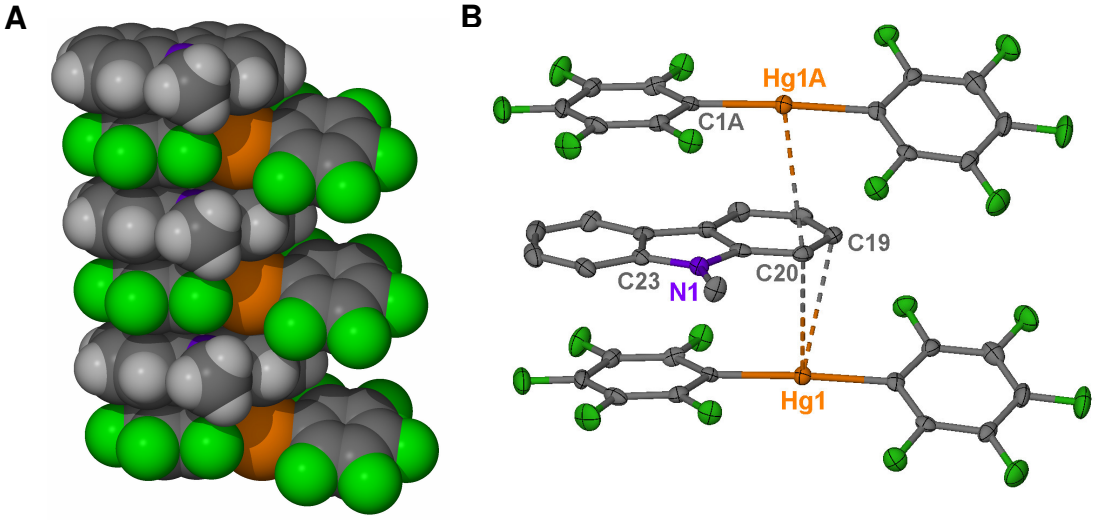

Figure V.4. Space filling (A) and ORTEP view (50% ellipsoid, B) of a stack in the structure of **16**. Representative intermolecular distances (Å): Hg(1)-C(19) 3.27, Hg(1)-C(20) 3.35; Hg(1A)-C(20) 3.44.

Table V.1. Crystal data, data collection, and structure refinement for **16**.

Crystal data	**16**
Formula	$C_{25}H_{11}F_{10}HgN$
M_r	715.94
Crystal size (mm^3)	0.13 x 0.09 x 0.04
Crystal system	Monoclinic
Space group	P2(1)/n
a (Å)	6.6746(6)
b (Å)	43.478(4)
c (Å)	7.8521(7)
α (°)	
β (°)	105.572(2)°
γ (°)	
V ($Å^3$)	2195.0(3)
Z	4
ρ_{calc} (gcm^{-3})	2.166
μ(Mo $K\alpha$)(mm^{-1})	7.112
F(000) (e)	1352
Data Collection	
T/K	120(2)
Scan mode	ω
hkl range	-8→6, -57→54, -10→8
Measured refl.	9405
Unique refl., [R_{int}]	4703, [0.0635]
Refl. used for refinement	4703
Absorption correction	none
T_{min}/T_{max}	
Refinement	
Refined parameters	334
R1, wR2 [I>2σ(I)]	0.0418, 0.0965
ρ_{fin} (max/min) ($eÅ^{-3}$)	3.357, -3.418

[a] $R1 = (F_o - F_c)/ F_o$. [b] $wR2 = \{[w(F_o^2 - F_c^2)^2]/ [w(F_o^2)^2]\}^{1/2}$; $w = 1/[\sigma^2(F_o^2) + (ap)^2 + bp]$; $p = (F_o^2 + 2F_c^2)/3$; $a = 0.0559$; $b = 0.0000$.

The pentafluoroaryl groups of **2** form arene–perfluoroarene interactions with one of the arene rings of *N*-methylcarbazole, as evidenced by the short distance of 3.411 Å separating the centroids of the phenyl ring containing C(23) and the perfluoroaryl ring containing C(1A) (Figure V.4). Cohesion of the two components is further supported by secondary Hg···π interactions with distances ranging from 3.27 to 3.44 Å. While arene adducts of **2** have shown that **2** adopts a planar structure, the dihedral angle between the

rings of the perfluoroaryl groups of **2** is 26° which is, however, lower than that observed for free **2** (59.4°).[100] As opposed to the adduct [**1**•*N*-methylcarbazole] which has short Hg···N interactions[71], the nitrogen atom in adduct **16** is not in close proximity to the mercury center. Unfortunately, the crystals of adduct **16** did not display any luminescence at room temperature or 77 K.

V.4. Luminescence of solid polymer blends with **1** and **2**

Encouraged by the observation of solution interactions, we attempted to isolate solid polymer blends with **1** or **2**. As seen in solution, the solid state luminescence for both PV2N and PVK is typically dominated by prompt excimer fluorescence.[98a,99d, 101]

When a 1:1 CH_2Cl_2 solution of PV2N with **1** or **2** is slowly evaporated, a clear film is obtained which appears uniform in composition. Both compounds **1** and **2** crystallize from CH_2Cl_2, and in the films of PV2N and **1** or **2**, no crystallites of the organomercurials can be observed. For the **1**•PV2N blend, the emission spectrum at 77 K corresponds to the $T_1 \rightarrow S_0$ phosphorescence of naphthalene, which is the monomer chromophore unit in PV2N (Figure V.5A).[85]

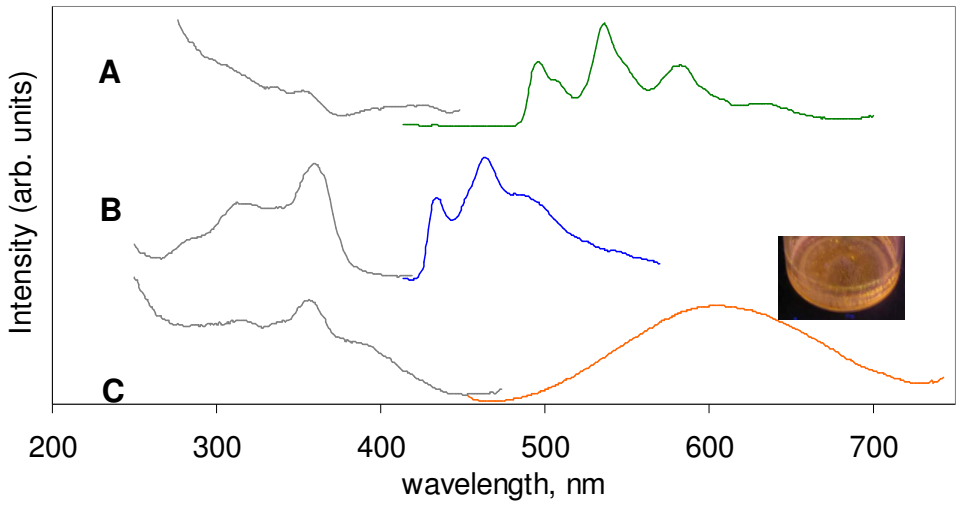

Figure V.5. Photoluminescence excitation and emission spectra of solids **1**•PV2N (A), **2**•PVK (B), and **1**•PVK (C) at 77 K.

Triplet emission has been observed in PV2N films under delayed emission conditions at 77 K, and the emission spectrum consists of an excimer band centered at 570 nm.[101] For frozen solutions of PV2N in MeTHF under similar conditions, the reported triplet emission correlates with the phosphorescence of naphthalene, which could be rationalized by the fluid nature of the solution allowing for the disruption of the necessary excimer overlap.[101] In the **1**•PV2N blend, the observed naphthalene phosphorescence suggests that the organomercurial is breaking the ordering the chromophores in the polymer. At 0.905 ms, the triplet lifetime of the **1**•PV2N blend is significantly shorter than that observed for solid PV2N (150 ms at 77 K)[101] and free naphthalene (2.3 s).[85] Unfortunately the PV2N blend with **2** was not luminescent at room temperature or 77 K, which could be due to the lack of rigidity of the polymer chain and insufficient spin–orbit coupling provided by **2**.

Scheme V.1. Representation of PVK interacting with **1** or **2**.

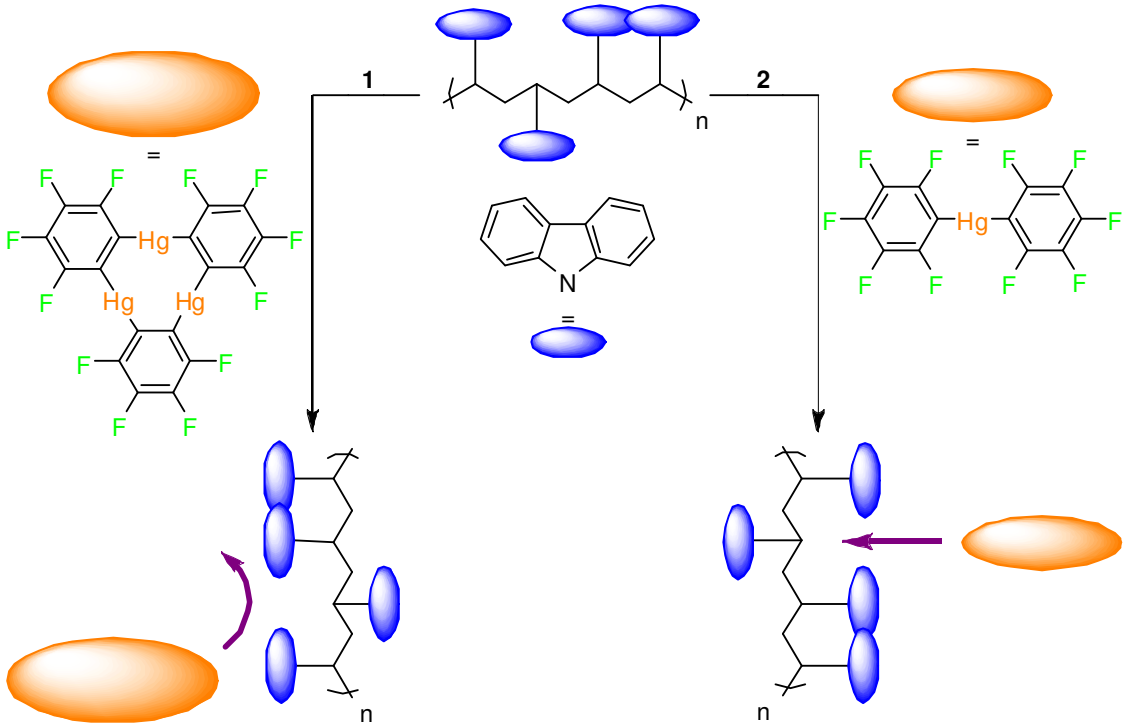

In order to understand how pure PVK behaves without the presence of **1** or **2**, we measured the emission spectra of commercially available PVK and observed a broad, structureless band centered at 423 nm which correspond to excimer fluorescence emission as previously reported.[99d]

In contrast, the blend **2**•PVK, prepared by slowly evaporating a 1:1 CH_2Cl_2 solution of PVK with **2**, displays a blue luminescence at 77 K. The energies and vibrational progression of this emission correspond to the phosphorescence previously reported for frozen solutions of PVK (Figure V.5B) and is attributed to *N*-alkylcarbazole monomer triplet emission.[102] We postulate that the small size of **2** allows the organomercurial to insert itself into the PVK chain thus isolating the chromophore, which then phosphoresces due to the external mercury heavy atom effect provided by **2** (Scheme V.1).

However the blend of organomercurial **1** and PVK presents quite different photoluminescent behavior. Rather than the usual blue fluorescence observed for pure PVK, **1**•PVK emits an intense orange color (Figure V.5C). The emission spectrum of this blend exhibits a broad, structureless band centered at 600 nm. With a measured lifetime of 18.15 μs, this band likely arises from a triplet emission. Using delayed emission conditions at 77 K, the triplet emission of solid PVK has been previously reported, and the spectrum displays an excimer band centered at 500 nm.[103]

The red-shifted band in **1**•PVK more than likely originates from a long range ordering of singlet excitons which, upon interaction with **1**, undergoes intersystem spin crossing to the triplet exciton. This triplet exciton then radiatively relaxes to the ground state.[104] In fact, it is highly probable that **1** acts as an energy "sink" for the moving singlet excitons.

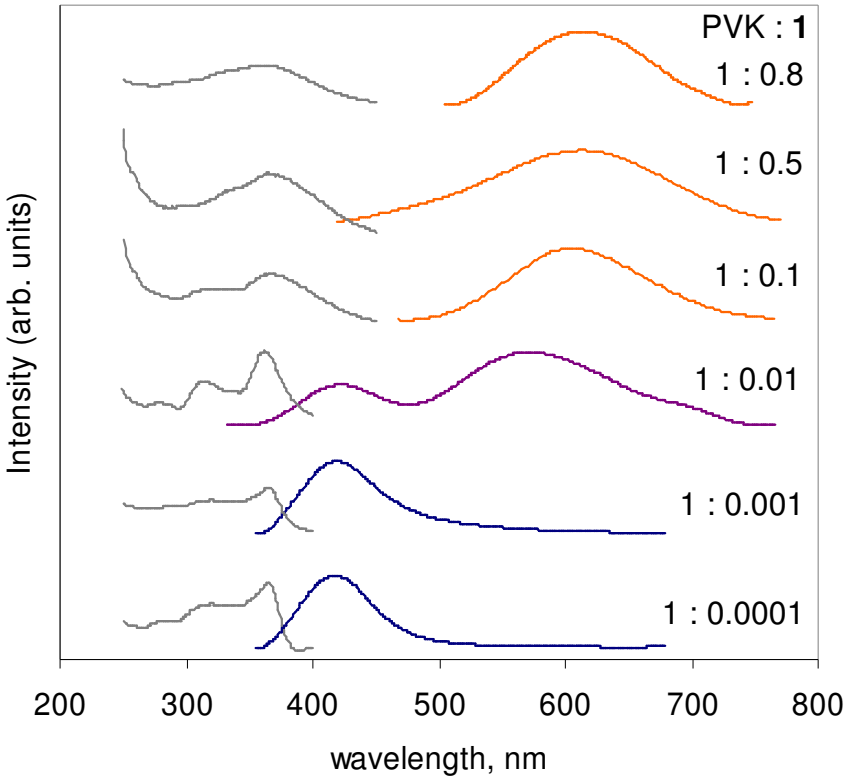

Figure V.6. Excitation and emission spectra of submolar blends of PVK and **1** at room temperature measured by Dr. El-bjeriami of UNT.

In order to investigate the length of the excitons and hence the number of chromophores involved, submolar blends of PVK and **1** were prepared using a similar approach mentioned above and their photoluminescence recorded. The PVK monomer unit : **1** ratio was varied from 1:1 to 1:0.0001, and the results are shown in Figure V.6. As seen in pure PVK, the blends 1:0.0001 and 1:0.001 display only blue excimer fluorescence, further evidenced by the lifetime measurement of 22 ns. Upon addition of 1% of **1**, the orange band centered at 600 nm, with a similar lifetime (18.36 μs) as seen in the 1:1 blend, appears along with the fluorescence band. Due to the presence of both the orange and blue bands, the blend 1:0.01 exhibits white emission. At a doping level of 10%, fluorescence is completely quenched, only the orange emission is observed. This suggests that the length of the extended exciton is between 10 and 100

chromophores along the polymer chain. PVK singlet excitons spanning up to 400 carbazole units have been previously reported, which is somewhat longer than the excitons measured in the **1**•PVK blend.[105] However, the structure of the blend could be considered altered due to the presence of bulky **1** as compared to the pure PVK solid, which might account for the up to one order of magnitude discrepancy in exciton lengths.

V.5. Conclusions

In recent reports dealing with phosphorescent OLEDs, Thompson and others have investigated heavy metal complexes as dopants in organic host materials, and these dopants are the triplet emitters of the OLED.[106,107] Our approach, however, focuses on generating a composite material where the dopant facilitates the emission of the host matrix itself. Both PV2N and PVK interact with **1** and **2** in solution as evidenced by fluorescence spectroscopy. The solid blend of **1**•PV2N displays the green phosphorescence of the monomer, naphthalene, at low temperatures, which suggests that the organomercurial is disrupting the long range ordering of the polymer. For the **2**•PVK blend, blue phosphorescence, attributed to the *N*-alkylcarbazole monomer, is observed due to the smaller size of **2** allowing for insertion in the polymer chain. On the other hand, the large organomercurial **1** is excluded from interaction with the chromophore of PVK. In fact, the **1**•PVK blend displays intense orange emission attributed to phosphorescence of an extended excimer comprising 10 to 100 chromophores. We have shown that in the case of PVK a small doping percentage (1%) of **1** can give rise to white emission, while larger percentages of **1** result in bright room temperature orange phosphorescence. Current efforts are focused on incorporating these composites in light emitting devices.

V.6. Experimental details

General. Due to the toxicity of the mercury compounds discussed, extra care was taken at all times to avoid contact with solid, solution, and air-borne particulate mercury compounds. The studies herein were carried out in a well aerated fume hood.

Atlantic Microlab, Inc., Norcross, GA, performed the elemental analyses. All commercially available starting materials and solvents were purchased from Aldrich Chemical and VWR, Inc. and used as provided. Compounds **1** and **2** were prepared according to the published procedure.[70,90] The fluorescence spectra were recorded with a SLM/AMINCO, Model 8100 spectrofluorometer equipped with a xenon lamp.

Synthesis of·[2•*N*-methylcarbazole] (16). Compound **2** (0.020 g, 0.037 mmol) was dissolved in CH_2Cl_2 (3 mL). In a separate vial, a CH_2Cl_2 solution of *N*-methylcarbazole (0.006 g, 0.037 mmol) was prepared. The two solutions were mixed. Upon concentration by slow evaporation of the solvent, crystals of **16** formed in 98% yield (0.0247 g, 0.037 mmol). mp 228 °C. Anal. Calcd for $C_{31}H_{10}F_{12}Hg_3$: C, 30.71; H, 0.83. Found: C, 30.97; H, 0.76.

Synthesis of Polymer Adducts. All compounds were prepared by mixing compound **1** or **2** with the corresponding polymer in CH_2Cl_2 (5–10 mL). Films formed upon evaporation of the solvent. Reagent quantities, yields, and melting points are provided for each adduct hereafter.

[**1•PV2N]: 1** (0.020 g, 0.019 mmol); PV2N (0.003 g, 0.019 mmol), 99% (0.023 g), mp 310 °C.

[**2•PV2N]: 2** (0.020 g, 0.037 mmol); PV2N (0.006 g, 0.037 mmol), 90% (0.023 g), mp 298°C.

[**1•PVK]:** 1:1–**1** (0.020 g, 0.019 mmol); PVK (0.003 g, 0.019 mmol), 98% (0.022 g) mp 345 °C.

0.8:1–**1** (0.025 g, 0.024 mmol); PVK (0.005 g, 0.0301 mmol), 97% (0.029 g), mp 348°C.

0.5:1–**1** (0.016 g, 0.015 mmol); PVK (0.005 g, 0.0301 mmol), 99% (0.021 g), mp 343°C.

0.1:1–**1** (0.003 g, 0.003 mmol); PVK (0.005 g, 0.0301 mmol), 99% (0.008 g), mp 345°C.

0.01:1–**1** (0.006 g, 0.006 mmol); PVK (0.100 g, 0.601 mmol), 97% (0.103 g), mp 322°C

0.001:1–**1** (0.003 g, 0.003 mmol); PVK (0.500 g, 3.01 mmol), 98% (0.492 g), mp 321°C

0.0001:1–**1** (0.003 g, 0.003 mmol); PVK (4.98 g, 30.0 mmol), 96% (4.78 g), mp 324°C

[**2•PVK]: 2** (0.020 g, 0.0374 mmol); PVK (0.0062 g, 0.0374 mmol), 95% (0.025 g), mp 310°C

Crystal Structure Determinations. X-ray data for **3** were collected on a Bruker SMART-CCD diffractometer using graphite-monochromated Mo Kα radiation (λ = 0.71073 Å). Specimens of suitable size and quality were selected and glued onto a glass fiber with freshly prepared epoxy resin. The structure was solved by direct methods, which successfully located most of the non-hydrogen atoms. Subsequent refinement on F^2 using the SHELXTL/PC package (version 6.1) allowed location of the remaining non-hydrogen atoms. Details of the crystal structure can be found in the CIF file.

Luminescence Titrations. The solution luminescence spectra were recorded with a SLM/AMINCO, Model 8100 spectrofluorometer equipped with a xenon lamp. Titration experiments were performed by adding aliquots of a CH_2Cl_2 solution of **1** (50 μL of 5.7 x 10^{-3} M) or **2** (50 μL of 6 x 10^{-3} M) to a quartz cuvette containing 3.00 mL of a CH_2Cl_2 solution of PV2N (6 x 10^{-4} M) or PVK (2 x 10^{-5} M). The samples were excited at $\lambda_{excited}$ = 337 nm (PV2N) and 334 nm (PVK) and the emission intensities at 379 nm (PV2N) and 383 nm (PVK) were monitored during the titration. The intensities were corrected for dilution and absorption using the following formula: $I_{corrected} = I_{observed}\left(\frac{V}{V_{initial}}\right)10^{0.5A}$ where V = volume of the sample, V_{intial} = volume of the sample prior to additions, and A = absorbance of the sample at the excitation wavelength.

Photophysical Measurements. Completed by Dr. El-bjeriami from the Omary group at the University of North Texas. Steady-state luminescence spectra were acquired with a PTI QuantaMaster Model QM-4 scanning spectrofluorometer. The excitation and emission spectra were corrected for the wavelength-dependent lamp

intensity and detector response, respectively. Lifetime data were acquired using fluorescence and phosphorescence subsystem add-ons to the PTI instrument. The pulsed excitation source was generated using the 337.1 nm line of the N_2 laser pumping a freshly prepared 1×10^{-2} M solution of the continuum laser dye, Coumarin-540A, in ethanol, the output of which was appropriately tuned and frequency doubled to attain the excitation wavelengths needed based on the luminescence excitation spectra for each compound. Cooling in temperature-dependent measurements for the crystals was achieved using an Oxford optical cryostat, model Optistat CF ST, interfaced with a liquid nitrogen tank.

CHAPTER VI

TERNARY SUPRAMOLECULAR COMPLEXES INVOLVING $[(o\text{-}C_6F_4)Hg]_3$ AND HYDROGEN BONDED COMPLEXES

VI.1. Introduction

Trimeric perfluoro-*ortho*-phenylene mercury (**1**) has been shown to interact with aromatic substrates to form supramolecular binary stacks where molecules of **1** and the arene alternate.[6,7,28-31,71,72] In these adducts, as a result of the close proximity of three mercury centers, the arene experiences an intense spin orbit perturbation resulting in room temperature phosphorescence of the arene.[6,7,71] Although the photophysics of adducts involving **1** has been extensively studied, the chemical consequences of complexation with **1** requires more attention. In search of possible systems, we investigated the ability of **1** to increase the acidity of aromatic derivatives.

Carbazole is a weakly acidic aromatic substrate which forms hydrogen bonds with various Lewis bases. In solution, hydrogen bonding of coordinating solvents with carbazole has been reported using various techniques including UV absorption, IR, and fluorescence spectroscopy. For instance, the absorption spectra of carbazole in coordinating solvents such as THF, diethylether, and 1,4-dioxane are red shifted with respect to the spectra of carbazole in cyclohexane.[108] The carbazole-pyridine complex has been observed through fluorescence spectroscopy[109], while the N-H stretching frequencies have been used to study the carbazole-THF complex[110]. Unfortunately, none of these carbazole complexes with coordinating solvents have been structurally characterized.

In this chapter, we intend to determine if the acidity and hydrogen bond donor ability of carbazole can be enhanced by cofacial complexation with **1**. In essence, the Lewis acid **1** will withdraw electron density from carbazole, thus increasing its acidity towards Lewis bases. Ultimately it can be envisaged that **1** could stabilize the fully

deprotonated form of carbazole. The results discussed in this chapter consequently represent the first structurally characterized hydrogen bonded complexes of carbazole and THF or triethylamine as well as the first reported ternary supramolecules involving **1** (Scheme VI.1). In addition to structure and characterization of these supramolecules, remarkable temperature dependent luminescent properties will be discussed.

Scheme VI.1.

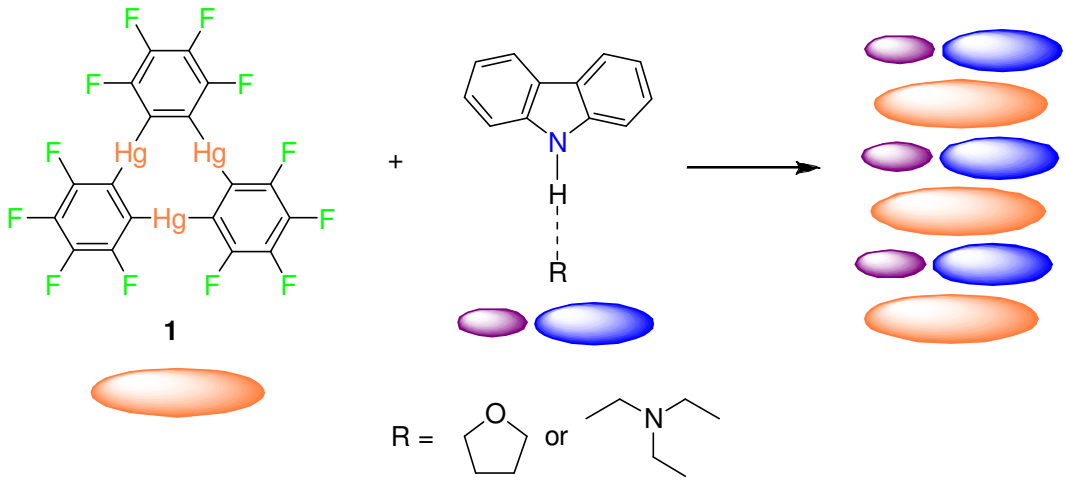

VI.2. Synthesis and structure of the adducts

When an equimolar THF solution of **1** and carbazole is mixed, slow evaporation of the solvent yields the crystalline adduct [**1**•($C_{12}H_8NH$•THF)] (**17**) whose composition has been confirmed by elemental analysis. If, however, a triethylamine (NEt_3) solution of carbazole is mixed with a THF solution of **1**, slow evaporation of the solvents results in the adduct [**1**•($C_{12}H_8NH$•NEt_3)] (**18**) whose stoichiometry has also been confirmed by elemental analysis. Although both adducts are air stable and soluble in polar solvents such as acetone and THF, long term storage of the crystalline adducts requires contact with the coordinating solvent. When a CH_2Cl_2 solution of **1** and carbazole is mixed,

slow evaporation produces the solvent free adduct [**1**•carbazole] as indicated by elemental analysis. While the solid state structure of [**1**•carbazole] has not been elucidated, the structures of adducts **17** and **18** have been determined using X-ray crystallography (Table VI.1). In both adducts, there are no unusual intramolecular bond distances or angles of the three components. The extended structures exhibit supramolecular stacks where molecules of **1** and the carbazole–solvent complex alternate (Figure VI.1). It is important to note that crystallization of pure carbazole from THF or NEt_3 yields only crystalline carbazole as evidenced by unit cell determination.

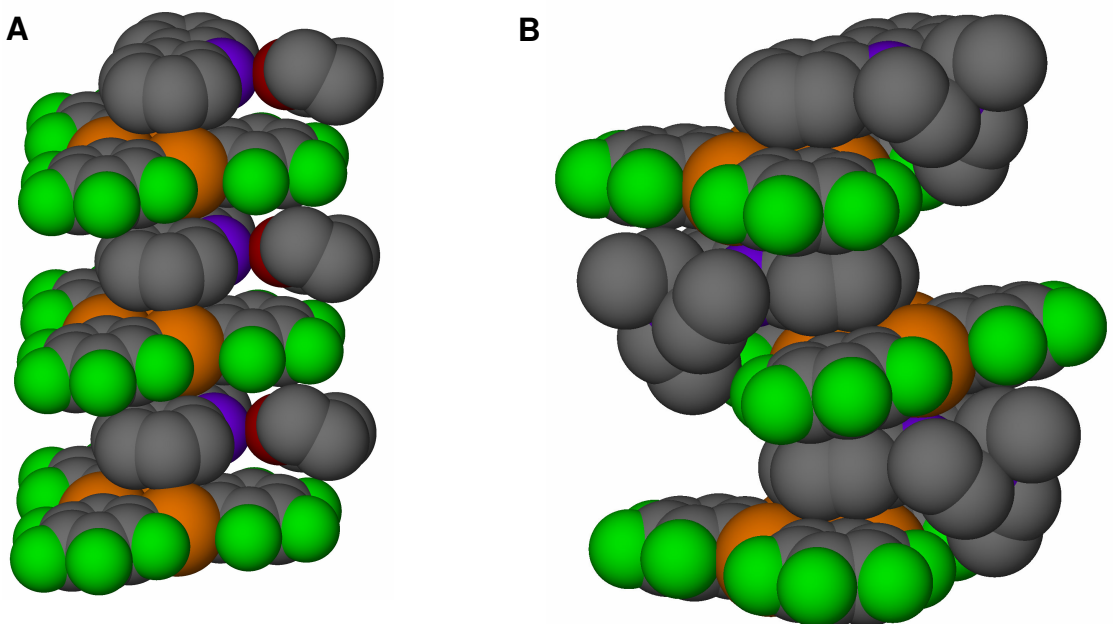

Figure VI.1. Space filling view of (A) **17** and (B) **18**.

Table VI.1. Crystal data, data collection, and structure refinement for **17** and **18.**

Crystal data	**17**	**18**
Formula	$C_{34}H_{17}F_{12}Hg_3NO$	$C_{36}H_{24}F_{12}Hg_3N_2$
M_r	1285.26	1314.34
Crystal size (mm^3)	0.18 x 0.09 x 0.04	0.24 x 0.17 x 0.08
Crystal system	Triclinic	Monoclinic
Space group	P-1	P2(1)/c
a (Å)	7.7605(16)	12.121(2)
b (Å)	14.167(3)	22.893(5)
c (Å)	16.065(3)	13.047(3)
α(°)	113.83(3)	
β(°)	96.00(3)	112.74(3)°
γ(°)	96.98(3)	
V ($Å^3$)	1580.5(6)	3338.9(12)
Z	2	4
ρ_{calc} (gcm^{-3})	2.701	2.615
μ(Mo $K\alpha$)(mm^{-1})	14.637	13.859
F(000) (e)	1168	2408
Data Collection		
T/K	110(2)	110(2)
Scan mode	ω	ω
hkl range	-9→9, -16→16, -19→19	-13→13, -26→24, -14→14
Measured refl.	11425	21747
Unique refl., [R_{int}]	5527, [0.0701]	5239, [0.1130]
Refl. used for refinement	5527	5239
Absorption correction	SADABS	SADABS
T_{min}/T_{max}	0.444896	0.382563
Refinement		
Refined parameters	346	478
R1, wR2 [I>2σ(I)]	0.0542, 0.1097	0.0538, 0.1245
ρ_{fin} (max/min) ($eÅ^{-3}$)	2.361, -3.045	3.441, -1.740

[a] $R1 = (F_o - F_c)/ F_o$. [b] $wR2 = \{[w(F_o^2 - F_c^2)^2]/ [w(F_o^2)^2]\}^{1/2}$; $w = 1/[\sigma^2(F_o^2) + (ap)^2 + bp]$; $p = (F_o^2 + 2F_c^2)/3$; a = 0.0470 (**17**), 0.0710 (**18**); b = 0.0000 (**17**), 0.0000 (**18**)

Compound **17** crystallizes in the triclinic space group *P*-1 with one molecule of **1**, one molecule of carbazole, and one molecule of THF in the asymmetric unit (Figure VI.2). The orientation of the carbazole component allows for the π-face of the heterocycle to be directly exposed to the trinuclear mercury core of **1**. The resulting Hg-C distances (3.25–3.41 Å) are within the sum of the van der Waals radii for Hg (1.7–2.0 Å) and $C_{aromatic}$ (1.5 Å), suggesting the presence of secondary Hg-π interactions. The

THF molecule does not engage in any close interactions with the mercury centers or the perfluoroaryl backbone of **1**. However, the short distance (2.76 Å) between N(1) of the carbazole molecule and O(1) of THF suggests the occurrence of a relatively strong hydrogen bond. The similarity of the C(27)-N(1)-O(1) and C(29)-N(1)-O(1) angles (127° and 125°, respectively) indicates that the N-H···O interaction is quite linear. Typical N···O distances range from 2.7 Å to 3.0 Å, and it has been previously proposed that the more linear angle indicates a stronger hydrogen bond.[111-114]

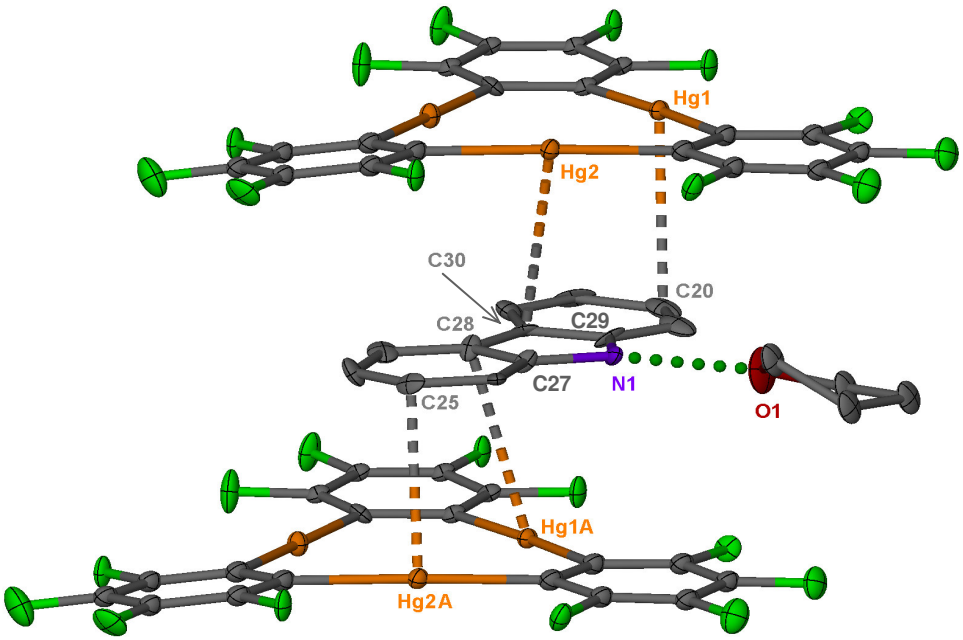

Figure VI.2. Structure of **17**. ORTEP view (50% ellipsoid) with hydrogen atoms omitted for clarity. Representative intermolecular distances (Å): N(1)-O(1) 2.760, Hg(1)-C(20) 3.328, Hg(1A)-C(28) 3.357, Hg(2)-C(30) 3.408, Hg(2A)-C(25) 3.251.

Compound **18** crystallizes in the monoclinic space group $P2_1/c$ with one molecule of **1**, one molecule of carbazole, and one molecule of NEt_3 in the asymmetric unit (Figure VI.3). As in the case of **17**, the carbon atoms of the carbazole component engage in secondary Hg-π interactions with the mercury centers of **1** as evidenced by the

short Hg-C distances (3.25–3.43 Å). Furthermore, there is a short Hg-N interaction of 3.38 Å between Hg(3A) and N(1). As with **17**, the NEt_3 molecule does not interact with the mercury centers or the perfluoroaryl backbone of **1**. The short N(1)···N(2) distance of 2.94 Å suggests a hydrogen bond between the NEt_3 nitrogen atom and the carbazole N-H moiety. Additionally, the C(27)-N(1)-O(1) and C(29)-N(1)-O(1) angles (136° and 114°, respectively) indicates that the N-H···N interaction is fairly linear. Typical N···N distances attributed to hydrogen bonding interactions typically range from 2.8–3.0 Å. Due to the increased crowding induced by the NEt_3 component, the molecules of **1** and carbazole are not planar with respect to one another. In fact, the plane of the mercury core of **1** containing Hg(1) and the carbazole would intersect at a 6.1° dihedral angle.

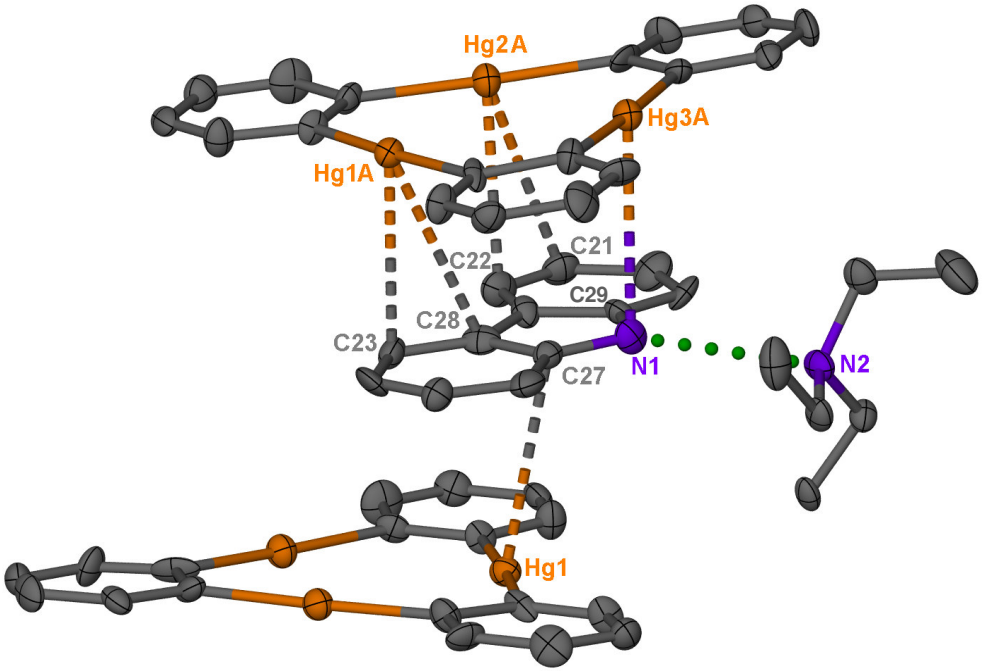

Figure VI.3. Structure of **18**. ORTEP view (50% ellipsoid) with hydrogen and fluorine atoms omitted for clarity. Representative intermolecular distances (Å): N(1)-N(2) 2.940, Hg(1)-C(27) 3.432, Hg(1A)-C(23) 3.141, Hg(1A)-C(28) 3.362, Hg(2A)-C(21) 3.432, Hg(2A)-C(22) 3.207, Hg(3A)-N(1) 3.375

In order to confirm the presence of a hydrogen bonding interaction between the carbazole N-H group and the solvent molecules, we analyzed the adducts by IR spectroscopy. The N-H stretching bands appear at 3460 cm^{-1} for [**1**•carbazole], 3419 cm^{-1} for **17**, and 3417 cm^{-1} for **18**. The vibrational frequency shifts ($\Delta\nu$) between the isolated carbazole in [**1**•carbazole] and the hydrogen bonded complexes **17** and **18** are 41 cm^{-1} and 43 cm^{-1}, respectively. This weakening of the N-H stretch in **17** and **18** is in agreement with the presence of a hydrogen bond interaction, an effect which has been previously discussed for other hydrogen bonded systems. [115]

VI.3. Solid state luminescence

At both room temperature and 77 K adduct [**1**•carbazole] emits blue light (Figure VI.4). Examination of its emission spectra recorded at both temperatures indicates that the observed luminescence corresponds to the phosphorescence of carbazole.[116] As previously proposed for the *N*-methylcarbazole adduct of **1**, the observed phosphorescence is a direct result of the external mercury heavy atom effect which promotes intersystem spin crossing from the S_1 to the T_1 state of the carbazole. At low temperature (77 K), adducts **17** and **18** also emit blue light with emission spectra which also corresponds to the triplet emission of carbazole (Figures VI.5-6). In both spectra, however, weak bands are observed at 578 nm and 567 nm. Remarkably, elevation of the temperature leads to a drastic increase in the intensity of these bands which results in a change of the color of the emission from blue to orange in the case of **17** and from blue to yellow in the case of **18**. The exact origin of these low energy bands cannot be confirmed at this time.

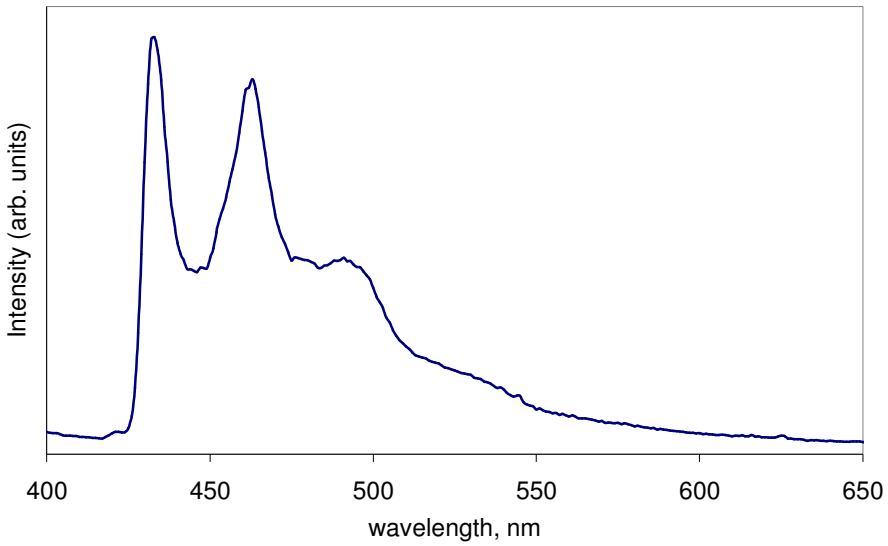

Figure VI.4. Emission spectra of [**1**•carbazole] at 77 K.

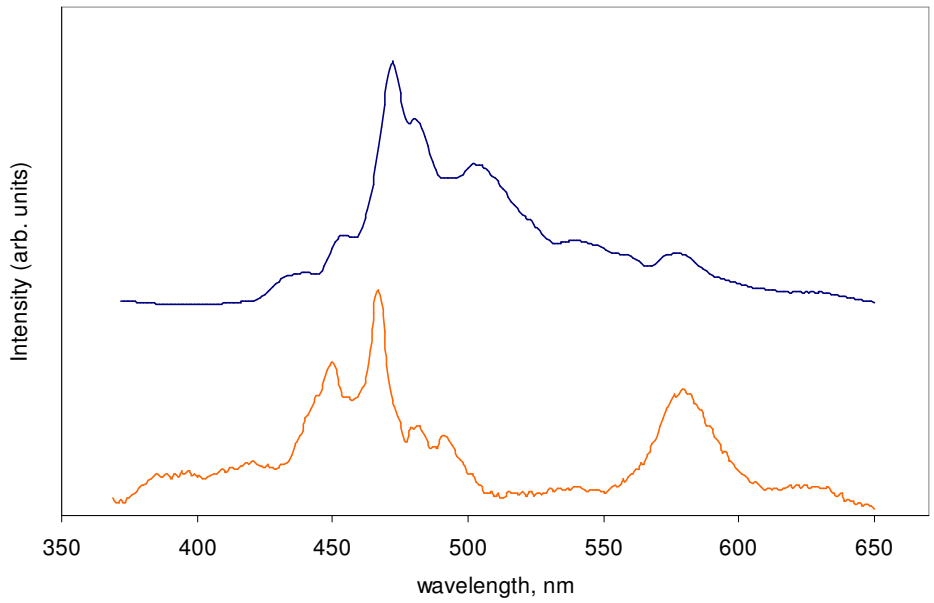

Figure VI.5. Emission spectra of **17** at (a) 77 K and (b) RT.

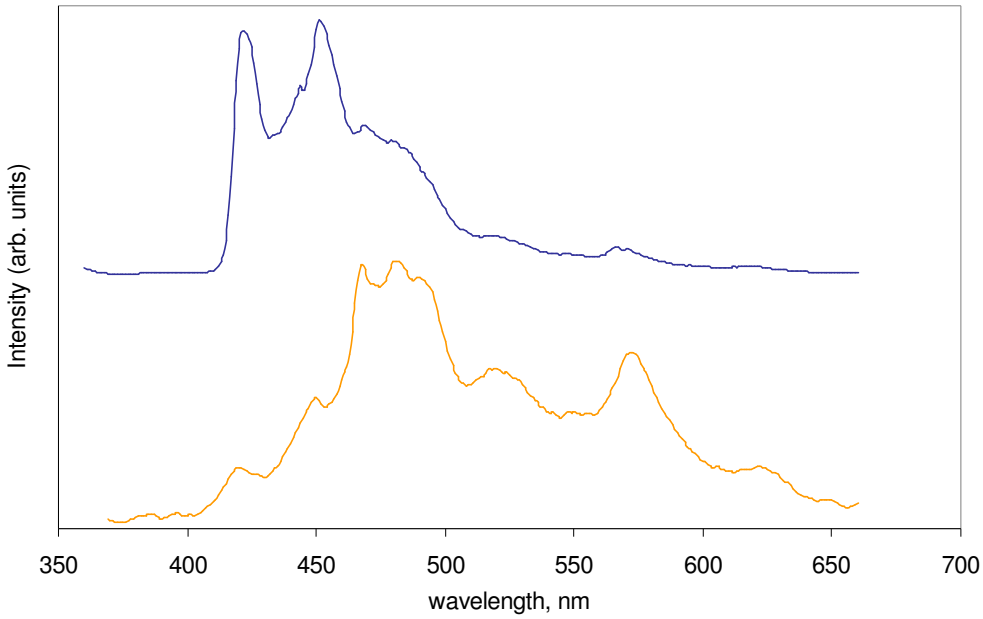

Figure VI.6. Emission spectra of **18** at (a) 77 K and (b) RT.

VI.4. Conclusions

This chapter describes the first structurally characterized hydrogen bonded complex of carbazole with coordinating solvents, specifically THF and NEt_3, which suggests that complexation to **1** allows for increased acidity of the carbazole substrate. In both adducts the extended structures exhibit supramolecular binary stacks where molecules of **1** and the carbazole-solvent complex alternate. Short Hg-C contacts involving molecules of **1** and carbazole indicate the presence of secondary Hg-π interactions, which can be considered largely electrostatic and/or dispersive in nature. Additionally, adducts **17** and **18** display a hydrogen bonding interaction between the acidic N-H moiety of carbazole and the Lewis basic site of the coordinating solvent. Both solid state structures and IR spectroscopy confirmed the presence of the hydrogen bond with short N···O and N···N distances (2.76 Å and 2.94 Å respectively) and the lower N-H stretching frequency compared to the solvent free [**1**•carbazole] adduct. Both adducts **17** and **18** are brightly luminescent indicating that the Lewis bases do not

quench the excited state of the chromophores.[117] This blue emission is the phosphorescence of free carbazole which is observed due to the external mercury heavy atom effect which promotes intersystem spin crossing from the S_1 to T_1 state.

VI.5. Experimental details

General. Due to the toxicity of the mercury compounds discussed, extra care was taken at all times to avoid contact with solid, solution, and air-borne particulate mercury compounds. The studies herein were carried out in a well aerated fume hood. Atlantic Microlab, Inc., Norcross, GA, performed the elemental analyses. All commercially available starting materials and solvents were purchased from Aldrich Chemical and VWR, Inc. and used as provided. Compound **1** was prepared according to the published procedure.[70] The luminescence spectra were recorded with a SLM/AMINCO, Model 8100 spectrofluorometer equipped with a xenon lamp. Low-temperature measurements were made in a cryogenic device of local design. Collodion was used to attach the powder samples to the holder. The collodion was scanned for a baseline subtraction. Liquid nitrogen was used to obtain the 77 K measurements. The solid state IR spectroscopy was performed on a Perkin Elmer Spectrum 100 FTIR.

Synthesis of [1•carbazole]. Compound **1** (0.020 g, 0.019 mmol) was dissolved in CH_2Cl_2 (5 mL). In a separate vial, a CH_2Cl_2 solution of carbazole (0.003 g, 0.019 mmol) was prepared. The two solutions were mixed. Upon concentration by slow evaporation of the solvent, crystals of [**1**•carbazole] formed in 96% yield (0.022 g, 0.0191 mmol). mp 310°C (decomp). Anal. Calcd for $C_{34}H_8F_{12}Hg_3$: C, 32.77; H, 0.65. Found: C, 32.54; H, 0.54.

Synthesis of [1•($C_{12}H_8NH$•THF)] (17). Compound **1** (0.020 g, 0.019 mmol) was dissolved in THF (3 mL). In a separate vial, a THF solution of carbazole (0.003 g, 0.019 mmol) was prepared. The two solutions were mixed. Upon concentration by evaporation of the solvent, crystals of **17** formed in 83% yield (0.020 g, 0.019 mmol). Extended storage required contact with THF. mp 349°C (decomp). Anal. Calcd for $C_{34}H_{17}NOF_{12}Hg_3$: C, 31.82; H, 1.34. Found: C, 31.67; H, 1.24.

Synthesis of [1•($C_{12}H_8NH$•NEt_3)] (18). Compound **1** (0.020 g, 0.019 mmol) was dissolved in THF (3 mL). In a separate vial, a triethylamine solution (5 mL) of carbazole (0.003 g, 0.019 mmol) was prepared. The two solutions were mixed. Upon concentration by evaporation of the solution, crystals of **18** formed in 78% yield (0.020 g, 0.019 mmol). Extended storage required contact with triethylamine. mp 316°C (decomp). Anal. Calcd for $C_{36}H_{23}N_2F_{12}Hg_3$: C, 32.92; H, 1.84. Found: C, 32.74; H, 1.63.

Crystal Structure Determinations. X-ray data for **17** and **18** were collected on a Bruker SMART-CCD diffractometer using graphite-monochromated Mo Kα radiation (=0.71073 Å). Specimens of suitable size and quality were selected and glued onto a glass fiber with freshly prepared epoxy resin. The structure was solved by direct methods, which successfully located most of the non-hydrogen atoms. Subsequent refinement on F^2 using the SHELXTL/PC package (version 5.1) allowed location of the remaining non-hydrogen atoms.

CHAPTER VII

COMPLEXATION OF NEUTRAL SUBSTRATES USING MONO- AND TRIFUNCTIONAL ORGANOMERCURIALS*

VII.1. Introduction

Polyfunctional organomercurial Lewis acids have been extensively used as building blocks for supramolecular species. Electron withdrawing substituents are used to enhance the Lewis acidity of these polyfunctional organomercurials, allowing these derivatives form adducts with neutral and anionic substrates. For instance, trimeric perfluoro-*ortho*-phenylene mercury (**1**) has been extensively studied as an anion receptor. In addition to halides[21], larger anions such as $[B_{10}H_{10}]^{2-}$, $[Fe(CN)_6]^{3-}$ and SCN^- also interact with **1** to form multidecker sandwiches.[23,25,118] Likewise, bis(pentafluorophenyl)mercury (**2**) complexes anions such as bromide and iodide to form T-shaped complexes where the halide is terminally ligated to the mercury center.[19] Neutral electron rich substrates have also been complexed with polyfunctional organomercurial derivatives. The coordination chemistry of **2** has been limited to Lewis basic substrates containing nitrogen[119], phosphorus, and arsenic[79] as donor atoms. In our contributions to this area, we found that **1** interacts with aromatic substrates to form extended binary supramolecules where **1** and the arene alternate.[28-31,71,72] This approach has been employed with a variety of aromatic substrates including naphthalene, biphenyl, triphenylene, and pyrene. [6,7] The mercury centers of the trinuclear complex approach the π-face of the aromatic substrate and engage in polyhapto secondary Hg-C interactions. Due to the extended structures of these solids, each arene is surrounded by

---

* Reprinted in part with permission from *Dalton Trans.*, Taylor, T. J.; Burress, C. N.; Pandey, L.; Gabbaï, F. P., "Structural and photophysical studies of phenanthrene adducts involving C_6F_5HgCl and $[o\text{-}C_6F_4Hg]_3$" *in press*, Copyright 2006 by Royal Society of Chemistry.

six mercury atoms. As a result, the arene experiences an intense spin-orbit perturbation manifested by the $T_1 \rightarrow S_0$ monomer phosphorescence of the arene. Moreover, the triplet excited state lifetimes fall in the ms range, which represents shortening by 3-4 orders of magnitude in comparison to the lifetimes of the free arene.

In this chapter, the synthesis and characterization of additional adducts of **1** and **2** will be presented (Scheme VII.1). In addition to the structural and luminescent properties of these adducts, attempts at increasing the Lewis acidity of **1** by using the fluorinated backbone as a transition metal ligand will also be discussed.

Scheme VII.1.

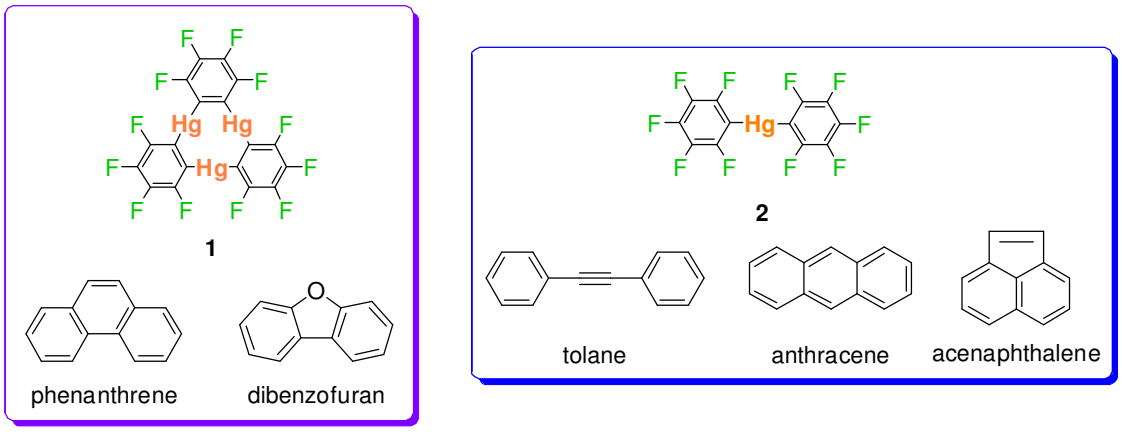

VII.2. Synthesis and structures of arene adducts with **2**

When a CH_2Cl_2 solution of **2** is mixed with a solution of tolane, anthracene, or acenaphthalene, slow evaporation of the solvent yields the 1:1 adduct of [**2**•tolane] (**19**), [**2**•anthracene] (**20**), and [**2**•acenaphthalene] (**21**), whose stoichiometries were confirmed by elemental analysis. These adducts, which are air stable, have been studied by single crystal X-ray crystallography (Table VII.1). The extended structures exhibit binary stacks where molecules of **2** alternate with the aromatic substrate. In all three adducts,

there are no unusual intermolecular bond distances or angles of the components. The closest known analog of such binary compounds is an adduct involving **2** and 2,2'-dipyridyl diselenide.[80] This adduct forms extended stacks that are supported by Hg–Se interactions, rather than Hg–C interactions.

Compound **19** crystallizes in the triclinic space group *P*-1 with half a molecule of **2** and half a molecule of tolane in the asymmetric unit (Figure VII.1). The short centroids distance of 3.579 Å between the phenyl group of the tolane and the pentafluorophenyl group of **2** indicates the presence of arene–perfluoroarene interactions. The tolane is oriented such that perfluoroarene–arene interactions are maximized with a centroid to centroid distance of between one of the fluoroarene rings of **2** and one of the six-membered rings of the tolane. This interaction resembles that encountered in several purely organic arene-fluoroarene assemblies.[120-123] The shortest contact between the mercury atom Hg(1) and the sp-hybridized carbon center (C(7)) is 3.62 Å, which is slightly longer than typical secondary Hg-C_{sp} interactions[72] but is within the sum of the van der Waals radii for Hg (r_{vdw} = 1.73–2.00 Å)[65] and $C_{aromatic}$ (r_{vdw} = 1.7 Å)[66]. Although there could be some overlap between the mercury center and the π system of the C≡C, more than likely perfluoroarene–arene interactions are largely responsible for the cohesion of the adduct.

Table VII.1. Crystal data, data collection, and structure refinement for **19**, **20**, **21.**

Crystal data	**19**	**20**	**21**
Formula	$C_{26}H_{10}F_{10}Hg$	$C_{26}H_{10}F_{10}Hg$	$C_{24}H_8F_{10}Hg$
M_r	712.93	712.93	686.89
Crystal size (mm^3)	0.18 x 0.09 x 0.04	0.23 x 0.05 x 0.07	0.20 x 0.08 x 0.05
Crystal system	Triclinic	Monoclinic	Monoclinic
Space group	P-1	P2(1)/c	P2(1)/c
a (Å)	6.0478(5)	7.5160(15)	14.672(6)
b (Å)	7.1879(6)	6.3341(13)	6.813(3)
c (Å)	13.2749(11)	22.400(5)	21.561(8)
α(°)	104.5790(10)°		
β(°)	92.8480(10)°	90.68(3)°	109.656(7)°
γ(°)	94.3980(10)°		
V ($Å^3$)	555.42(8)	1066.3(4)	2029.6(13)
Z	1	2	4
ρ_{calc} (gcm^{-3})	2.131	2.220	2.248
μ(Mo $K\alpha$)(mm^{-1})	7.025	7.319	7.685
F(000) (e)	336	672	1288
Data Collection			
T/K	110(2)	110(2)	110(2)
Scan mode	ω	ω	ω
hkl range	-8→7, -9→9, -17→17	-9→9, -7→8, -29→28	-16→16, -7→7, -24→24
Measured refl.	4719	8670	11788
Unique refl., [R_{int}]	2474, [0.0191]	2498 [0.0281]	3179, [0.1990]
Refl. used for refinement	2474	2498	3179
Absorption correction	SADABS	SADABS	none
T_{min}/T_{max}	0.411839	0.176692	
Refinement			
Refined parameters	169	169	316
R1, wR2 [I>2σ(I)]	0.0201, 0.0523	0.0242, 0.0634	0.0489, 0.1160
ρ_{fin} (max/min) ($eÅ^{-3}$)	1.213, -2.086	1.380, -1.508	1.559, -3.444

[a] $R1 = (F_o - F_c)/ F_o$. [b] $wR2 = \{[w(F_o^2 - F_c^2)^2]/ [w(F_o^2)^2]\}^{1/2}$; $w = 1/[\sigma^2(F_o^2) + (ap)^2 + bp]$; $p = (F_o^2 + 2F_c^2)/3$; *a* = 0.0290 (**17**), 0.0400 (**18**), 0.0500 (**21**); *b* = 1.2222 (**17**), 1.8000 (**18**), 4.4000 (**21**)

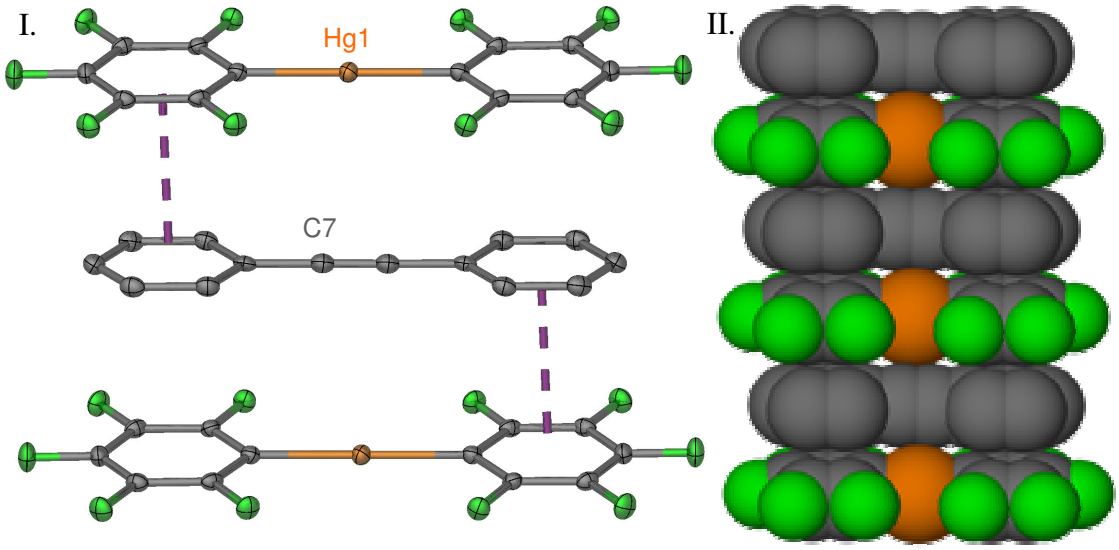

Figure VII.1. Structure of **19.** Hydrogen atoms omitted for clarity: I. ORTEP view (50% ellipsoids) displaying centroid–centroid interaction at 3.579 Å. II. Space-filling view of a portion of a stack.

Compound **20** crystallizes in the monoclinic space group $P(2)_1/c$ with half a molecule of **2** and half a molecule of anthracene in the asymmetric unit (Figure VII.2). Unlike in the structure of **19**, the shortest Hg-C contact is within the van der Waals radii of Hg and $C_{aromatic}$ (3.38 Å between Hg(1) and C(11)), suggesting that secondary Hg-π interactions contribute to the cohesion of these supramolecules. Perfluoroarene–arene interactions are also observed in adduct **20** as evidenced by the centroid–centroid distance of 3.74 Å between one of the fluoroarene rings of **2** and the six-membered ring of the anthracene containing C(11).

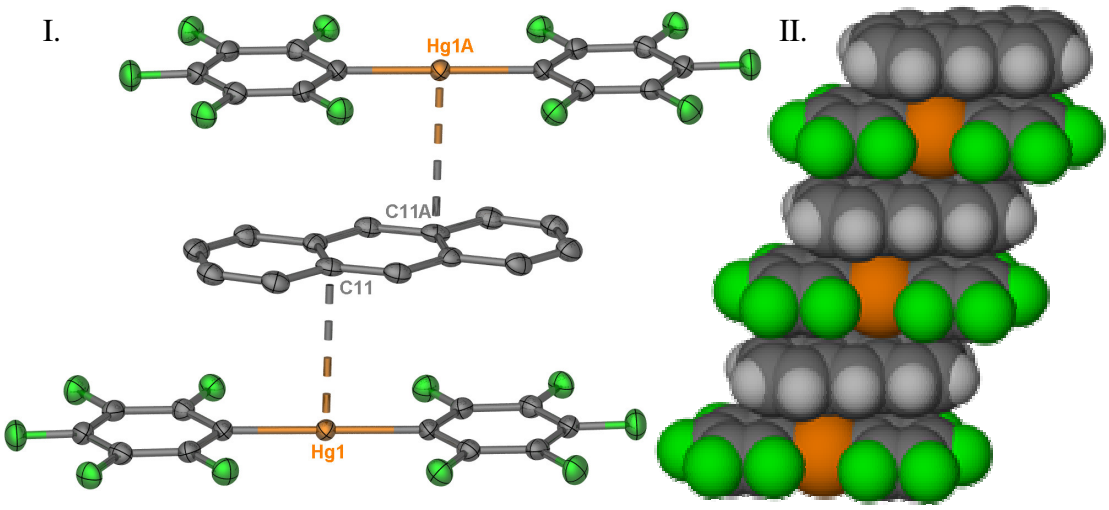

Figure VII.2. Structure of **20**: I. ORTEP view (50% ellipsoids) with hydrogen atoms omitted for clarity. The representative close intermolecular distance Hg(1)–C(11) is 3.38 Å. II. Space filling view of a portion of a stack.

Compound **21** crystallizes in the monoclinic space group $P(2)_1/c$ with one molecule of **2** and one molecule of acenaphthalene in the asymmetric unit (Figure VII.3). The acenaphthalene component is weakly π-coordinated to the nearby mercury centers of **2**. The two mercury centers Hg(1) and Hg(1A) sandwich the acenaphthalene moiety via η^2 and η^1 interactions, respectively, involving carbon atoms C(19), C(20), and C(24) (3.28–3.40 Å). As a result of these interactions, the acenaphthalene moiety is slightly tilted with respect to the plane containing **2** with which it forms an angle of 4.0°. This angle is very similar to that observed in the [**2**•naphthalene] adduct, which has an angle of 4.6° between the planes of the two components. As opposed to both **19** and **20**, the acenaphthalene component does not engage in perfluoroarene–arene interactions with the pentafluorophenyl rings of **2**.

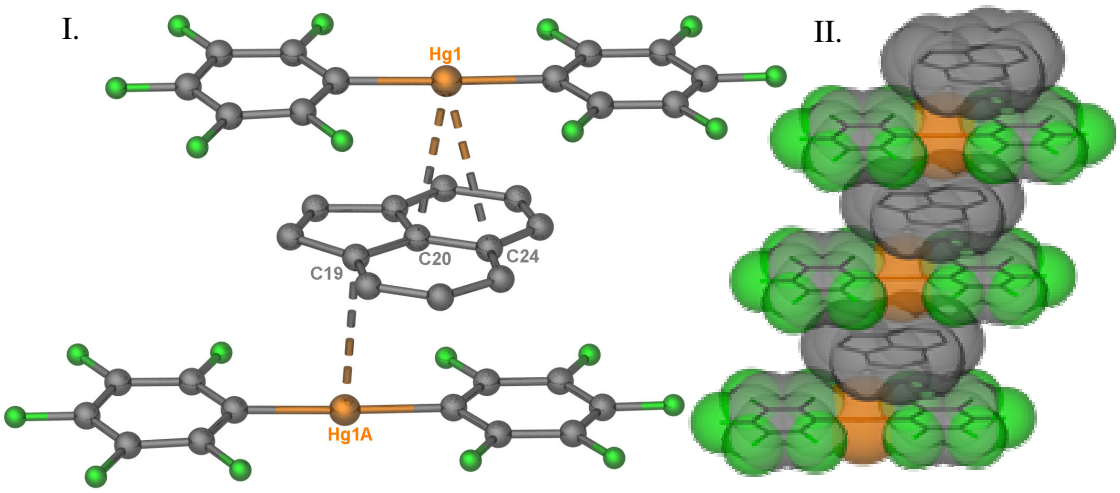

Figure VII.3. Molecular structure of **21**. I. Intermolecular representative Hg-C distances (Å): Hg(1)-C(20) 3.31, Hg(1)-C(24) 3.40, Hg(1A)-C(19) 3.28. II. Space filling view of a portion of a stack.

As shown by the structural studies of these adducts, complexation of aromatic substrates can be achieved with simple organomercurials, specifically **2**. The electron withdrawing backbone allows for sufficient Lewis acidity at the mercury center for the formation of supramolecules with arenes in the case of **20** and **21**. The interactions in these stacks are perhaps largely dispersive and/or electrostatic in nature, as has been previously proposed for aromatic adducts of **1**.

VII.3. Synthesis and structures of adducts with **1**

In spite of the extensive work on luminescent adducts with **1**, the phenanthrene and dibenzofuran adducts of **1** had not been synthesized previously. These adducts form similar extended binary stacks in the solid state as seen with the previous arene adducts of **1**. [6,7,28,29] When a CH_2Cl_2 solution of **1** is added to a solution of phenanthrene in the same solvent, upon slow evaporation, the 1:1 adduct (**22**) crystallizes in an 87% yield. Compound **22** crystallizes in the monoclinic space group $P2_1/m$ with half a molecule of **1** and half a molecule of phenanthrene in the asymmetric unit (Table VII.2 and Figure VII.4). The Hg···$C_{aromatic}$ distances range from 3.28–3.41 Å, indicating the presence of

secondary Hg–π interactions. Unlike adducts **19** and **20** of **2**, the perfluoroaryl backbone of **1** does not engage in perfluoroarene–arene interactions with the phenanthrene molecule. The perfluoroaryl rings of **1** slightly bend away from the Hg centers, where the plane of the perfluoroaryl backbone and the plane of the three Hg centers would intersect at a 6° dihedral angle.

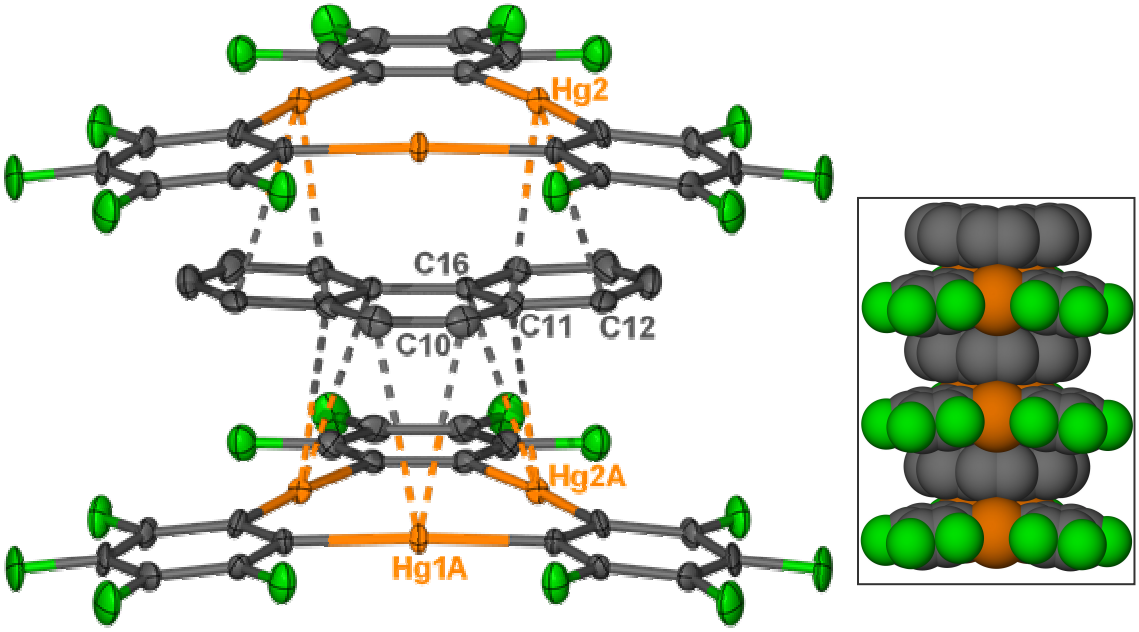

Figure VII.4. ORTEP view of **22** (50% ellipsoids, hydrogen atoms are omitted for clarity). Representative intermolecular distances (Å): Hg(1A)-C(10) 3.40, Hg(2A)-C(11) 3.55, Hg(2A)-C(16) 3.41, Hg(2)-C(11) 3.28, Hg(2)-C(12) 3.34. Inset: Space filling view of a portion of a stack.

Table VII.2. Crystal data, data collection, and structure refinement for **22** and **23.**

Crystal data	**22**	**23**
Formula	$C_{32}H_{10}F_{12}Hg_3$	$C_{30}H_8F_{12}Hg_3O$
M_r	1224.17	1214.13
Crystal size (mm^3)	0.31 x 0.15 x 0.07	0.19 x 0.10 x 0.06
Crystal system	Monoclinic	Orthorhomic
Space group	P2(1)/m	Pna2(1)
a (Å)	6.6663(13)	17.770(4)
b (Å)	20.640(4)	22.211(4)
c (Å)	10.143(2)	6.9177(14)
α (°)		
β (°)	94.23(3)	
γ (°)		
V ($Å^3$)	1391.8(5)	2730.3(10)
Z	2	4
ρ_{calc} (gcm^{-3})	2.921	2.954
μ(Mo $K\alpha$)(mm^{-1})	16.605	16.936
F(000) (e)	1100	2176
Data Collection		
T/K	110(2)	110(2)
Scan mode	ω	ω
hkl range	-7→7, -26→10, -13→6	-20→20, -25→22, -7→7
Measured refl.	7834	17666
Unique refl., [R_{int}]	3111 [0.0295]	4258 [0.1007]
Refl. used for refinement	3111	4258
Absorption correction	SADABS	SADABS
T_{min}/T_{max}	0.241723	0.300563
Refinement		
Refined parameters	214	393
R1, wR2 [I>2σ(I)]	0.0372, 0.0932	0.0583, 0.1295
ρ_{fin} (max/min) ($eÅ^{-3}$)	2.139, -2.945	1.883, -1.655

[a] $R1 = (F_o - F_c)/ F_o$. [b] $wR2 = \{[w(F_o^2 - F_c^2)^2]/ [w(F_o^2)^2]\}^{1/2}$; $w = 1/[\sigma^2(F_o^2) + (ap)^2 + bp]$; $p = (F_o^2 + 2F_c^2)/3$; a = 0.055300 (**22**); 0.0608 (**23**); b = 23.053200 (**22**), 155.1072 (**23**).

Upon slow evaporation of a CH_2Cl_2 solution of equimolar amounts of **1** and dibenzofuran, the 1:1 adduct (**23**) crystallizes in 82% yield. Compound **23** crystallizes in the orthorhombic space group *P*na2_1 with one molecule of **1** and one molecule of dibenzofuran in the asymmetric unit (Table VII.2 and Figure VII.5). The shortest Hg–C distances range from 3.26–3.43 Å suggesting the presence of Hg–π interactions. In

addition, the Hg–O distance is 3.58 Å which is within the van der Waals radii of the two elements. In the analogous *N*-methylcarbazole adduct of **1** (**12**), there are two crystallographically distinct stacks which differ by the orientation of the *N*-methylcarbazole unit with respect to the trinuclear mercury core. Compound **23**, however, does not show this ambiguity in the solid state, which may be a result of the preference that Lewis acidic mercury sites display for the Lewis basic oxygen atom.

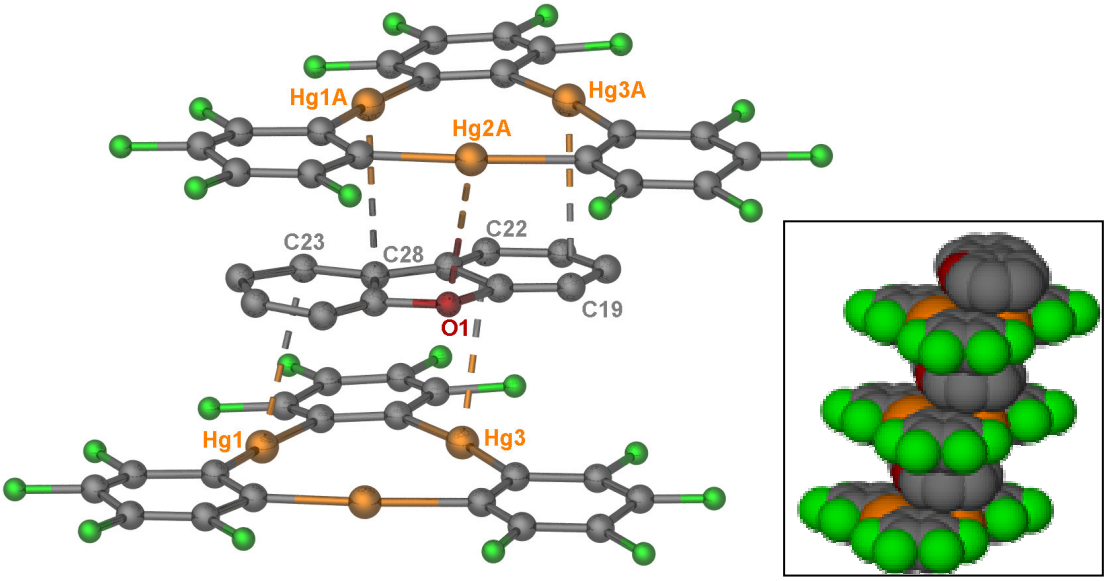

Figure VII.5. Molecular structure of **23** (Hydrogen atoms are omitted for clarity). Representative intermolecular distances (Å): Hg(1)-C(23) 3.36, Hg(1A)-C(28) 3.26, Hg(2A)-O(1) 3.58, Hg(3)-C(22) 3.43, Hg(3A)-C(19) 3.36. Inset: Space filling view of a portion of a stack.

VII.4. Solid state luminescence

Adducts **19** and **22** give rise to intense room temperature phosphorescence in the visible region. The emission spectrum of solid **19** corresponds to both the fluorescence (325–425 nm) and phosphorescence (458–590 nm) previously observed for free tolane

(Figure VII.6).[124] However, the lower energy band at 642 nm has not been reported. Although the exact assignment of this band cannot be confirmed, it may possibly correspond to formally forbidden transitions which could not be observed using traditional techniques. While the solid state structure shows that there is little interaction between the mercury and carbon centers, the observed phosphorescence of tolane suggests that the external heavy atom effect does indeed affect the photophysical properties of the tolane.

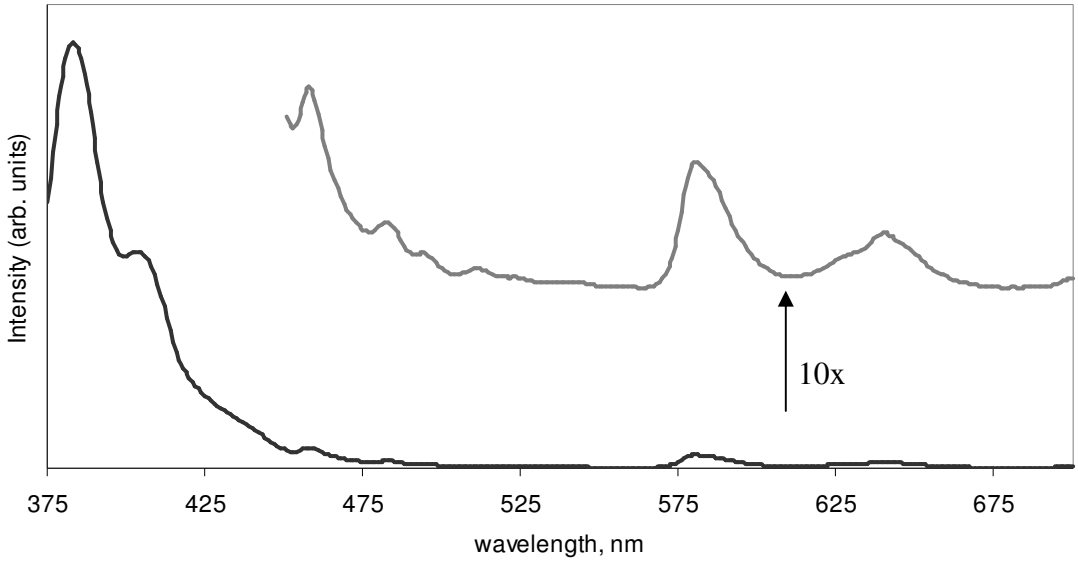

Figure VII.6. Emission spectrum of crystalline **19** at 77 K (λ_{exc} = 355 nm).

The energies and vibrational progression observed in the emission spectra of compound **22** corresponds very closely to that reported for the phosphorescence spectra of free phenanthrene in an EPA matrix (Figure VII.7).[125] As previously proposed for other arene adducts of **1**, the observed phosphorescence is a result of the external mercury heavy atom effect which promotes intersystem spin crossing from the S_1 to the T_1 state of the phenanthrene. In order to further assess the external heavy atom effect

induced by **1**, the kinetics of the radiative decay was analyzed by the Omary group of the University of North Texas. The measured lifetimes (τ^P = 1.338 ms, 0.857 ms at room temperature and 77 K, respectively) are much shorter than the reported triplet lifetime for free phenanthrene (3.4 seconds at 77 K).[126] This shortening is a direct result of the strong spin-orbit coupling effect of the mercury centers, which makes the phosphorescence transition a more allowed transition, hence leading to a shorter triplet lifetime than that exhibited by pure phenanthrene where the phosphorescence is strongly forbidden.

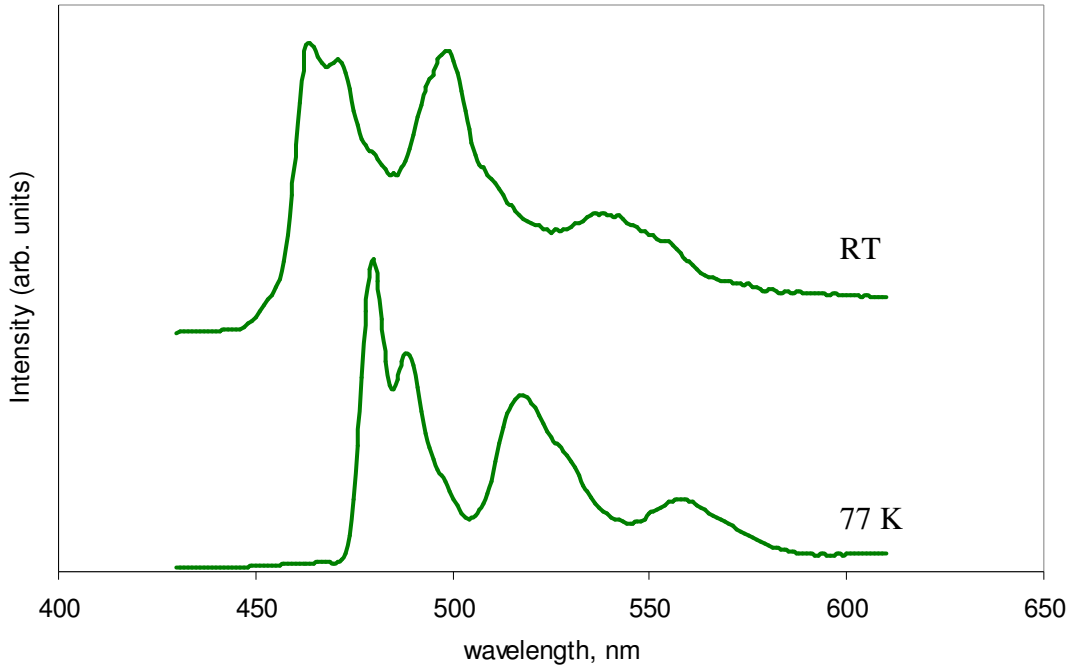

Figure VII.7. Emission spectra of crystalline **22** at RT and 77 K (λ_{exc} = 314 nm).

VII.5. Increasing acceptor properties of **1** by complexation of a transition metal

Although the body of work involving **1** as a polyfunctional Lewis acid is extensive, the fundamental chemistry of **1** is still an active area of research. As a general

goal, we have been interested in enhancing the Lewis acidic properties of **1**. Atwood and coworkers have shown that metalating macrocyclic calix[4]arenes with cationic metal centers including Ru, Ir, and Rh results in significant improvement in the accepting ability of the calixarene.[127] Consequently, anionic species were incorporated into the molecular cavity of the metalated calixarene.[127]

In order to apply this strategy to the case of **1**, it is necessary to determine suitable transition metal ions that complex fluorinated arenes. Although several metals form η^2- and η^4-π-complexes with hexafluorobenzene[128], the cationic $[Cp^*Ru]^+$ fragment has been shown to easily form sandwich η^6-π-complexes with various fluorinated arenes.[129] Due to the ease of synthesis of these η^6 complexes with Ru, we decided to investigate the ability of **1** to serve as a ligand in Ru sandwich complexes.

Following the addition of $[Cp^*Ru(CH_3CN)_3]PF_6$ to a THF solution containing an excess amount of **1** at ambient temperature, ether was added, and an orange brown precipitate was formed. The solution was filtered and allowed to slowly evaporate, resulting in the crystallization of a Ru sandwich complex with **1**. Although the quality of the refinement does not allow for a detailed discussion of bond distances and angles, the solid state structure was elucidated using single crystal X-ray diffraction. Unfortunately the stoichiometry was never confirmed by elemental analysis due to the highly unstable nature of these crystals. Compound $[\mathbf{24}\bullet(\mu^3\text{-Cl})(THF)_2]^{2+}(PF_6)_2$ crystallizes in the triclinic space group *P*-1 with two molecules of **24**, four molecules of THF, two chloride and four PF_6 anions in the asymmetric unit (Figure VII.8). The chloride anion probably originates from an impurity in the starting material, $[Cp^*Ru(CH_3CN)_3]PF_6$, which is synthesized from the tetramer $[Cp^*RuCl]_4$ and CH_3CN.[130]

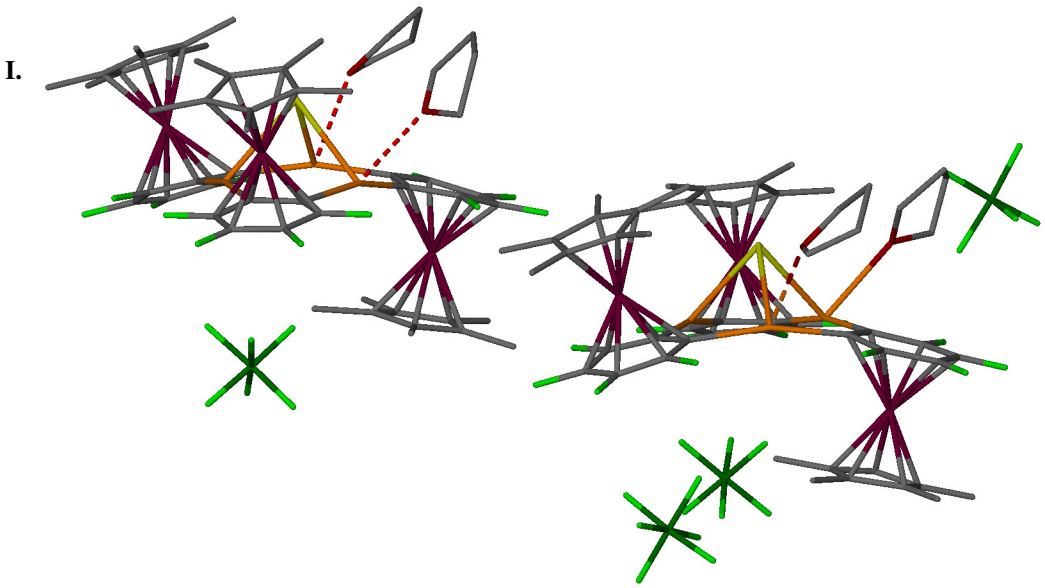

Figure VII.8. Asymmetric unit of $[\mathbf{24}\bullet(\mu^3\text{-Cl})(THF)_2]^{2+}(PF_6)_2$ showing all PF_6 counteranions. Hydrogen atoms omitted for clarity.

All three perfluoroaryl rings of **1** are π-coordinated to a Ru center in a η^6 fashion. Two of the $[Cp^*Ru]^+$ fragments are above the plane of the three mercury centers, and one of the $[Cp^*Ru]^+$ fragments is oriented below the plane. This conformation of the Ru centers is probably due to the sterics involved in adding another Ru center on the same face of **1**. Although **1** is typically planar, the perfluoroaryl rings of **1** in compound **24** bend away from the mercury core, where the plane of the perfluoroaryl ring and the plane of the mercury centers would intersect at angles ranging from 8.9° to 19.1°. Such unprecedented distortion possibly originates from steric effects or results from chloride complexation.

The adduct $[\mathbf{1}\bullet Cl]^-$ had been previously isolated but not structurally characterized. In $[\mathbf{24}\bullet(\mu^3\text{-Cl})(THF)_2]^{2+}$, the chloride is bound to all three mercury atoms via short Hg-Cl bonds of 2.8–3.0 Å, which are much shorter than the van der Waals radii for both elements (Figure VII.9). In addition to the chloride complexation, two THF molecules are η^1 coordinated via the oxygen atom to two of the mercury centers of **1**.

Previously structurally characterized halide complexes of **1** display extended binary stacks and lack solvent molecules in the crystal lattice. However, the additional coordination of the THF molecules in [**24**•(μ^3-Cl)$(THF)_2$]$^{2+}$ suggests that the mercury centers in this complex are possibly more electron deficient than in pure **1**. While more studies are necessary to substantiate this claim, complex [**24**•(μ^3-Cl)$(THF)_2$]$^{2+}$ shows that the Lewis acidic properties of **1** can be altered by complexation with a transition metal moiety.

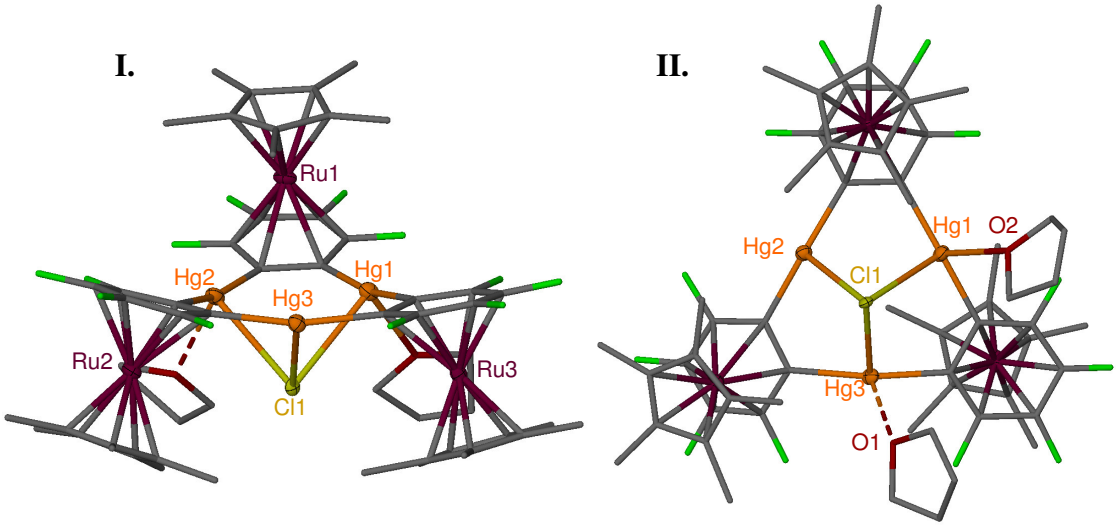

Figure VII.9. (I) Side-on view of one molecule of [**24**•(μ^3-Cl)$(THF)_2$] $^{2+}(PF_6)_2$ with hydrogen atoms and THF molecules omitted for clarity; (II) Top view of the μ^3-chloride complexation.

VII.6. Concluding remarks

The results reported in these studies indicate that simple mononuclear organomercurials such as **2** readily assemble with aromatic substrates to form supramolecules. While adducts **20** and **21** display short Hg···C interactions in the solid state, perfluoroarene–arene interactions are largely responsible for the cohesion of the stack in adduct **19**. DFT calculations carried out on **2** have shown the existence of a

positively charged electrostatic potential surface around the mercury center, which suggests that electrostatic forces play a role in the formation of adducts **20** and **21**. Keeping in mind that mercury is soft and polarizable, the involvement of dispersion forces should not be ruled out and may also contribute to the stability of the adducts. These studies also clearly demonstrate that the trinuclear derivative **1** regularly forms supramolecular binary stacks with aromatic substrates. As has been previously proposed for other adducts of **1** and aromatic substrates,[6,7] the formation of these adducts is probably largely dispersive or electrostatic in nature. The phenanthrene adduct, **22**, displays room temperature phosphorescence of the free arene with shortened triplet lifetimes. This observation is a result of the external mercury heavy atom effect which promotes intersystem spin crossing from the S_1 to the T_1 state. Finally, these studies illustrate that the accepting properties of **1** can be altered by complexation of a transition metal to the perfluorinated backbone of **1**. As a result, this metalated organomercurial complexes chloride anions in an μ^3 fashion**.**

VII.7. Experimental details

General. Due to the toxicity of the mercury compounds discussed, extra care was taken at all times to avoid contact with solid, solution, and air-borne particulate mercury compounds. The studies herein were carried out in a well aerated fume hood. Atlantic Microlab, Inc., Norcross, GA, performed the elemental analyses. All commercially available starting materials and solvents were purchased from Aldrich Chemical and VWR, Inc. and used as provided. Compounds **1** and **2** were prepared according to the published procedure.[70,90] The luminescence spectra were recorded with a SLM/AMINCO, Model 8100 spectrofluorometer equipped with a xenon lamp. Low-temperature measurements were made in a cryogenic device of local design. Collodion was used to attach the powder samples to the holder. The collodion was scanned for a baseline subtraction. Liquid nitrogen was used to obtain the 77 K measurements.

Synthesis of [2•tolane] (19). Compound **2** (0.020 g, 0.037 mmol) was dissolved in CH_2Cl_2 (3 mL). In a separate vial, a CH_2Cl_2 solution of tolane (0.0030 g, 0.037 mmol) was prepared. The two solutions were mixed. Upon concentration by slow evaporation

of the solvent, crystals of **19** formed in 96% yield (0.022 g, , 0.0374 mmol). mp 312°C (decomp). Anal. Calcd for $C_{26}H_{10}F_{10}Hg$: C, 43.80; H, 1.41. Found: C, 43.95; H, 1.26.

Synthesis of [2•anthracene] (20). Compound **2** (0.020 g, 0.037 mmol) was dissolved in CH_2Cl_2 (3 mL). In a separate vial, a CH_2Cl_2 solution of anthracene (0.0067 g, 0.037 mmol) was prepared. The two solutions were mixed. Upon concentration by slow evaporation of the solvent, crystals of **20** formed in 75% yield (0.020 g, 0.0374 mmol). mp 326°C (decomp). Anal. Calcd for $C_{26}H_{10}F_{10}Hg$: C, 43.80; H, 1.41. Found: C, 43.99; H, 1.17.

Synthesis of [2•acenaphthalene] (21). Compound **2** (0.020 g, 0.0374 mmol) was dissolved in CH_2Cl_2 (3 mL). In a separate vial, a CH_2Cl_2 solution of acenapthhalene (0.0030 g, 0.0374 mmol) was prepared. The two solutions were mixed. Upon concentration by slow evaporation of the solvent, crystals of **21** formed in 86% yield (0.022 g, , 0.0374 mmol). mp 142°C. Anal. Calcd for $C_{24}H_8F_{10}Hg$: C, 41.97; H, 1.17. Found: C, 41.63; H, 1.29.

Synthesis of [1•phenanthrene] (22). Compound **1** (0.020 g, 0.0191 mmol) and phenanthrene (0.0039 g, 0.019 mmol) were dissolved in CH_2Cl_2 (10 mL). Upon concentration by slow evaporation of the solvent, crystals of **22** formed in 87% yield (0.020 g, 0.0191 mmol). mp 321°C (decomp). Anal. Calcd for $C_{32}H_{10}F_{12}Hg_3$: C, 31.27; H, 0.82. Found: C, 30.88; H, 0.84.

Synthesis of [1•dibenzofuran] (23). Compound **1** (0.020 g, 0.0191 mmol) and dibenzofuran (0.003 g, 0.0191 mmol) were dissolved in CH_2Cl_2 (10 mL). Upon concentration by slow evaporation of the solvent, crystals of **23** formed in 82% yield (0.018 g, 0.0191 mmol). mp 287°C (decomp). Anal. Calcd for $C_{30}H_8F_{12}Hg_3$: C, 29.68; H, 0.66. Found: C, 29.41; H, 0.59.

Synthesis of [24•(μ^3-Cl)(THF)$_2$]. Compound **1** (0.062 g, 0.059 mmol) in THF (5 mL) was added to a solution of $[Cp^*Ru(CH_3CN)_3]PF_6$ (0.020 g, 0.039 mmol) in the same solvent (15 mL) at room temperature. After two days of stirring, diethyl ether (5 mL) was added, and the resulting solution was filtered. Upon concentration of the

solution phase by slow evaporation, crystals of [**24**•(μ^3-Cl)$(THF)_2$] formed in 10% yield (0.005 g, 0.039 mmol).

Crystal Structure Determinations. X-ray data for all adducts were collected on a Bruker SMART-CCD diffractometer using graphite-monochromated Mo Kα radiation (=0.71073 Å). Specimens of suitable size and quality were selected and glued onto a glass fiber with freshly prepared epoxy resin. The structure was solved by direct methods, which successfully located most of the non-hydrogen atoms. Subsequent refinement on F^2 using the SHELXTL/PC package (version 5.1) allowed location of the remaining non-hydrogen atoms.

CHAPTER VIII

GENERAL CONCLUSIONS

This dissertation has focused on studying the phosphorescence of organic chromophores using **1** and **2** as external heavy atom effect inducers. In order to ascertain the suitability of these luminescent adducts for OLED applications, several research objectives have been investigated including shortening the triplet lifetimes of the complexes, synthesis of phosphorescent noncrystalline adducts processable into films, and fundamental studies on the interaction of **1** and **2** with aromatic substrates.

To reduce the triplet lifetimes of adducts involving **1**, we developed a strategy which combines both internal and external heavy atom effects. Specifically, we investigated complexes involving **1** and the *N*-heterocycles as well as the 1-halonaphthalenes, wherein the nitrogen atom or the halogen atom (Cl, Br, and I) acts as internal spin-orbit coupling perturbers. With the substrate *N*-methylcarbazole, the interaction of the two components in solution could be confirmed by fluorescence spectroscopy. In the solid state, these adducts form supramolecular binary stacks where the molecules of **1** alternate with the aromatic substrate (Figure VIII.1). Short Hg–C contacts indicate the presence of secondary Hg–π interactions which are probably dispersive and/or electrostatic in nature. Additionally, Hg···X (where X = N, Cl, Br, or I) interactions are also observed in the supramolecular stacks (Figure VIII.2) As a result of the mercury external heavy atom effect, all of these adducts display intense room temperature phosphorescence of the free arene. In the case of the 1-halonaphthalene adducts, the triplet lifetimes are significantly decreased as compared to the triplet lifetime of free naphthalene; however, the lifetimes of the adducts are similar to that of [**1**•naphthalene]. This could be explained by the presence of Hg···halogen interactions which prevent the arene chromophore from directly interacting with the mercury atoms of **1**. However, triplet state lifetimes of [**1**•*N*-heterocycle] were drastically reduced to

below 100 μs, and this reduction most likely results from the synergy of the internal nitrogen and external mercury heavy atom effects (Figure VIII.1).

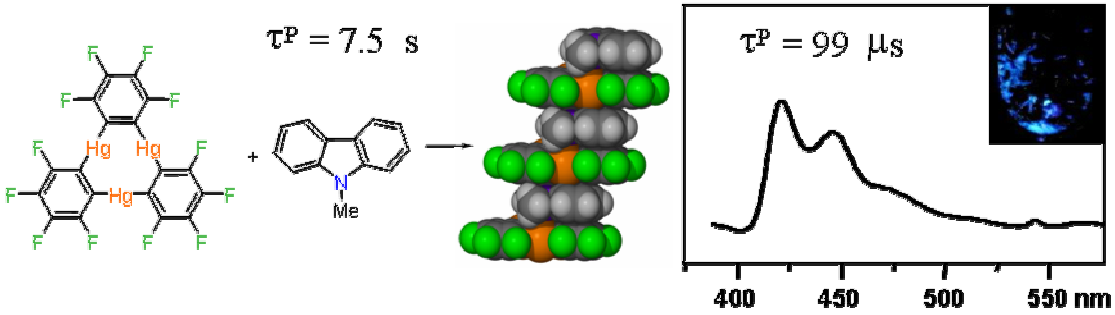

Figure VIII.1. Depiction of the reaction of *N*-methylcarbazole with **1** which yields phosphorescent supramolecular stacks. As a result of both internal and external heavy atom effects, a five order of magnitude reduction in triplet lifetimes is observed.

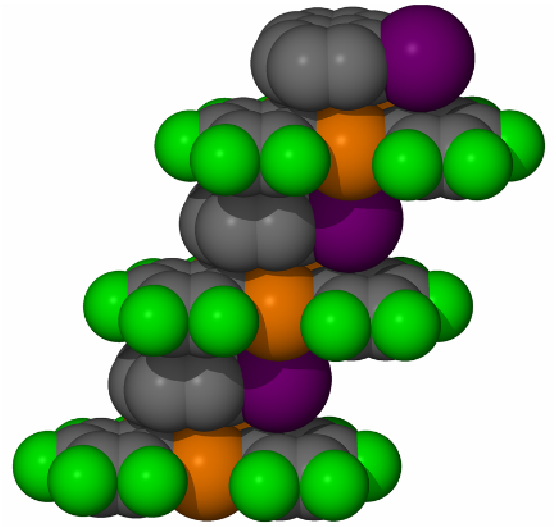

Figure VIII.2. Space filling view of [**1**•1-iodonaphthalene] displaying both Hg-C and Hg-I interactions.

With the ultimate goal of incorporating these luminescent materials in OLEDs, polymeric materials which are amenable to deposition in thin layers by spin-coating techniques were investigated as substrates for **1** and **2**. Both PV2N and PVK interact with **1** in solution as evidenced by fluorescence spectroscopy. The solid blend **1**•PV2N displays the green phosphorescence of the naphthalene monomer at low temperatures, which suggests that the organomercurial is disrupting the long range ordering of the polymer. For the blend **2**•PVK, blue phosphorescence, attributed to the *N*-alkylcarbazole monomer, is observed due to the small size of **2** allowing for insertion in the polymer chain. In the case of the solid blend **1**•PVK, a small doping percentage (1%) of **1** can give rise to white emission, while larger percentages of **1** result in bright room temperature orange excimer emission.

To determine if the attraction between **1** and aromatic substrates is due to the close proximity of the three mercury centers, **2** was studied as a monofunctional analog to **1**. By utilizing fluorescence spectroscopy, the interaction of naphthalene and **1** has been detected in solution and the Stern-Volmer constant determined. The solid state structure of the adducts with **2** reveal the existence of supramolecular stacks with short Hg–C contacts which suggest secondary Hg–π interactions (Figure VIII.3). In the case of [**2**•biphenyl] and [**2**•fluorene], perfluoroarene–arene interactions also provide cohesion to the stacks. All of the arene adducts of **2** studied exhibit room temperature phosphorescence with shortened triplet lifetimes. Comparison of the photophysical results supports the occurrence of cooperative effects between the Lewis acidic mercury centers of **1**, which make it a more efficient external heavy-atom effect inducer.

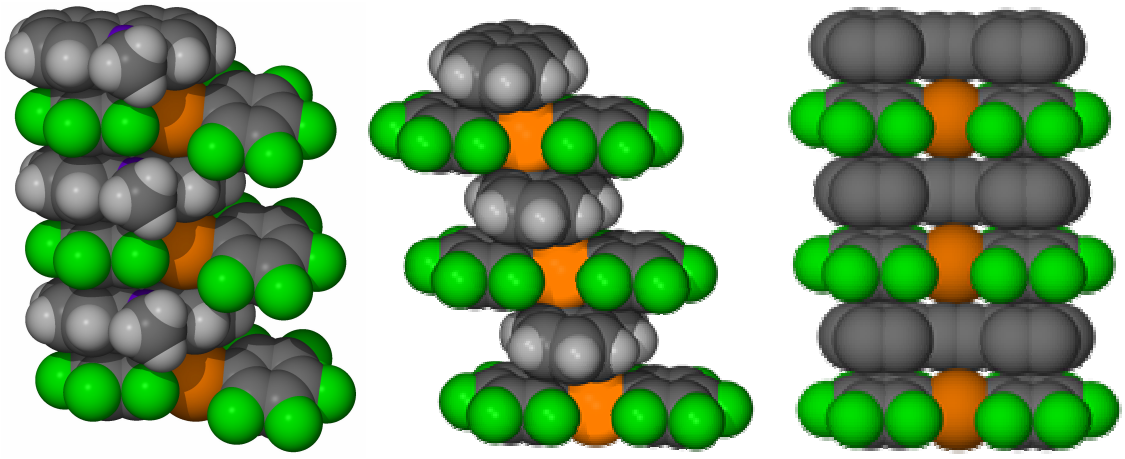

[**2**•*N*-methylcarbazole] [**2**•naphthalene] [**2**•tolane]

Figure VIII.3. Space filling view of [**2**•*N*-methylcarbazole], [**2**•naphthalene] and [**2**•tolane] highlighting the different interactions observed in adducts with **2**.

In addition to naphthalene, biphenyl, and fluorene, the solid state structure of other arene adducts of **2** have been studied, all of which exhibit binary supramolecular stacks with slight variations in their structures. For instance, as opposed to the other arene adducts, the molecule of **2** in adduct [**2**•*N*-methylcarbazole] does not lie planar between the *N*-heterocycles (Figure VIII.3). In fact, the dihedral angle between the perfluoroaryl groups of **2** is 26°. As seen in [**2**•biphenyl], secondary Hg–π interactions along with perfluoroarene–arene interactions are observed in this adduct. Other arene adducts with **2** display only one type of interaction in the supramolecular stack. In the case of [**2**•naphthalene] and [**2**•acenaphthalene], only short Hg-C contacts are detected, suggesting the presence of secondary Hg–π interactions, while [**2**•tolane] only exhibits perfluoroarene–arene interactions (Figure VIII.3).

These studies also clearly demonstrate that the trinuclear derivative **1** regularly forms supramolecular binary stacks with aromatic substrates. In the case of phenanthrene, the solid state structure of the 1:1 adduct displays short Hg-C contacts ranging from 3.28 Å to 3.41 Å suggesting the presence of secondary Hg–π interactions.

This adduct exhibits room temperature phosphorescence of the pure phenanthrene with shortened triplet lifetimes (Figure VIII.4).

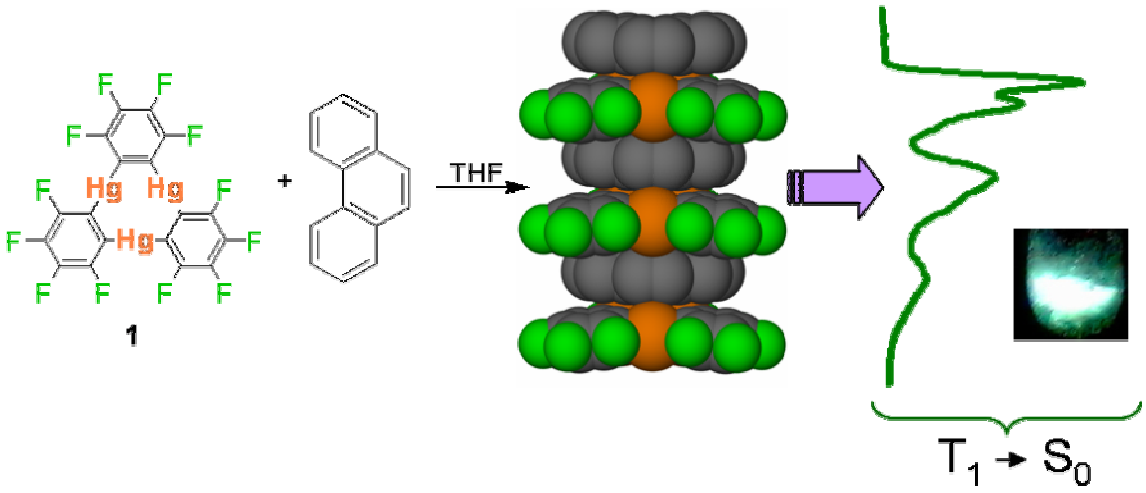

Figure VIII.4. Reaction of **1** with phenanthrene resulting in phosphorescent supramolecular stacks

Although various examples of binary supramolecular stacks involving **1** and aromatic substrates have been reported, this dissertation presents the first structurally characterized ternary complex with **1**, carbazole, and coordinating solvents THF and triethylamine. The acidic N-H moiety of the carbazole interacts with the Lewis basic site of the solvent by hydrogen bonding as evidenced by IR spectroscopy and short N···O and N···N distances in the solid state. In the extended structure, molecules of **1** and the hydrogen bonded complex alternate to form supramolecules. Short Hg–C contacts involving molecules of **1** and carbazole indicate the presence of secondary Hg–π interactions. These supramolecules exhibit thermochromic luminescent properties; at 77 K, the blue phosphorescence of free carbazole is observed due to the external mercury heavy atom effect.

In summary, the results presented herein indicate that fluorescence spectroscopy is a valid tool for observing the interaction of organomercurials **1** and **2** with aromatic substrates in solution. While **2** was not always found to interact with arenes, **1** displays a high affinity for aromatic substrates in solution. Both organomercurials **1** and **2** quench the fluorescence of the aromatic substrates as a result of the external mercury heavy atom effect where the singlet excited state is effectively depopulated. A summary of the Stern-Volmer constants reported in this dissertation is provided in Table VIII.1.

Table VIII.1. Summary of K_{SV} values using organomercurials as fluorescence quenchers

Organomercurial	Substrate	K_{SV} (M^{-1})
1	*N*-methylcarbazole	383 ± 24
1	naphthalene	159 ± 6
1	poly(vinylcarbazole)	2567 ± 91
1	poly(vinyl-2-naphthalene)	198 ± 30
2	poly(vinylcarbazole)	151 ± 15

These results also show that stacked supramolecular structures are not limited to adducts involving **1**. In fact, both fluorinated organomercurials **1** and **2** readily assemble with aromatic substrates to form supramolecules, where **1** and **2** engage in a variety of interactions with the aromatic substrates. In these adducts, both **1** and **2** typically induce the phosphorescence of the aromatic chromophore with a shortening of the triplet state lifetime due to the external mercury heavy atom effect. A summary of the adducts presented in this dissertation along with their luminescent properties is presented in Table VIII.2

Table VIII.2. Summary of solid state adducts of **1** and **2** and their luminescent properties

Adduct	Luminescent properties	τ^P (77 K)
[**1**•*N*-methylcarbazole]	blue phosphorescence	0.099 ms
[**1**•*N*-methylindole]	blue phosphorescence	0.057 ms
[**1**•1-chloronaphthalene]	green phosphorescence	1.557 ms
[**1**•1-bromonaphthalene]	green phosphorescence	1.018 ms
[**1**•1-iodonaphthalene]	green phosphorescence	0.991 ms
[**1**•fluorene]	blue-green phosphorescence	0.436 ms
[**1**•carbazole]	blue phosphorescence	not measured
[**1**•($C_{12}H_8NH$•THF)]	blue phosphorescence (77 K)	not measured
[**1**•($C_{12}H_8NH$•NEt_3)]	blue phosphorescence (77 K)	not measured
[**1**•phenanthrene]	green phosphorescence	0.857 ms
[**1**•dibenzofuran]	green phosphorescence	2.43 ms
[**2**•naphthalene]	green phosphorescence	5.15 ms
[**2**•biphenyl]	blue phosphorescence	2.96 ms
[**2**•fluorene]	blue-green phosphorescence	1.56 ms
[**2**•*N*-methylcarbazole]	none observed	n/a
[**2**•tolane]	phosphorescence	not measured
[**2**•anthracene]	none observed	n/a
[**2**•acenaphthalene]	none observed	n/a

REFERENCES

1 For a review, see: Sibley S., Thompson, M.E., Burrows, P.E., Forrest, S.R. *Electroluminescence in Molecular Materials*. In *Optoelectronic Properties of Inorganic Compounds*, Roundhill, D.M., Fackler, J.P., Jr. (Eds), Plenum: New York, 1999, Chapter 5.

2 For a review on OLED phosphorescent dyes, see: Holder, E.; Langeveld, B. M. W.; Schubert, U. S. *Adv. Mater.* **2005**, *17*, 1109-1121.

3 S.M. Kelly, *Flat Panel Displays Advanced Organic Materials*, Royal Society of Chemistry: Cambridge, UK, 2000, pp 5-6, 134-135.

4 (a) Köhler, A.; Wilson, J. S.; Friend, R. H. *Adv. Mater.* **2002**, *14*, 701-707. (b) Baldo, M. A.; O'Brien, D. F.; Thompson, M. E.; Forrest, S. R. *Phys. Rev. B* **1999**, *60*, 14422-14428.

5 Adachi, C.; Baldo, M. A.; Thompson, M. E.; Forrest, S. R *J. Appl. Phys.* **2001**, *90*, 5048-5051.

6 Haneline, M.R., Tsunoda, M., and Gabbaï, F.P. *J. Am. Chem. Soc.* **2002,** *124,* 3737–3742.

7 Omary, M.A., Kassab, R.M., Haneline, M.R., Elbjeirami, O. and Gabbaï, F.P. *Inorg. Chem*. **2003,** *42,* 2176–2178.

8 McGlynn, S.P., Azumi, T., Kinoshita, M. *Molecular Spectroscopy of the Triplet State*, Prentice-Hall: Englewood Cliffs, NJ, 1969, pp 40-43, 183-187.

9 Frank, W.; Dincher, B. *Z. Naturforsch. B* **1987**, *42*, 828-834.

10 Ulvenlund, S.; Rosdahl, J.; Fischer, A.; Schwerdtfeger, P.; Kloo, L. *Eur. J. Inorg. Chem.* **1999**, 633-642.

11 Borovik, A.S.; Bott, S.G.; Barron, A.R. *Angew. Chem. Int. Ed.* **2000**, *39*, 4117-4118.

12 Borovik, A.S.; Bott, S.G.; Barron, A.R. *J. Am. Chem. Soc.*, **2001**, *123*, 11219-11228.

13 Branch, C.S.; Barron, A.R. *J. Am. Chem. Soc.,* **2002**, *124*, 14156-14161.

14 Delaigue, X.; Hosseini, M.W.; Kyritsakas, N.; De Cian, A.; Fischer, J. *Chem. Commun.* **1995**, 609-610.

15 Fowley, L. A.; Lee, J. C.; Crabtree, R. H.; Siegbahn, P. E. M. *J. Organomet. Chem.* **1995**, *504*, 57-67.

16 Fowley, L. A.; Lee, J. C.; Crabtree, R. H. *Organometallics*, **1996**, *15*, 1157-1165.

17 Tschinkl, M.; Bachman, R. E.; Gabbaï, F. P. *J. Organomet. Chem.* **1999**, *582*, 40-44.

18 Viets, D.; Lork, E.; Watson, P. G.; Mews, R. *Angew. Chem. Int. Ed.* **1997**, *36*, 623-624.

19 Naumann, D.; Schulz, F.; Pantenburg, I.; Tyrra, W. *Z. Anorg. Allg. Chem.* **2004**, *630*, 529-534.

20 Schulz, F.; Pantenburg, I.; Naumann, D. *Z. Anorg. Allg. Chem.* **2003**, *629*, 2312-2316.

21 Shur, V. B.; Tikhonova, I.A.; Yanovskii, A.I.; Struchkov, Yu.T.; Petrovskii, P.V.; Panov, S.Yu.; Furin, G.G.; Vol'pin, M.E. *J. Organomet. Chem.* **1991**, *418*, C29-C32.

22 Koomen, J. M.; Lucas, J. E.; Haneline, M. R.; King, J. D. B.; Gabbaï, F. P., Russell, D. H. *Int. J. Mass Spectrom.* **2003**, *225*, 225-231.

23 Shubina, E. S.; Tikhonova, I. A.; Bakhmutova, E. V.; Dolgushin, F. M.; Antipin, M. Y.; Bakhmutov, V. I.; Sivaev, I. B.; Teplitskaya, L. N.; Chizhevsky, I. T.; Pisareva, I. V.; Bregadze, V. I.; Epstein, L. M.; Shur, V. B. *Chem. Eur. J.* **2001**, *7*, 3783-3790.

24 Saitkulova, L. N.; Bakhmutova, E. V.; Shubina, E. S; Tikhonova, I. A.; Furin, G. G.; Bakhmutov, V. I.; Gambaryan, N. P.; Chistyakov, A. L.; Stankevich, I. V.; Shur, V. B., Epstein, L. M. *J. Organomet. Chem.* **1999**, *585*, 201-210.

25 Tikhonova, I. A.; Dolgushin, F. M.; Tugashov, K. I.; Ellert, O. G.; Novotortsev, V. M.; Furin, G. G.; Antipin, M. Y.; Shur, V. B. *J. Organomet. Chem.* **2004**, *689*, 82-87.

26 Gardinier, J. R., Gabbai, F. P. *Dalton Trans.* **2000**, *16,* 2861 – 2865.

27 M. Tsunoda, F. P. Gabbaï, *J. Am. Chem. Soc.* **2000**, *122*, 8335-8336.

28 Haneline M. R.; Taylor R. E.; Gabbaï F. P. *Chem. Eur. J.* **2003**, *9*, 5189-5193.

29 Haneline, M. R.; King, J. B.; Gabbaï, F. P. *J. Chem. Soc. Dalton Trans.* **2003**, *13*, 2686-2690.

30 Haneline, M.R.; Gabbaï, F.P. *C. R. Chimie* **2004**, *7*, 871-876.

31 Haneline, M.R.; Gabbaï, F.P. *Angew.Chem. Int. Ed. Engl.* **2004**, *43*, 5471-5474.

32 Kasha, M. *J. Chem. Phys* **1952**, *20*, 71-74.

33 Tsubomura, H.; Mulliken, R.S. *J. Am. Chem. Soc.* **1960**, *82*, 5966-5974.

34 See the following and the references therein: (*a*) Azumi, T. *Chem. Phys. Lett.* **1973**, *19*, 580-583; (*b*) Chandra, A. K.; Turro, N. J.; Lyons, A. L.; and Stone, P. *J. Am. Chem. Soc.* **1978**, *100*, 4964-4968; (*c*) Minaev, B. F.; Knuts S.; and Agren, H. *Chem. Phys.* **1994**, *181*, 15-28; (*d*) Chattopadhyay, N.; Serpa, C.; Pereira, M. M.; Seixas de Melo, J.; Arnaut L. G.; and Formosinho, S. J. *J. Phys. Chem. A* **2001**, *105*, 10025-10030; (*e*) Gould, I. R.; Boiani, J. A.; Gaillard, E. B.; Goodman J. L.; and Farid, S. *J. Phys. Chem. A* **2003**, *107*, 3515-3524.

35 Giachino, G.; Kearns, D. R. *J. Chem. Phys.* **1970,** *52*, 2964-2974.

36 Giachino, G.; Kearns, D. R. *J. Chem. Phys.* **1970**, *53*, 3886-3891.

37 Colson, S. D.; Gash, B. R. *Chem. Phys. Lett.* **1972**, *15*, 625-626.

38 Colson, S. D.; Gash, B. R. *J. Chem. Phys.* **1973**, *59*, 3528-3533.

39 Colson, S. D.; Gash, B. R. *Chem. Phys. I* **1973**, 182-190.

40 van Leeuwen, W. H.; Langelaar, J.; van Voorst, J. D. W. *Chem. Phys. Lett*, **1972**, *13*, 622-624.

41 Priestley, E. B.; Haug, A. *J. Chem. Phys.* **1968**, *49*, 622-629.

42 Hochstrasser, R. M.; Prasad, P. N. *J. Chem. Phys*. **1972**, *56*, 2814-2823.

43 Romanova, Z. S.; Deshayes, K.; Piotrowiak, P. *J. Am. Chem. Soc.* **2001**, *123*, 2444-2445.

44 For a representative example, please see: Bower, E. L.; Winefordner, J. D. *Anal. Chim. Acta.* **1978**, *102*, 1-13.

45 Vander Donckt, E.; Vogels, C. *Spectrochim. Acta* **1971**, *27A,* 2157-2163.

46 Vander Donckt, E.; Matagne, M.; Sapir, M. *Chem. Phys. Lett.* **1973**, *20*, 81-84.

47 For a recent review, please see: Peng, Y.L.; Wang, Y.T.; Wang, Y.; Jin, W. J. *J. Photochem. & Photobio. A* **2005**, *173*, 301-308.

48 Femia; R. A.; Love, L. J. C. *J. Phys. Chem.***1985**, *87*, 1897-1901.

49 Li, L.; Hai, X.; Tong, A. *Spectrochim. Acta Part A* **2000**, *56*, 1513-1521.

50 Scypinski, S.; Love, L. J. C. *Anal. Chem.* **1984**, *56*, 322-327.

51 Hamai, S.; Kuduo, T. *J. Photochem. & Photobio. A* **1998**, *113*, 135-140.

52 Ramamurthy. V.; Caspar. J. V.; Corbin, D. R.; Eaton, D. F. J. *Photochem. Photobio. A* **1989,** *50,* 157-158.

53 Ramamurthy, V.; Caspar, J. V.; Eaton, D. F.; Kuo, E. W.; Corbin, D. R. *J. Am. Chem. Soc.* **1992**, *114*, 3882-3892.

54 Mohamed, A. A.; Rawashdeh-Omary, M. A.; Omary, M. A.; Fackler, J. P. *Dalton Trans.* **2005**, 2597-2602.

55 Lower, S. K.; El-Sayed, M. A. *Chem. Rev.* **1966**, *66*, 199-241.

56 Ramamurthy, V.; Caspar, J. V.; Eaton, D. F.; Kuo, Erica W.; Corbin, D. R. *J. Am. Chem. Soc.* **1992**, *114*, 3882-3892.

57 For a general review, see: Shur, V. B.; Tikhonova, I. A. *Russ. Chem. Bull.* **2003**, *52*, 2539-2554.

58 Baldo, M. A.; Thompson, M. E.; Forrest, S. R. *Pure Appl. Chem.* **1999**, *71*, 2095-2106.

59 Such lifetimes are necessary for the rapid on/off switching of the emission required in displays. See: Stoffers, C.; Yang, S.; Zhang, F.; Jacobsen, S. M.; Wagner, B. K.; Summers, C. J. *Appl. Phys. Lett.* **1997**, *71,* 1759-1761.

60 McGlynn, S. P. *Chem. Rev.* **1958**, *58*, 1113-56.

61 Nijegorodov, N.; Mabbs, R. *Spectrochim. Acta, Part A.* **2001**, *57*, 1449-1462.

62 Lakowicz, J. *Principles of Fluorescence Spectroscopy*, Kluwer/Plenum: New York, NY, 1999.

63 (a) Perry, A.W., Tidwell, P., Cetorelli, J., Windefordner, J. *Anal. Chem.* **1971**, *43*, 781-782. (b) Lessard, G., Durocher, G., *J. Phys. Chem*. **1978**, *82*, 2812-2819.

64 Lessard, G., Durocher, G. *J. Phys. Chem.* **1978**, *82*, 2812-2819.

65 P. Pyykkö, M. Straka, *Phys. Chem. Chem. Phys.* **2000**, *2*, 2489–2493.

66 C. Caillet, P. Claverie, *Acta Crystallogr. A* **1975**, 31, 448-461.

67 Bondi, A. *J. Phys. Chem.,* **1964**, *68*, 441-451.

68 Yang, X.; Knobler, C.; Zheng, Z; Hawthorne, M. F. *J. Am. Chem. Soc.* **1994**, *116*, 7142-7159.

69 R.G. Pearson, *Chemical Hardness*, Wiley, VCH: Weinheim, 1997.

70 Sartori, P.; Golloch, A. *Chem. Ber.* **1968**, *101*, 2004-2009.

71 Burress, C.; Elbjeirami, O.; Omary, M.; Gabbaï, F.P. *J. Am. Chem. Soc*. **2005**, *127,* 12166-12167.

72 Taylor, T.J.; Gabbaï, F.P. *Organometallics* **2006**, *25*, 2143-2147.

73 Tikhonova, I. A.; Tugashov, K. I.; Dolgushin, F. M.; Yakovenko, A. A.; Strunin, A. B.; Petrovskii, P. V.; Furin, G. G.; Shur, V. B. *Inorg. Chim. Acta* **2006**, *359*, 2728-2735.

74 McClure, D. S. *J. Chem. Phys*. **1949**, *17*, 905-913.

75 Wilkinson, D.L.; Riede, J.; Muller, G. *Z. Naturforsch B: Chem. Sci.***1991**, *46*, 285.

76 Brock, C.P.; Dunitz, J.D. *Acta Cryst.* **1982**, *B38*, 2218.

77 Kunchur, N. R.; Mathew, M. *Chem. Commun.* **1966**, 71-73.

78 Puhl, W.H. Henneike, H.F. *J. Phys. Chem*. **1973**, *77*, 558-562.

79 Canty, A.J.; Gatehouse, B.M. *J. Chem. Soc. Dalton Trans.* **1972**, 511-514.

80 Kientiz, C.; Thone, C.; Jones, P. *Inorg.Chem*. **1996**, *35*, 3990-3997.

81 Almenningen, A.; Bastiansen, O.; Fernholt, L.; Cyvin, B. N.; Cyvin, S. J.; Samdal, S. *J. Mol. Struct. (THEOCHEM)* **1985**, *128*, 59-76.

82 Grein, Friedrich, *J. Phys. Chem. A* **2002**, *106*, 3823-3827.

83 (a) Sekiya, R.; Nishikiori, S. *Chem. Eur. J.* **2002**, *8*, 4803-4810. (b) Biradha, K.; Mahata, G. *Cryst. Growth Des*. **2005**, *5*, 61-63.

84 Gustav, K.; Seydenschwanz, C. *Chem. Phys. Lett.* **1984**, *109*, 156-159.

85 Ramamurthy, V.; Eaton, D. F.; and Caspar, J. V. *Acc. Chem. Res*. **1992**, *25*, 299-307.

86 (a) Najbar, J.; Barzyk, W. *J. Lumin*. **1974**, *8*, 242-251. (b) Bree, A.; Zwarich, R. *J. Chem. Phys.* **1969**, *51*, 903-912.

87 Miller, J. C.; Meek, J. S.; Strickler, S. J. *J. Am. Chem. Soc.* **1977,** *99*, 8175-8179.

88 Melhiush, W. H.; Metcalf, W. S. *J. Chem. Soc.* **1958**, 480-482.

89 Haneline, M. R.; Gabbai, F. P. *Inorg. Chem.* **2005**, *44*, 6248-6255.

90 Jukes, A.E.; Gilman, H. *J. Organomet. Chem*. **1969**, *17*, 145-148.

91 Frisch, M. J.; Trucks, G. W.; Schlegel, H. B.; Scuseria, G. E.; Robb, M. A.; Cheeseman, J. R.; Zakrzewski, V. G.; Montgomery, J. A.; Stratmann, R. E.; Burant, J. C.; Dapprich, S.; Millam, J. M.; Daniels, A. D.; Kudin, K. N.; Strain, M. C.; Farkas, O.; Tomasi, J.; Barone, V.; Cossi, M.; Cammi, R.; Mennucci, B.; Pomelli, C.; Adamo, C.; Clifford, S.; Ochterski, J.; Petersson, G. A.; Ayala, P. Y.; Cui, Q.; Morokuma, K.; Malick, D. K.; Rabuck, A. D.; Raghavachari, K.; Foresman, J. B.; Cioslowski, J.; Ortiz, J. V.; Stefanov, B. B.; Liu, G.; Liashenko, A.; Piskorz, P.; Komaromi, I.; Gomperts, R.; Martin, R. L.; Fox, D. J.; Keith, T.; Al-Laham, M. A.; Peng, C. Y.; Nanayakkara, A.; Gonzalez, C.; Challacombe, M.; Gill, P. M. W.; Johnson, B.; Chen, W.; Wong, M. W.; Andres, J. L.; Gonzalez, A. C.; Head-Gordon, M.; Replogle, E. S.; Pople, J. A. *Gaussian 98*, revision A.11.3; Gaussian, Inc.: Pittsburgh, PA, 1998.

92 Becke, A. D. *J. Chem. Phys.* **1993**, *98*, 5648-56552.

93 Lee, C.; Yang, W.; Parr, R. G. *Phys. Rev. B* **1988**, *37*, 785-789.

94 Parr, R. G.; Yang, W. *Density Functional Theory of Atoms and Molecules*, Oxford University Press: New York, 1989.

95 Ditchfield, R.; Hehre, W. J.; Pople, J. A. *J. Chem. Phys.* **1971**, *54*, 724-728.

96 Bergner, A.; Dolg, M.; Kuchle, W.; Stoll, H.; Preuss, H. *Mol. Phys*. **1993**, *80*, 1431-1441.

97 S.M. Kelly, *Flat Panel Displays Advanced Organic Materials*, Royal Society of Chemistry: Cambridge, UK, 2000, pp 5-6, 134-135.

98 (a) Harrah, L. A. *J. Chem. Phys.* **1972**, *56*, 385-389. (b) Fox, R. B.; Price, T. R.; Cozzens, R. F.; McDonald, J. R. *J. Chem. Phys.* **1972**, *57*, 534-541. (c) Semerak, S. N.; Frank, C. W. *Macromolecules* **1981**, *14*, 443-449. (d) Webber, S. E.; Avots-Acotins, P. E. *Macromolecules* **1981**, *14*, 105-110. (e) De Schryver, F. C.; Demeyer, K.; van der Auweraer, M.; Quanten, E. *Ann. N. Y. Acad. Sci.* **1981**, *366,* 93-109.

99 (a) Klöpffer, W. *J. Chem. Phys.* **1969**, *50*, 2337-2343. (b) David, C.; Piens, M.; Geuskens, G. *Eur. Polym. J.* **1972**, *8*, 1291-1297. (c) Yokoyama, M.; Tamamura, T.; Atsumi, M.; Yoshimura, M.; Shirota, Y.; Mikawa, H. *Macromolecules* **1975**, *8*, 101-104.

100 Kunchur, N.R.; Mathew, M. *J. Chem. Soc., Chem. Commun.,* **1966**, 71-73.

101 Kim, N.; Webber, S. E. *Macromolecules* **1980**, *13*, 1233-1236.

102 (a) Burkhart, R. D. *Macromolecules* **1976**, *9*, 234-239. (b) Yokoyama, M.; Tamamura, T.; Nakano, T.; Mikawa, H. *J. Chem. Phys.* **1976**, *65*, 272-279.

103 Burkhart, R. D.; Dawood, I. *Macromolecules* **1986**, *19*, 447-452.

104 Pearson, J. M. ; Stolka, M. *Poly(N-vinylcarbazole)*; Huglin, M. B., Ed.; Gordon and Breach, Science Publishers: New York, NY, 1981; Vol. 6, Chapter 8, pp 130-146.

105 (a) Itaya, A.; Okamoto, K.; Kusabayashi, S. *Bull. Chem. Soc. Japan* **1976,** *49,* 2037-2042. (b) Itaya, A.; Okamoto, K.; Kusabayashi, S. *Bull. Chem. Soc. Japan* **1977**, *50*, 22-26.

106 For a review on OLED phosphorescent dyes, see: Holder, E.; Langeveld, B. M. W.; Schubert, U. S. *Adv. Mater*. **2005**, *17*, 1109-1121.

107 Adachi, C.; Baldo, M. A.; Thompson, M. E.; Forrest, S. R *J. Appl. Phys*. **2001**, *90*, 5048-5051.

108 Sannigrahi, A. B.; Chandra, A. K. *J. Phys. Chem.* **1963**, *67*, 1106-1109.

109 Martin. M. M.; Ware, W. R. *J. Phys. Chem.* **1978**, *82*, 2770-2776.

110 Thyagarajan, G.; Rao, D. S. R. *Z. Phys. Chem.-Leipzig* **1974**, *255*, 97-102.

111 Desiraju, G. R. *Crystal Engineering: The Design of Organic Solids*; Elsevier: Amsterdam, 1989.

112 Garcia-Tellado, F.; Geib, S. J.; Goswami, S.; Hamilton, A. D. *J. Am. Chem. Soc.* **1991**, *113*, 9265-9269.

113 Wardell, J. L.; Low, J. N.; Glidewell, C. *Acta Crystallogr. C* **2006**, *62*, o318-o320.

114 Kuduva, S. S.; Blaser, D.; Boese, R.; Desiraju, G. R. *J. Org. Chem.* **2001**, *66*, 1621-1626.

115 (a) Grubbs, T. W.; Doughtery, R. P.; Heilweil, E. J. *J. Phys. Chem*. **1995**, *99*, 10716-10722. (b) Esenturk, O.; Walker, R. A. *Phys. Chem. Chem. Phys*. **2003**, *5*, 2020-2026. (c) Shukla, J. P.; Walker, S.; Warren, J. *J. Chem. Soc. Farad. T 1* **1978**, *74*, 2045-2050. (d) Nozari, M. S.; Drago, R. S. *J. Am. Chem. Soc.* **1970**, *92*, 7086-7090.

116 Skrilec, M.; Love, L. J. C. *J. Phys. Chem.* **1981**, *85*, 2047-2050.

117 Mataga, N.; Tanaka, F.; Kato, M. *Acta Phys. Pol.* **1968**, *64*, 733-745.

118 Tikhonova, I. A.; Dolgushin, F. M.; Yanovsky, A. I.; Struchkov, Y. T.; Gavrilova, A. N.; Saitkulova, L. N.; Shubina, E. S.; Epstein, L. M.; Furin, G. G.; Shur, V. B. *J. Organomet. Chem.* **1996**, *508*, 271-273.

119 Puhl, W.H. Henneike, H.F. *J. Phys. Chem*. **1973**, *77*, 558-562.

120 (a) Coates, G. W.; Dunn, A. R.; Henling, L. M.; Dougherty, D. A.; Grubbs, R. H. *Angew. Chem., Int. Ed. Engl.* **1997**, *36*, 248-251. (b) Coates, G. W.; Dunn, A.

R.; Henling, L. M.; Ziller, J. W.; Lobkovsky, E. B.; Grubbs, R. H. *J. Am. Chem. Soc.* **1998**, *120*, 3641-3649. (c) Weck, M.; Dunn, A. R.; Matsumoto, K.; Coates, G. W.; Lobkovsky, E. B.; Grubbs, R. H. *Angew. Chem., Int. Ed.* **1999**, *38*, 2741-2745.

121 (a) Renak, M. L.; Bartholomew, G. P.; Wang, S.; Ricatto, P. J.; Lachicotte, R. J.; Bazan, G. C. *J. Am. Chem. Soc*. **1999**, *121*, 7787-7799. (b) Bartholomew, G. P.; Bazan, G. C.; Bu, X.; Lachicotte, R. J. *Chem. Mater.* **2000**, *12*, 1422-1430. (c) Bartholomew, G. P.; Bu, X.; Bazan, G. C. *Chem. Mater.* **2000**, *12*, 2311-2318.

122 Aspley, C. J.; Boxwell, C.; Buil, M. L.; Higgitt, C. L.; Long, C.; Perutz, R. N. *Chem. Commun.* **1999**, 1027-1028.

123 (a) Collings, J. C.; Batsanov, A. S.; Howard, J. A. K.; Marder, T. B. *Acta Crystallogr., Sect. C: Cryst. Struct. Commun.* **2001**, *57*, 870-872. (b) Dai, C.; Nguyen, P.; Marder, T. B.; Scott, A. J.; Clegg, W.; Viney, C. *Chem. Commun.* **1999**, 2493-2494.

124 (a) Nagano, Y.; Ikoma, T.; Akiyama, K.; Tero-Kubota, S. *J. Chem. Phys.* **2001**, *114*, 1775-1784. (b) Ferrante, C.; Kensy, U. Dick, B. *J. Phys. Chem.* **1993**, *97*, 13547-13463. (c) Gutmann, M.; Gudipati, M.; Schonzart, P. F.; Hohlneicher, G. *J. Phys. Chem.* **1992**, *96*, 2433-2442.

125 Langelaar, J.; Rettschnick, R. P. H.; Lambooy, A. M. F.; Hoytink, G. J. *Chem. Phys. Lett.* **1968**, *1*, 609-612.

126 (a) Porter, G. and Wright, F.J. *Trans. Faraday Soc*. **1955**, *51*, 1205-1211. (b) Porter, G. and Wright, F.J., *Discussions Faraday Soc.* **1954**, *17*, 178-186. (c) McClure, D.S. *J. Chem. Phys.*, **1951**, *19*, 670-675. (d) Craig, D.P., Ross, I.G., *J. Chem. Soc.*, **1954**, 1589-1606.

127 Holman, K. T.; Halihan, M. M.; Jurisson, S. S.; Atwood, J. L.; Burkhalter, R. S.; Mitchell, A. R.; Steed, J. W. *J. Am. Chem. Soc.* **1996**, *118*, 9567 -9576

128 (a) Bell, T.W., Helliwell, M., Partridge, M.G., Perutz, R.N., *Organometallics,* **1992**, *11*, 1911-1918. (b) Barker, J.J., Orpen, A. G., Seeley, A.J., Timms, P.T. *J.*

Chem. Soc. Dalton Trans., **1993**, 3097-3102. (c) Gastinger, R. G.; Anderson, B. B.; Klabunde, K. J. *J. Am. Chem. Soc.***1980**, *102*, 4959-66.

129 Koelle, U., Hörnig, A., Englert, U., *Organometallics,* **1994**, *13*, 4064-4066.

130 Mbaye, D. M.; Demerseman, B.; Renaud, J. L.; Toupet, L.; Bruneau, C. *Adv. Synth. Catal.* **2004**, *346*, 835-841.

VITA

CHARLOTTE NICOLE BURRESS

c/o Prof. François Gabbaï
Department of Chemistry
Texas A&M University
College Station, TX 77843-3255

Education:

Ph.D. in chemistry from Texas A&M University
Graduated: December 2006

B.S. in chemistry from Newcomb College of Tulane University
Graduated: May 2002

Publications:

Taylor, T. J.; Burress, C. N.; Pandey, L.; Gabbaï, F. P. "Structural and photophysical studies of phenanthrene adducts involving C_6F_5HgCl and $[o\text{-}C_6F_4Hg]_3$." *Dalton Trans.* **2006,** *in press.*

Burress C. N.; Melaimi, M.; Taylor T. J.; Gabbaï F. P. "Mercury and Cadmium" *Comprehensive Organometallic Chemistry - 3rd Edition* **2006**, *in press*.

Burress, C.; Elbjeirami, O.; Omary, M. A.; Gabbaï, F. P. "Five-Order-of-Magnitude Reduction of the Triplet Lifetimes of N-Heterocycles by Complexation to a Trinuclear Mercury Complex." *J. Am. Chem. Soc.* **2005**, *127* 12166-12167.

Awards:

Martell Travel Award, Spring 2005
Regent's Graduate Fellowship, Texas A&M University
O. M. Chamberlain Memorial Scholarship, Newcomb College